THERMODYNAMICS, KINETICS AND MODELING STUDIES OF MAGNESIUM HYDRIDE ENHANCED BY CATALYSTS FOR HYDROGEN STORAGE APPLICATIONS

BY

SAIDI TEMITOPE SABITU

A DISSERTATION

Submitted in partial fulfillment of the requirements for the Doctoral Degree in the Applied Chemistry Graduate Program of Delaware State University

DOVER, DELAWARE

Fall 2012

DEDICATION

This thesis is dedicated to God Almighty, who makes all things possible. This is all YOU and none of ME. My wife, Folashade and son, Mororeoluwa who I hold forever dearly in my heart. Your love and support is incomparable. My parents Elder Moses Sabitu and Deaconess Victoria Sabitu who sacrificed everything for me to have the opportunities they never had. My siblings, Funmi, Seun, Bunmi, Isaiah and Anu, for supporting and praying for me. My friends through thick and thin, Tolu, Sam, Tunji and Gbenga. To friends and the Chemistry Department of Delaware State University, who supported me throughout my stay and during the course of my study.

ACKNOWLEDGEMENTS

My sincere appreciation goes to Dr. Andrew Goudy for his support and encouragement throughout my course of study. Thank you so much for believing in me and helping me realize my potentials. Thank you for looking beyond my flaws and letting me be me. It's a privilege coming across you on the face of the earth and certainly God ordained. Without your efforts, this thesis could not have been a success. I'm very grateful sir. Many thanks to Dr. Workie, Dr. Mohammed, Dr. Winstead, Dr. Marcano and Mrs. Sanchez for their encouragement and support throughout my research and during my stay at Delaware State University. I would also like to thank my colleagues, friends and well wishers for their support towards the success of this project, Dr. Yang, Adeola, Esosa, Jalaal, The Mayowas, Opes, Ibrahims, Ajeigbes, Gbadebos, Ibrahims and Akinwandes.

ABSTRACT

In this research, the effect of additives such as TiH_2, Mg_2Ni, Nb_2O_5, NbF_5 and transition metal oxides catalysts on the thermodynamics and hydrogen desorption kinetics of MgH_2 was investigated. The kinetics measurements were done using a method in which the ratio of the equilibrium plateau pressure to the opposing pressure was the same for all the reactions. The data showed NbF_5 to be vastly superior to the other catalysts studied in improving the hydrogen storage potentials of MgH_2. It has the lowest hydrogen desorption temperature and improved the reaction kinetics of MgH_2 the most. Kinetics modeling measurements showed that chemical reaction at the phase boundary to be the likely process controlling the reaction rates. Kissinger plots also showed the mixture of MgH_2 and NbF_5 to have the lowest activation energy when compared to other systems studied.

Apart from MgH_2, the effect of NbF_5 on the composite mixture of $2LiBH_4 + MgH_2$ which shows excellent hydrogen capacity but sluggish kinetics was also investigated and compared to Nb_2O_5 and Mg_2Ni. NbF_5 also proved to be a better catalyst in improving the hydrogen desorption temperature and kinetics of the composite mixture. Modeling studies indicated that chemical reaction at the phase boundary was the most likely process controlling the reaction rates of the catalyzed mixtures.

TABLE OF CONTENTS

LIST OF TABLES

LIST OF FIGURES

1.0 INTRODUCTION

The vision for world's sustainable energy is centered on reducing global carbon dioxide (CO_2) emissions caused by human activities, improve local air quality, ensure security of energy supply and create a new industrial and technological energy base which is very crucial for economic security [1]. Hydrogen has the potential to revolutionize transportation and our entire energy system. It has attracted worldwide interest as an energy carrier in the last decade and this has lead to comprehensive research and investigations on the science and technology involved and how to solve the problems of production, storage and applications of hydrogen [2]. The interest in hydrogen as the energy of the future is due to it being a clean energy, the most abundant element in the universe, the lightest fuel and richest in energy per unit mass [2]. Hydrogen is an attractive alternative to carbon-based fuels and part of its attraction is that it can be produced from diverse resources, both renewable (hydro, wind, solar, biomass, geothermal) and non-renewable (coal, natural gas, nuclear) [1]. Hydrogen can be utilized to provide clean electricity, run factories and hydrogen villages, cater for all our domestic energy requirements and high-efficiency power generation systems, including fuel cells for both vehicular transportation and distributed electricity generation [1, 2]. The fuel cells convert hydrogen directly into electricity using a low-temperature electrochemical process [1]. Producing hydrogen and using it in fuel cell vehicles holds the promise of virtually pollution-free transportation and independence from imported petroleum [3]. However, before hydrogen can become a significant fuel in the U.S. energy picture, many new systems must be built to produce hydrogen efficiently and to store and move it safely. Many miles of new pipelines will have to be constructed and consumers will have

to be educated on how to use it [4]. Infrastructures that will deliver hydrogen from where it's produced to the point of end-use, such as a dispenser at a refueling station or stationary power site have to be put in place. Such infrastructure includes not only pipelines but trucks, storage facilities, compressors and dispensers involved in the process of fuel delivery [5]. With advancements in hydrogen and fuel cell technologies, hydrogen as an energy carrier has the potential to provide a large amount of clean and renewable energy in the near future [4].

1.1 OBJECTIVES OF THE U.S. DEPARTMENT OF ENERGY

The goal of the U.S. Department of Energy Hydrogen Program for hydrogen fuel is to produce ten percent of our energy consumption by year 2030. The activities of the Department of Energy's hydrogen storage research and development are aimed at increasing the gravimetric and volumetric energy density and reducing the cost of hydrogen storage systems for transportation [6]. The proposed material must have the ability to carry enough hydrogen on-board a vehicle to enable a driving range of greater than 300 miles within packaging, cost constraints and preferably at low pressure. According to the long-term vision for hydrogen-storage applications published by the U.S. Department of Energy, the minimum hydrogen-storage capacity should be 6.5 wt% and 65 g/L hydrogen available at decomposition temperature between 60 and 120 ^{o}C for commercial viability. Other targets of the U.S. Department of Energy include; lowering the cost of manufacturing the fuel cells to be competitive with internal combustion engines while keeping toxicity, safety, permeation and leakage at a level required meeting the federal applicable standard [7].

1.2 THE NATIONAL HYDROGEN STORAGE PROJECT

The National Hydrogen Storage Project is made up of three centers of excellence as well as independent projects in applied and basic research and development. This is as a result of President Bush's Hydrogen Fuel Initiative announced in 2003, which pledged $1.2 billion to accelerate hydrogen research. The result of this research and development effort will be the development of hydrogen storage systems capable of meeting the 2015 Department of Energy's performance targets [8]. These centers of excellence involved multidisciplinary teams of multiple academic, industrial and federal laboratory partners. The Metal Hydride Center focuses on the development of advanced metal hydrides including lightweight advanced complex hydrides, destabilized binary hydrides, intermetallic hydrides, modified lithium amides and other on-board reversible hydrides. The Center on Chemical Hydrogen Storage focuses on storing hydrogen in covalent chemical bonds where hydrogen can be released via on-board chemical reactions of molecular system such as borohydride-water, dehydrogenation of boron hydrides such as amine boranes and polyhedral boranes, and investigations of non-boron-based materials including organics and nanoparticles. The Carbon Center focuses on breakthrough concepts for storing hydrogen in high surface area sorbents such as hybrid carbon nanotubes, aerogels, and nanofibers, as well as metal-organic frameworks and conducting polymers [8].

The National Hydrogen Storage Project also involves independent projects on new hydrogen storage materials and concepts, materials testing and system and life cycle analyses. Examples being studied include nanostructured metal hydrides and absorbent

materials, amine borane complexes, clathrates, lithium nitrides, and activation processes for enhanced storage [8].

1.3 HYDROGEN BENEFITS

Hydrogen holds promise for economic growth in both the stationary and transportation energy sector. Its application spans from energy, to transportation and manufacturing industries with even greater number of benefits which includes:

Public Health and Environmentally Friendly:

About half of the U.S population lives in areas where air pollution levels are high enough to impact public health and the environment negatively. The emissions from gasoline and diesel-powered vehicles such as nitrogen oxides, hydrocarbons and particulate matter are major sources of air pollution [9]. Hydrogen –powered fuel cell vehicles don't emit any of these harmful substances [9]. When combusted, hydrogen's only products are heat and water. The emission is free from carbon dioxide (CO_2), which is the largest contributing factor to global warming. By not producing carbon dioxide, hydrogen provides an environmentally friendly source of energy, which makes it far more favorable than fossil fuels [10]. The public health and environmental benefits are even greater when the hydrogen is produced from low or zero-emission sources such as wind, solar, nuclear energy and fossil fuels with advanced emission controls and carbon sequestration. Since the transportation sector accounts for one-third of U.S. carbon dioxide emissions, producing hydrogen for transportation from these sources can slash greenhouse gas emissions [9].

Renewable and Reliable:

Hydrogen is a renewable carrier of energy which can be produced from replenishable resources. Ninety three percent of the total energy we use today comes from non-renewable resources which are in limited supply and rapidly depleting. By using hydrogen, power generation from renewable resources will increase significantly. Hydrogen is a reliable carrier of energy in a number of ways. It provides an uninterrupted supply of power and responds to increasing energy demands and environmental standards. It is globally sustainable and can be made from renewable resources, making it a reliable energy carrier for current and future needs [9, 11].

Energy Security:

The United States imports about half of its petroleum, two-thirds of which is used to fuel vehicles in the form of gasoline and diesel. With most of the worldwide petroleum reserves located in politically volatile countries, the United States is vulnerable to supply disruptions. Hydrogen can be domestically produced from resources like natural gas, coal, solar energy, wind and biomass. When used to power highly efficient fuel cell vehicles, hydrogen holds the promise of offsetting petroleum currently being imported for transportation use [9].

Reduces dependence on fossil fuels:

By using hydrogen as an energy carrier, dependence on fossil fuels, oil import vulnerabilities, energy infrastructures, large scale power stations, national grids and long distance pipelines can be reduced. These large-scale infrastructures can be costly to secure and expensive to manage [10].

Efficient and Creates new economy:

Hydrogen has the highest energy content per unit weight of any known fuel and burns more efficiently than gasoline. Also, its long-term costs, including environmental costs are low. Hydrogen can fuel a new economy worth billions of dollars in revenue and help create jobs that are no longer dependent on oil related fluctuations such as imports and inflation [10].

1.4 CHALLENGES

The principal challenges to improving hydrogen storage technologies relate to increasing their efficiency, size and weight, capacity and ultimately their cost. Durability remains an issue, as does the development of unified international codes and safety standards to facilitate safe deployment of commercial technologies.

Cost and Durability:

The cost of on-board hydrogen storage systems is currently too high, particularly in comparison with conventional storage systems for petroleum fuels. Low-cost materials and components for hydrogen storage systems are needed, as well as low-cost, high-volume manufacturing methods. The durability of some hydrogen storage systems is inadequate. Materials and components are needed that produce hydrogen storage systems with a lifetime in excess of 1500 refueling cycles [12].

Weight and Volume:

The weight and volume of hydrogen storage systems are presently too high, resulting in inadequate vehicle range compared to conventional petroleum fueled vehicles. Materials

and components are needed for all compact, lightweight hydrogen storage systems that allow driving ranges similar to those available today for light-duty vehicle platforms [12].

Efficiency and Refueling time:

Energy efficiency is a challenge for all hydrogen storage approaches. The energy required to get hydrogen in and out of storage is an issue of reversible solid-state materials storage systems. In addition, the energy associated with compression and liquefaction must be factored in when considering compressed and liquid hydrogen storage technologies. Refueling times are currently too long. There is a need to develop hydrogen storage systems with refueling times of less than three minutes, over the lifetime of the system [12].

Codes and Standards:

Applicable codes and standards for hydrogen storage systems and interface technologies, which will facilitate implementation/commercialization and assure safety and public acceptance, have not yet been established. Standard hardware and operating procedures are also required [12].

Public Acceptance:

The hydrogen economy will be a revolutionary change from the world we know today. Education of the general public, training personnel in handling and maintenance of hydrogen system components, adoption of codes and standards, and development of certified procedures and training manuals for fuel cells and safety will foster hydrogen's acceptance as a fuel [12].

1.5 HYDROGEN STORAGE

Hydrogen storage describes the methodologies for storing hydrogen for subsequent use. The methodologies span many approaches, including high pressures, but usually focus on chemical compounds that reversibly release hydrogen upon heating. Hydrogen storage is a topical goal in the development of a hydrogen economy. Today, hydrogen for transportation application is compressed and stored in high pressure metal and composite tanks. Hydrogen is also stored by cooling it to its liquid form and containment in super-insulated tanks [12]. The goal for hydrogen storage is to pack hydrogen as close as possible, i.e. to reach the highest volumetric density by using as little additional materials as possible. Hydrogen storage implies the reduction of an enormous volume of hydrogen gas. At ambient temperature and atmospheric pressure, 1 kg of the gas has a volume of 11 m^3. To increase hydrogen density, work must either be applied to compress the gas, decrease the temperature below the critical temperature, or reduce the repulsion by the interaction of hydrogen with other material [13]. The second important criterion for a hydrogen storage system is the reversibility for uptake and release. Materials that interact with hydrogen as well as inert materials are important. This reversibility criterion excludes all covalent hydrogen-carbon compounds because hydrogen is only released if they are heated to temperatures above 800 ^oC, or if the carbon is oxidized [13]. Hydrogen can be stored in a number of ways, each with specific advantages and disadvantages. The basic method for reversible hydrogen storage with a high volumetric and gravimetric density includes the following:

Metal Hydrides:

Hydrogen reacts with many transition metals and their alloys at elevated temperatures to form hydrides. The electropositive elements such as Sc, Y, lanthanides, actinides and members of the Ti and V groups are the most reactive. The binary hydrides of transition metals are metallic in character and are usually referred to as metallic hydrides. They are very good conductors with a metallic or graphite-like appearance [13]. Depending on the binding energy between metal adsorbents and hydrogen, the storage of hydrogen in molecular and/or atomic form can be achieved. Heat is either absorbed (endothermic) or released (exothermic) during metal-hydrogen interaction. This makes metal hydrides excellent candidates for heat storage systems [14]. A typical metal-hydrogen reaction is stated as:

$$M + \frac{x}{2} H_2 \longrightarrow MH_x \qquad (1)$$

Many of these compounds, (MH_x), show large deviations from ideal stoichiometry (n = 1, 2, 3) and can exist as multiphase systems. The lattice structure is that of a typical metal with hydrogen atoms on the interstitial sites. They are called interstitial hydrides for that reason. This type of structure is limited to the compositions MH, MH_2, and MH_3, with the hydrogen atoms fitting into tetrahedral or octahedral holes in the metal lattice or a combination of the two [13]. Metal hydrides of intermetallic compounds, in the simplest case the ternary system AB_xH_n are particularly interesting because the variation of the elements allows the properties of these hydrides to be tailored. Element A is usually a rare earth or alkaline earth metal and tends to form a stable hydride while element B is often a transition metal that forms only unstable hydrides. Some well defined ratios of

B:A, where x = 0.5, 1, 2, 5, have been found to form hydrides with a hydrogen to metal ratio of up to two [13].

The discovery of hydrogen sorption by intermetallic compounds created great hopes and stimulated research and development efforts worldwide. Alloys derived from $LaNi_5$ show some very promising properties including reversibility, fast kinetics and good cycling life [15]. However, because lanthanum and nickel are heavy elements, the proportion of hydrogen in $LaNi_5H_6$ is below 2 wt% and as such cannot meet the targets for mobile applications. However, for stationary applications such as large hydrogen cylinders in hydrogen productions spots, refueling stations and residential blocks, intermetallic hydrides are very useful because weight is not a problem here [15, 16]. A higher mass density is reachable with light elements such as calcium and magnesium. Mg forms ionic, transparent MgH_2 which contains 7.6 wt% hydrogen. However, its formation from bulk Mg and gaseous hydrogen is very slow and the plateau pressure of 1 atm occurs at temperatures around 300 ^oC [15]. The desorption kinetics of MgH_2 at this temperature is slow. Therefore, temperature in excess of 400 ^oC is needed for faster desorption kinetics [17]. Recent studies on the effects of catalyst on MgH_2 have shown faster desorption and absorption kinetics, lower dehydrogenation temperature and lower activation energy. Other methods to achieve this include high-energy ball milling of Mg and precipitation of Mg from metal organic solutions to obtain micro- or nanostructured Mg [15].

Another approach is by alloying Mg before the hydride formation. Mg_2Ni forms a ternary complex hydride Mg_2NiH_4 which contains 3.6 wt% hydrogen. The hydride forms fairly rapidly owing to the presence of Ni as a catalyst but thermodynamically it still requires a temperature of about 280 ^oC to desorb the hydrogen contained in it. Other Mg alloys that

have been studied include Mg_2Cu, $Mg_{17}La_2$ and MgAl. Although there is a little reduction in the dehydrogenation temperature, this is accompanied by weight penalty. Also reversibility is only attained at high temperatures [15]

Complex Hydrides:

Group 1, 2 and 3 light metals, e.g. Li, Mg, B, and Al give rise to a large variety of metal-hydrogen complexes. They are especially interesting because of their light weight and the number of hydrogen atoms per metal atom, which is two in many cases [13]. Complex hydrides are interesting candidates for hydrogen storage due to their high hydrogen capacity (5-20 wt%) both volumetrically and gravimetrically (e.g., $KAlH_4$: 5.5 wt%, $LiBH_4$: 18 wt%) [14]. In contrast to the interstitial hydrides, where hydrogen sits on and comes out of interstitial sites without affecting the lattice of the host, desorption of hydrogen from complex hydrides lead to complete decomposition of the complex hydride phase. Two types of complex hydrides which are investigated in detail for hydrogen storage are complex borohydrides and complex aluminum hydrides. Upon decomposition, complex hydrides liberate hydrogen through more than two steps and form binary hydride phase. Therefore, part of the storage capacity is usually retained in the form of stable binary light metal hydrides [14].

Complex boron hydrides:

Boron is known to form unstable polymeric hydrides (e.g. $(BH_3)_x$) [18]. The monomer BH_3 is a strong lewis acid which achieves electronic saturation by dimerization [diborane (B_2H_6)]. Boron can also make complex hydride $[BH_4]^-$ through additional charge localization in the boron atom. The H atoms are located at the corners of the tetrahedral

$[BH_4]^-$ where boron coordinates the hydrogen atoms located at the center. Localization of additional charge for the stabilization of the complex boron-hydrogen tetrahedron is usually achieved by charge transfer from alkali or alkaline earth or by few transition metals [19]. A correlation has been found between the electronegativity of the cation and the frequency of the bending and stretching modes of hydrogen in the anion as well as the melting temperature of the complex hydride [20]. The thermodynamic stabilities for a series of metal tetrahydroborates $M[BH_4]_n$ (M=Li, Na, K, Cu, Mg, Zn, Sc, Zr and Hf; n=1-4) has been investigated using first-principle calculations. The results indicated that the bond between $(M_+)^n$ cations and $[BH_4]^-$ anions in $M[BH_4]_n$ is ionic and the charge transfer to $[BH_4]^-$ anions from $(M^+)_n$ cations is responsible for the stability of $M[BH_4]_n$ [21, 22]. The general decomposition reaction of alkali metal tetrahydroborates is stated as:

$$ABH_4 \longrightarrow ABH_2 + H_2 \longrightarrow AH + B + 3/2H_2 \quad (2)$$

For alkaline earth metal tetrahydroborates, the decomposition reaction is

$$E(BH_4)_2 \longrightarrow EH_2 + 2B + 3H_2 \quad (3)$$

To a large extent, the physical properties of the tetrahydroborates are still unknown. They are also less promising candidates than aluminohydrides for hydrogen storage due to their unfavorable thermodynamic properties. However, they are at currently being considered as interesting candidates for hydrogen production due to their high hydrogen capacity [14].

Complex aluminum hydrides:

Reaction of hydrogen with aluminum leads to the formation of the covalently bonded binary hydride called alane (AlH_3). As in the case of complex borohydrides, the 8 electron octet configuration can be achieved by localizing one more electron and a hydrogen atom in the alane [14]. Electropositive elements such as Na, K, Li, Mg, and Ca can be used to localize the additional charge in Al leading to the formation of the $[AlH_4]^-$ complex. As a result, there is ionic bonding between M (Alkali or alkaline earth metal) and AlH_4^- due to the transfer of electrons [23]. $LiAlH_4$ has been investigated for its potential hydrogen storage usage due to its high storage capacity of 10.5 wt%. However, it has not yet been considered for commercial applications because of its irreversible dehydrogenation reactions. Recently, the possibility of reversible hydrogenation in the Li-Al-H system has been reported. An activated mixture of LiH and Al was made using $TiCl_3$ catalyst and the hydrogenation of the mixture was accelerated by Me_2O solvent. Although a capacity of about 6 wt% was reversibly generated with good desorption performances, the capacity was affected by the concentration of the $TiCl_3$ and repeated runs did not seem to provide consistent capacity [24, 25]. When catalysts like Ti, Nb_2O_5 and $NbCl_5$ were employed, the result was not reproducible [14].

The pristine $NaAlH_4$ releases hydrogen above its melting point (183 ^oC) and the desorption kinetics is very slow [14]. The dehydrogenated products recombine to form $NaAlH_4$ only above high pressure hydrogen (>150 atm) at 200 ^oC. Due to these reasons, sodium alanate was not considered a viable candidate for reversible hydrogen storage. The total hydrogen capacity of $NaAlH_4$ is 7.4 wt% and hydrogen liberation occurs by the following reactions:

$$3NaAlH_4 \longrightarrow Na_3AlH_6 + 2Al + 3H_2 \ (3.75 \text{ wt\% at } 170\text{-}230\ ^oC) \quad (4)$$

$$Na_3AlH_6 \longrightarrow 3NaH + Al + \frac{3}{2}H_2 \quad (1.85 \text{ wt\% at } 230\text{-}260\ ^oC) \quad (5)$$

$$3NaH \longrightarrow 3Na + \frac{3}{2}H_2 \ (1.8 \text{ wt\% } > 400\ ^oC) \quad (6)$$

The first and second step reactions takes more than 50 hours for the liberation of about 5 wt% hydrogen at temperatures less than its melting point 183 ^oC [26]. The third step reaction is usually not considered because the desorption temperature 400 ^oC is too high for fuel cell applications. Moreover, the reversibility is only possible under severe reaction conditions. Bogdanovic et al. investigated the thermodynamic effect of metal catalysts such as Ti, Zr, Fe, Mn etc. on $NaAlH_4$ and found Ti to be the most effective catalyst. Other researchers have studied the desorption behavior of $NaAlH_4$ using different catalysts, however still the performance deviated much from the actual thermodynamic data [14]. Recent studies have proven that the hydrogen storage performance of $NaAlH_4$ is particle size dependent [27]. The studies reported that desorption of nano $NaAlH_4$ occurs rapidly at about 50 ^oC. The hydrogen desorption of $NaAlH_4$ with sizes in the range of 2-10 nm occurs at temperatures less than 100 ^oC while sizes in the range of 1-10 µ occurs above 100 ^oC and goes beyond 200 ^oC. The activation energies of $NaAlH_4$ with sizes of 1-10 nm, 19-30 nm and 1-10 µ was observed to be 58, 79 and 116 kJ/mol respectively [27]. This shows that there are still lots of areas to be explored in this system and the possibility of obtaining favorable thermodynamic conditions.

Potassium alanate ($KAlH_4$) is a reversible hydride even in the absence of catalysts. It has a hydrogen storage capacity of 5.7 wt%. Limited studies have been carried out on $KAlH_4$ due to the fact that it is not commercially available. The dehydrogenation reaction of $KAlH_4$ goes through three decomposition reaction steps stated as follows:

$$3KAlH_4 \longrightarrow K_3AlH_6 + 2Al + 3H_2 \quad (7)$$

$$K_3AlH_6 \longrightarrow 3KH + Al + \frac{3}{2}H_2 \quad (8)$$

$$3KH \longrightarrow K + \frac{1}{2}H_2 \quad (9)$$

The first dehydrogenation occurs at about 300 ^oC with the release of 2.9 wt% hydrogen. The second step releases further 1.4 wt% hydrogen at about 340 ^oC and the third step further releases 1.4 wt% hydrogen at 430 ^oC [28]. It has been observed that $TiCl_3$ catalyst reduces the desorption temperature of the first reaction step from 300 to about 250 ^oC with no significant reduction in the second reaction step [29]. Due to these thermodynamic limitations and the low hydrogen capacity, $KAlH_4$ has not been extensively considered for practical hydrogen storage although it is very useful in the synthesis of mixed complex hydrides which show enhanced thermodynamic characteristics for high capacity reversible hydrogen storage [30].

Magnesium alanate ($Mg(AlH_4)_2$) is another high capacity complex hydride that has received considerable attention for onboard hydrogen storage applications [31, 32]. It has a hydrogen capacity of 9.3 wt% but it is not commercially available due to lack of synthesis techniques affordable for bulk scale synthesis of $Mg(AlH_4)_2$. The thermal

dehydrogenation of $Mg(AlH_4)_2$ does not follow the general dehydrogenation reaction of alkali metal alanates where the desorption goes through a hexahydroaluminate phase. The irreversible dehydrogenation reaction proceeds through a two step reaction path as follows:

$$Mg(AlH_4)_2 \longrightarrow MgH_2 + 2Al + 3H_2 \quad (10)$$

$$2Al + MgH_2 \longrightarrow \frac{1}{2}Al_3Mg_2 + \frac{1}{2}Al + H_2 \quad (11)$$

The first step occurs at about 140 ^oC releasing 6.9 wt% hydrogen. The remaining hydrogen gets liberated at about 340 ^oC with the formation of the intermetallic compound Al_3Mg_2. Studies have shown that the desorption kinetics of $Mg(AlH_4)_2$ can be significantly improved by Ti catalyst. However, $Mg(AlH_4)_2$ cannot be regenerated under the studied conditions [31]. Other ways to increase the desorption kinetics and reversibility of $Mg(AlH_4)_2$ has been investigated but were unsuccessful due to thermodynamic reasons [32, 33].

Liquid Hydrogen:

Hydrogen does exist in a liquid state, but only at extremely cold temperatures. Liquid hydrogen is stored in cryogenic tanks at 21.2 K (-253 ^oC) at ambient pressure. The temperature requirements for liquid hydrogen necessitate expending energy to compress and chill the hydrogen into its liquid state. The cooling and compressing process requires energy, resulting in a loss of about 30% of the energy that the liquid hydrogen is storing. The storage tanks are well insulated to preserve temperature and are reinforced to store the liquid hydrogen under pressure [13, 34]. Because of the low critical temperature of

hydrogen (33 K), the liquid form can only be stored in open systems, as no liquid phase can exist above the critical temperature. The pressure in a closed storage system at room temperature could increase to about 10^4 bar [13]. The simplest liquefaction cycle is the Joule-Thompson cycle. The gas is first compressed and then cooled in a heat exchanger, before it passes through a throttle valve where it undergoes an isenthalpic Joule-Thompson expansion, producing some liquid. The cooled gas is separated from the liquid and returned to the compressor via the heat exchanger [35]. The large amount of energy necessary for liquefaction and the continuous boil-off of hydrogen limit the possible use of liquid hydrogen storage systems to applications where the cost of hydrogen is not an issue and the gas is consumed in a short time, e.g. air and space applications [13]. Other options include storing hydrogen as a constituent in other liquids, such as $NaBH_4$ solutions, rechargeable organic liquids, or anhydrous ammonia NH_3 [36]. Borohydride ($NaBH_4$) solutions can be used as a liquid storage medium for hydrogen. The catalytic hydrolysis reaction is:

$$NaBH_4\ (l) + 2H_2O\ (l) \longrightarrow 4H_2\ (g) + NaBO_2\ (s) \quad \text{(Ideal reaction)} \qquad (12)$$

The theoretical maximum hydrogen energy storage density for this reaction is 10.9 wt. % H_2. The main advantage with using $NaBH_4$ solutions is that it allows for safe and controllable onboard generation of hydrogen. The main disadvantage is that the reaction product $NaBO_2$ must be regenerated back to $NaBH_4$ off-board. Although the use of $NaBH_4$ solutions in vehicles may be prohibitively expensive, there do exist a few commercial companies that promote the technology (Millennium Cell in the US and MERIT in Japan). The required cost reduction is unlikely because of the unfavorable

thermodynamics. However, $NaBH_4$ solutions may be usable in high-value portable and stationary applications [36].

Some organic liquids can also be used to indirectly store hydrogen in liquid form. The concept can be summarized in three steps. First, an organic liquid is dehydrogenated to produce H_2 gas onboard. Second, the dehydrogenated product is transported from the vehicle tank to a central processing plant, while simultaneously refilling the tank with fresh H_2-rich liquid. Finally, the H_2-depleted liquid needs to be re-hydrogenated, brought back to the starting compound and returned to the filling station. An example of a rechargeable organic liquid process is the dehydrogenation and hydrogenation of methylcyclohexane (C_7H_{14}) and toluene (C_7H_8) [36].

Clathrates and Zeolites:

Another way of storing hydrogen is by encapsulating the gas inside a guest (solid) structure to form a clathrate from which the hydrogen can be released by pressure and temperature swing [37]. A clathrate is a chemical substance consisting of a lattice of one type of molecule trapping and containing a second type of molecule (e.g. methane clathrates, also known as methane hydrates). Reports on hydrogen clathrate hydrates first appear in 1999 prompting extensive investigation on hydrogen clathrates as potential materials for hydrogen storage. Lee et al. [38] have reported that the hydrogen storage capacities in THF-containing binary clathrate hydrates can be increased to about 4 wt% at moderate pressure by tuning their composition to allow the hydrogen guests to enter both the larger and smaller cages, while retaining low-pressure ability. Capturing H_2 in H_2O cages to give clathrate hydrogen hydrate is a breakthrough in the development of

hydrogen storage materials. However, pure H_2 hydrate is only stabilized under high pressure. Hence, storage of hydrogen using clathrates is still an area that needs extensive investigation mainly to stabilize the clathrates under affordable operating conditions [14].

Zeolites are porous aliminosiicate networks usually accommodating a large variety of cations such as Na^+, K^+, Ca^{2+}, Mg^{2+} etc [39]. The positive ions are held loosely and they can readily be exchanged in contact solution. The interest in zeolites as potential hydrogen storage candidates is because the diameter of the cages and the channels can be controlled by exploiting their ion-exchange property to modify the valence state and size of the exchangeable cations [40]. Langmi et al. [40] also reported that zeolites can store about 0.3 wt% of hydrogen and higher hydrogen storage capacities of about 1 wt% can be attained under cryogenic conditions. Although promising, from the capacity and applications point of view zeolites are not yet candidates for hydrogen storage systems.

Carbonaceous nanomaterials (carbon nanotubes, fullerenes etc)

Carbonaceous materials are attractive candidates for hydrogen storage because of a combination of adsorption ability, high specific surface area, pore microstructure, and low-mass density. Despite extensive results available on hydrogen uptake by carbonaceous materials, the actual mechanism of storage still remains a mystery. The interaction may be based on van der Walls attractive forces (physisorption) in which the hydrogen to carbon ratio is limited to less than one hydrogen atom per two carbon atoms or chemisorption with a ratio of two hydrogen atoms per one carbon atom [41, 42, 43].

Carbon nanotubes are microscopic tubes of carbon, two nanometers across, that store hydrogen in microscopic pores on the tubes and within the tube structures. Similar to

metal hydrides in their mechanism for storing and releasing hydrogen, they hold the potential to store a significant volume of hydrogen [12]. Dillon et al. presented the first report on hydrogen storage in carbon nanotubes and triggered a worldwide tide of research on carbonaceous materials. Hydrogen can be physically adsorbed on activated carbon and be "packed" on the surface and inside the carbon structure more densely than if it has just been compressed [44]. The best result achieved with carbon nanotubes to date confirmed by the National Renewable Energy Laboratory are hydrogen storage density corresponding to about 10% of the nanotubes weight [45]. In present world, carbon nanostructures are not as supreme as complex hydrides or intermetallic hydrides for reversible hydrogen storage. However, they play a dramatic role in energy storage and conversion devices through their excellent performances in electrochemical devices [46]. Metal organic frameworks (MOFs) are crystalline solids that contain multidentate organic ligands connecting metal ions or small metal containing clusters. MOFs have a three dimensional framework that encloses uniform pores which are interconnected forming an ordered network of channels. They are synthesized by a self-assembly process in which different combinations of organic linkers and metal nodules lead to materials having a wide range of varying topologies and pore sizes [47]. Since MOFs have an interpenetrated dynamic framework with high porosity, it is possible to adsorb hydrogen under affordable operating conditions. Since the metal atom attaches surfaces possessing high catalytic activity, the system gets catalyzed and desorbs hydrogen under lower temperatures [48]. An interesting relationship between the surface area of many MOFs and hydrogen uptake capacity has been demonstrated. At moderate pressures in the range of 10-90 atm, storage of about 10 wt% hydrogen is possible using MOF having a surface

area in excess of 6000 m^2/g. However, a lower pressure in the range of 1-2 atm does not offer any considerable hydrogen absorption capacity [49]. Although MOFs are gaining considerable attention in hydrogen storage, they are still not yet considered as the preferred materials for applications due to insufficient reversible hydrogen storage behavior under mild operating conditions and also due to their poor micro-structural stability.

Fullerene is a potential hydrogen storage material based on the ability to react with hydrogen via hydrogenation of carbon-carbon double bonds. This theory predicts that a maximum of 60 hydrogen atoms can be attached to both the inside and outside of the fullerene spherical surface. Thus, a stable $C_{60}H_{60}$ isomer can be formed with the theoretical hydrogen content of about 7.7 wt%. Although the fullerene hydride reaction is reversible, it is only possible at very high temperatures, about 823-873 K [50].

Hydrogen can also be stored in glass microspheres of approximately 50 μm diameter. The microspheres can be filled with hydrogen by heating them to increase the glass permeability to hydrogen. A pressure of 25MPa is achieved at room temperature resulting in a storage density of 14% mass fraction and 10 kg H_2/m^3. At 62 MPa, a bed of glass microspheres can store 20 kg H_2/m^3. The release of hydrogen occurs by reheating the spheres to again increase the permeability [50].

Chemical Hydrides:

Chemical hydrides slurries or solutions can be used as hydrogen carriers or storage media. The hydrogen in the hydride is released through a reaction with water. Controlled injection of H_2O during vehicle operation is used to generate hydrogen via hydrolysis

reactions. The liberation of hydrogen is exothermic and does not require waste heat from the vehicle power source. Chemical hydride systems are irreversible and require thermal management and regeneration of the carrier to recharge the hydrogen content. An essential feature of the process is recovery and reuse of spent hydride at a centralized processing plant [12, 36].

1.6 MAGNESIUM HYDRIDE AS A HYDROGEN STORAGE MATERIAL

Magnesium hydride is considered as one of the promising hydrogen storage materials for vehicular application because it has a high gravimetric hydrogen content of 7.6 wt%, high volumetric density of 110 g/l, low cost and it releases hydrogen reversibly via a simple one-step process without any byproduct. It also possesses good-quality functional properties such as heat-resistance, vibration absorbing, reversibility and recyclability. However, it's high thermal stability, low rates of hydrogen absorption/desorption and high reactivity toward air and oxygen are major obstacles to its usefulness for hydrogen storage [51-60]. Thermodynamic properties of the magnesium hydride system have been investigated and the results showed an operating temperature which is too high for practical on-board applications. The high thermodynamic stability of MgH_2 results in relatively high desorption enthalpy, which corresponds to an unfavorable desorption temperature of 300 ^oC at 1 bar H_2 [52, 61]. In the past years, several attempts have been made to improve the hydrogenation/dehydrogenation properties of the MgH_2 system by reducing the particle size, forming binary or ternary magnesium-based metal hydrides and alloying with transition metal elements (e.g. Ti, Ni, Co, V, Mn, Fe and Cr) for their catalytic effect [59, 62, 63] Liang et al. [57] found that these elements had different catalytic effects on the reaction kinetics of the Mg-H system and that the activation

energy for hydrogen desorption from magnesium hydride was drastically reduced. Sohn and Enami [62] reported the loss of hydrogen capacity as a result of adding a transition metal to the system although the dehydrogenation temperature of the mixture was lowered compared to the MgH_2. Consequently, a little amount of these elements or their compounds need to be used to prevent a significant decrease of the hydrogen storage capacity of MgH_2, while improving the reaction kinetics. Huot et al. [64] ball milled a mixture of Mg and Ni under hydrogen atmosphere and found that the presence of Ni reduced the onset temperature for hydrogen desorption from MgH_2 from 440.7 ^oC to 225.4 ^oC. However, the presence of Mg_2Ni slowed the decomposition kinetics of MgH_2. Oelerich et al. [56] investigated the catalytic effect of cheap metal oxide with multiple valence states (e.g. Sc_2O_3, TiO_2, V_2O_5, Cr_2O_3, Mn_2O_3, Fe_3O_4, CuO, Al_2O_3 and SiO_2) on the reaction rates of MgH_2 and found that as little as 0.2 mol% was sufficient to provide fast sorption kinetics. Barkhordarian et al. [65] investigated the efficiency of Nb_2O_5 as a catalyst for the hydrogen sorption reaction of magnesium and how it compares to other metal and oxide catalysts. They found that the catalytic effect of Nb_2O_5 is superior for both the absorption and desorption reactions. Further studies [53] showed that at 250 ^oC, 6 wt% of hydrogen was absorbed in 60 secs and desorbed in 500 secs from a mixture of Mg-H and 0.5 mol% Nb_2O_5. They also found that the activation energy for the desorption reaction varies exponentially with Nb_2O_5 concentration. Luo et al [60] researched the influence of NbF_5 as an additive on the hydrogen sorption kinetics of MgH_2. They found that NbF_5 reduces the desorption temperature of MgH_2 by 64K and the hydrogen sorption capacity and sorption kinetics of the composites were dependent on the amount of NbF_5 added as well as the milling time. They recorded the fastest kinetics using 2 mol% NbF_5.

None of these studies attempted to compare the intrinsic reaction rates of catalyzed MgH_2 using constant pressure thermodynamic forces. This is important because, without constant pressure driving forces, results will vary largely as the conditions change. Goudy et al. first developed this unique method and showed its importance when they studied the kinetics of a series of intermetallic hydrides that were based on of $LaNi_5$ [66]. Since then they have used this method to study the kinetics of other materials such as sodium alanate [67], $CaH_2/LiBH_4$ [68], and $LiNH_2/MgH_2$ [69] systems. To better understand the effect of catalysts on reaction temperature and rates Sabitu et al. [70, 71] studied the thermodynamic effects of TiH_2 and Mg_2Ni additives on the hydrogen storage properties of MgH_2 and compared it's intrinsic dehydriding kinetics when ball milled with TiH_2, Mg_2Ni and Nb_2O_5 using constant pressure thermodynamic driving forces. In other studies, Sabitu and Goudy [72, 73] studied the thermodynamic behaviors of adding NbF_5 and transition metal oxide catalysts to MgH_2 and compare their kinetic behaviors and modeling patterns. The results from these studies will be presented in the results and discussion section.

1.7 LITHIUM BOROHYDRIDE AS A HYDROGEN STORAGE MATERIAL

$LiBH_4$ has attracted considerable attention as a potential hydrogen storage material due to its high gravimetric and volumetric hydrogen capacity [74, 75]. It has a gravimetric capacity of 18.5 wt% and a volumetric hydrogen density of 121 kg/m^3 [74-83]. However, its usage for on-board hydrogen storage application is limited due to both thermodynamic and kinetics deficiencies [80]. For $LiBH_4$ to be a viable hydrogen storage material, it must be have fast kinetics, must be reversible and capable of operating at low temperature and moderate pressure [74, 82]. In the past years, several attempts have been

made to reduce the desorption enthalpy and improve the hydrogenation/dehydrogenation kinetics of the $LiBH_4$ system by alloying with transition metals, oxides, carbon, amides and halides [74, 76, 77, 79, 82]. Most of them have been found to improve the kinetics and thermodynamics of $LiBH_4$ effectively [76]. Modifications using nanoporous carbon scaffolds has been used to enhance the kinetics of $LiBH_4$ [83]. However, this is accompanied by a reduction in the hydrogen storage capacity due to the additional weight of the supporting substrate.

Vajo et al. [84] reported that the addition of MgH_2 to $LiBH_4$ can lower the dehydrogenation enthalpy by 25 kJ/mol H_2.

$$2LiBH_4 + MgH_2 \longrightarrow 2LiH + MgB_2 + 4H_2 \quad (13)$$

Other studies have shown that hydrogen release does not proceed directly according to reaction 13, but with an intermediate reaction step [75, 77]. This slow intermediate step made it possible to destabilize reaction 13 thermodynamically but not kinetically [77]. Vajo et al. [84, 85] reported several catalysts such as $TiCl_3$, VCl_3, $NiCl_2$ and TiF_3 that have been added to the $LiBH_4$-MgH_2 system to improve the reaction kinetics. Fan et al. [82] doped Nb_2O_5 into $LiBH_4$-MgH_2 composite to form a more destabilized and reversible composite system and found that Nb_2O_5 decreases the activation energy of the $LiBH_4$-MgH_2 composite. In terms of kinetics, at 400 ^oC the addition of Nb_2O_5 significantly improved the dehydrogenation/hydrogenation kinetics due to the formation of NbH_2 which facilitates hydrogen diffusion.

Xia et al. [76] reported that the hydrogen storage properties of $LiBH_4$-MgH_2 composite were enhanced by the catalytic effect of $MoCl_3$. Particularly for the sample with molar

ratio of 2:1, the activation energy for hydrogen desorption of the composite mixture with $MoCl_3$ was lower than that of the pure $LiBH_4$-MgH_2 system indicating that the kinetics of the $LiBH_4$-MgH_2 composite was significantly improved by the introduction of Mo. Jiang and Liu [75] reported that the dehydrogenation kinetics of $LiBH_4$-MgH_2 (2:1) was enhanced by hydrogen back pressure and $CuCl_2$ catalyst. They applied hydrogen back pressure to significantly influence the rate at which hydrogen was released from the uncatalyzed and $CuCl_2$-catalyzed composite and found that it significantly improved the dehydrogenation kinetics of the $CuCl_2$-catalyzed mixture. They suggested that the hydrogen back pressure plays a role in the formation of MgB_2 which is the determining factor for the reaction pathway and dehydrogenation kinetics of the $LiBH_4$-MgH_2 (2:1) composite.

Zhou et al. [74] showed that a reactive composite of $LiBH_4$-$_xLa_2Mg_{17}$ was successfully prepared mechanically by reacting $LiBH_4$ with MgH_2 and LaH_3. They reported that the MgH_2 and LaH_3 additives provided a synergetic thermodynamic and kinetic destabilization on the dehydrogenation/hydrogenation of $LiBH_4$. It should be noted that none of these studies attempted to compare the intrinsic reaction rates of the catalyzed $LiBH_4$-MgH_2 composite using constant pressure thermodynamic forces. As explained earlier, without constant pressure driving forces, the conditions for measuring kinetics will differ and it will affect the results greatly. The importance of this unique technique was first demonstrated by Goudy and coworkers when they analyzed the kinetic behavior of a series of $LaNi_5$-based intermetallic hydrides [66, 86, 87].

Sabitu et al. [72] compared the intrinsic dehydriding kinetics of MgH_2 ball milled with TiH_2, Mg_2Ni, Nb_2O_5 and NbF_5 using constant pressure thermodynamic driving forces.

They showed that the reaction rate is in the order $NbF_5 > Nb_2O_5 > Mg_2Ni > TiH_2$. Since these catalysts were effective for MgH_2, Sabitu and Goudy studied the thermodynamic behavior of the $LiBH_4$-MgH_2 (2:1) system after adding Nb_2O_5, Mg_2Ni and also NbF_5 to the mixture. This provided more insight on how catalysts affect reaction temperature and rates. The results from the study will be presented in the results and discussion section.

1.8 GOALS OF THE RESEARCH

The goals for this research are highlighted below:

- Studying the thermodynamic effect of TiH_2 and Mg_2Ni on the hydrogen storage properties of magnesium hydride. The hydrogen sorption behavior of magnesium hydride ball milled with either or mixture of both catalysts was also compared.

- Studying and comparing the dehydrogenation kinetics and modeling of magnesium hydride enhanced with additives such as TiH_2, Mg_2Ni and Nb_2O_5 at constant pressure thermodynamic driving forces. The effect of each catalyst on the activation energy of magnesium hydride was also compared.

- Thermodynamics, dehydrogenation kinetics and modeling studies of magnesium hydride enhanced by NbF_5 catalyst using constant pressure thermodynamic forces. The effect of the catalyst on the activation energy of magnesium hydride was also studied.

- Studying the thermodynamic effect of transition metal oxide catalysts on magnesium hydride and comparing the dehydrogenation kinetics and modeling

using constant pressure thermodynamic forces. The effect of each transition metal oxide catalyst on the activation energy of magnesium hydride was also studied.

- Destabilizing lithium borohydride with magnesium hydride and studying the thermodynamic effect of adding catalyst such as Mg_2Ni, Nb_2O_5 and NbF_5 to the composite. The dehydrogenation kinetics and modeling were also compared using constant pressure thermodynamic forces.

2.0 EXPERIMENTAL DETAILS

2.1 SAMPLE PREPARATIONS

The starting materials used in this research were obtained commercially from the Sigma Aldrich Corporation. They were used as received in powder form without further purification. The MgH_2 powder was hydrogen storage grade and according to the supplier, the total amount of trace metal contaminants in this material was less than 0.1%. All sample handling, weighing and loading were performed in a vacuum atmospheres argon-filled glove box that was capable of achieving less than 1 ppm oxygen and moisture. The glove box was vacuum-cleaned several times using purified argon gas to remove air and moisture.

2.2 SAMPLE PREPARATION VIA BALL MILLING

Prior to analysis, the samples and composite mixtures with and without catalysts were prepared by mechanical milling for up to 10 hours in a SPEX 8000M Mixer/Mill that had an argon-filled stainless steel pot that contained four small stainless steel balls. Before use, the stainless steel sample holder and the balls were washed and dried in the oven for thirty minutes, after which they were removed and cooled to room temperature. They were then transferred to the ante chamber of the glove box. The ante chamber was vacuum cleaned about seven times to remove air and moisture trapped in it during the transfer of the stainless steel holder and balls into it. The ante chamber was opened from the inside of the glove box and the sample holder was placed inside the glove box.
The analytical balance that was in the glove box was tarred and the required amount of each sample was weighed. Approximately 0.96 mol% of magnesium hydride was

weighed and 4 mol% of each catalyst was added. A composite mixture of $2LiBH_4$ + MgH_2 was also prepared with 4 mol% of catalysts. The sample holder was tightly closed to prevent spillage and avoid air or moisture contamination when it's taken out of the glove box. Afterwards, the sample holder was removed from the glove box and transferred to the SPEX 8000M Miller/Mill. It was placed in the clamp jaws of the mixer and the crank was tightened firmly. The small locking tab on the treaded rod was also tightened to prevent the jaws from unclamping while the mixer was shaking. The machine was turned on and the duration of mixing was set at 10 hours for all the samples. After ball milling, the sample holder was returned to the glove box through the process described earlier and the mixed samples or the newly formed product were transferred into clean sample bottles for further analysis. The pictures of the glove box that served as the working station and the SPEX 8000M Mixer/Mill are shown in figures 2a and 2b below.

Figure 2a. Glove box

Figure 2b. SPEX 800M Mixer/Mill

2.3 X-RAY DIFFRACTION ANALYSIS

X-ray powder diffraction analysis was used to determine whether a new phase was formed during the sample ball milling process. A PANalytical X'pert Pro MPD Analytical X-ray Diffractometer Model PW 3040 Pro was used for this analysis and it is shown in figure 2c below. A clean and dry X-ray analysis sample holder was placed in the glove box through the vacuum-cleaned ante chamber on the side of the glove box. The process of cleaning and transferring materials inside the glove box has been described earlier in the sample preparation section. The samples were transferred into the X-ray sample holder and a razor was used to level the samples to ensure an even surface. A thin transparent film was used to cover the sample to prevent exposure to air and moisture when it was out of the glove box and the lid was fastened to hold the thin film

tightly onto the X-ray sample holder. The sample holder was then transferred from the glove box to the PANalytical X'pert Pro X-ray Diffractometer. The sample holder was mounted on the stage and the doors of the instrument were tightly shut. The program for running the X-ray diffraction analysis was started by clicking the X'pert data collector icon on the desktop which prompted the instrument's connection. The analysis took few minutes from start to completion. The result analysis was performed by using the X'pert data viewer software on the desktop which helped in analyzing the ball-milled mixtures and determine whether new phases were formed.

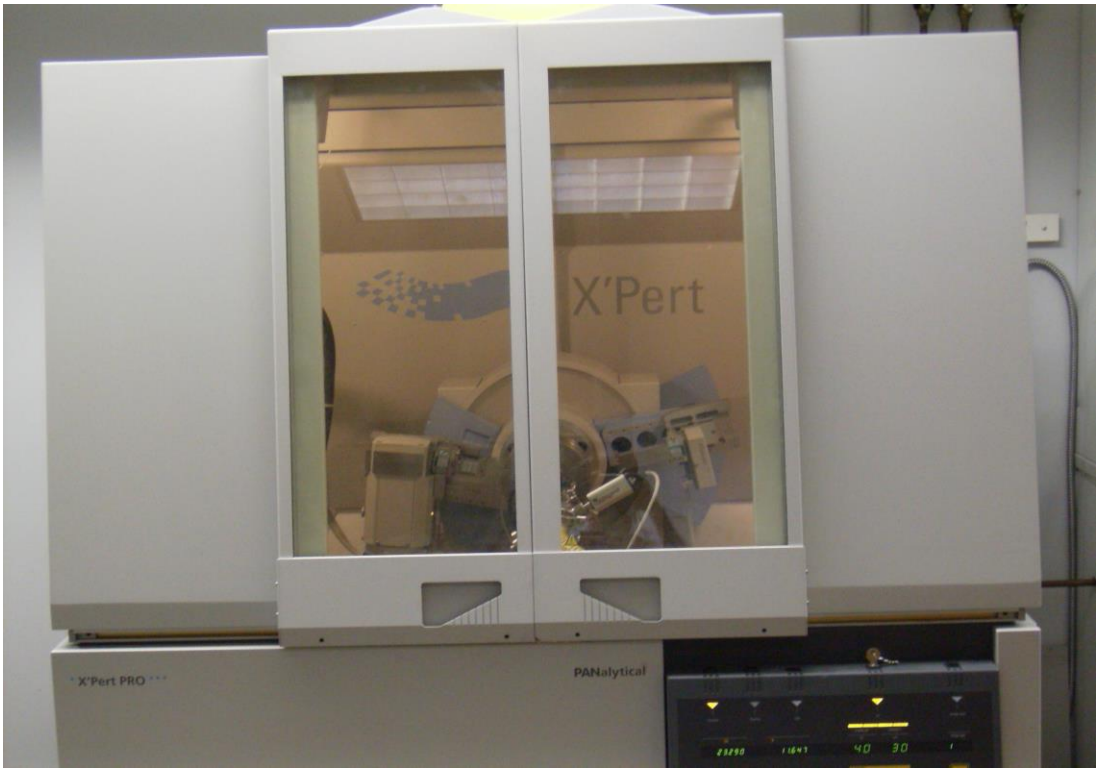

Figure 2c. PANalytical X-ray Diffractometer

2.4 THERMAL GRAVIMETRIC AND DIFFERENTIAL THERMAL ANALYSIS (TG/DTA)

Simultaneous thermal analysis, a combination of Thermal Gravimetric and Differential Thermal Analysis (TG/DTA), was conducted to determine the thermal stability of the mixtures using a Perkin Elmer Diamond TG/DTA shown in figure 4 below. The instrument was placed inside the glove box to prevent sample contamination by air and moisture. It was turned on with the power button and allowed to stand for some minutes until option “linkwait” appeared on the LCD monitor. The pyris program was started and the sample and program information were entered. The sample stage was opened by pushing the open button on the side of the TG/DTA instrument. Two identical pans were located on the two beams covered by the stage. The one to the left was the reference pan while the one on the right served as the sample pan. The two pans were inspected to make sure there were no leftover samples on them. The sample stage was then closed by pushing the close button on the side of the TG/DTA. The weight of the two pans was zeroed. This was repeated three times to ensure equilibration of the weight of the pans. The sample stage was then opened and the sample pan was carefully removed with forceps. A small amount of the sample to be analyzed was put into the pan and carefully placed on the beam. The stage was closed and the weight of the sample was measured by clicking on the weigh icon on the program file displayed on the computer monitor. This was repeated three times to ensure equilibration. The desired heating rate was set and the program was started using the automated program. The picture of the TG/DTA instrument is shown in Fig 2d below.

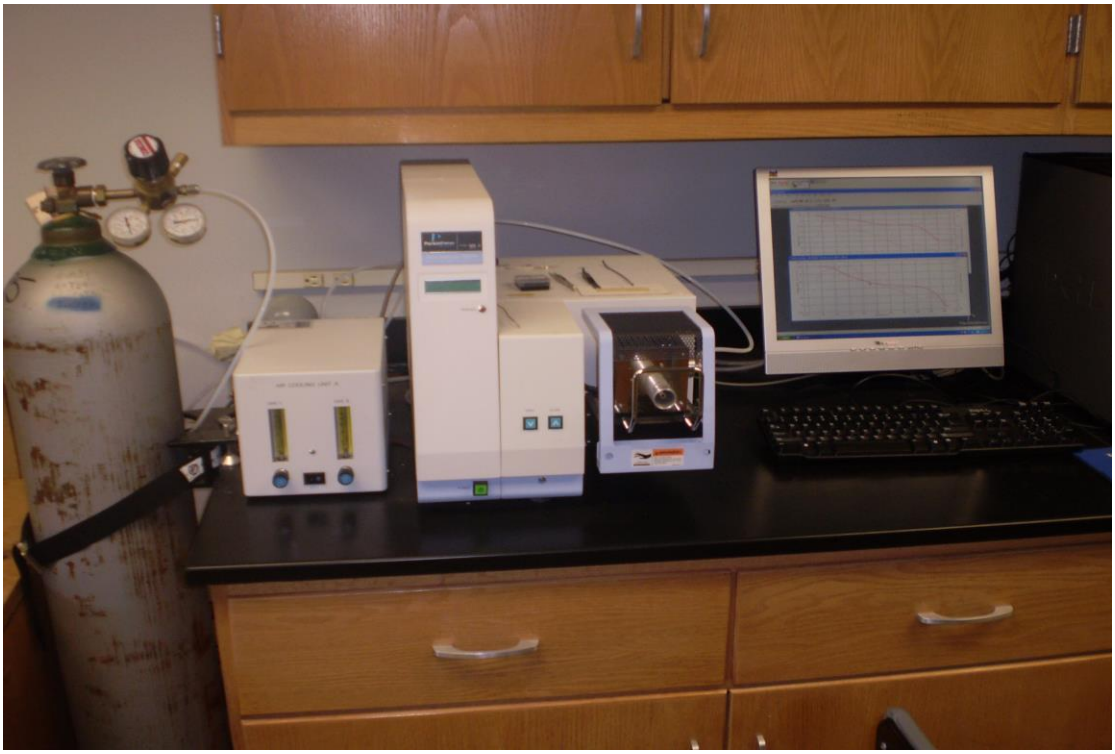

Figure 2d. Thermogravimetric Analyzer

2.5 TEMPERATURE PROGRAMMED DESORPTION (TPD) AND PRESSURE COMPOSITION ISOTHERM (PCI) ANALYSIS

Temperature Programmed Desorption (TPD) and Pressure Composition Isotherm (PCI) analyses were done in a gas reaction controller unit to evaluate the dehydrogenation properties of each sample. This apparatus was manufactured by the Advanced Materials Corporation in Pittsburgh, PA. The unit was fully automated and controlled by a Lab View-based software program. The TPD and PCI analyses were done on freshly ball-milled samples, and no activation procedure was necessary. Before analysis, the sample chamber was detached from the instrument, cleaned and transferred to the glove box where the samples were loaded into it. Approximately 0.6g of each sample was placed inside the sample holder. The chamber was attached to the instrument via a quick connect

fitting. Labview software installed on the computer that was interfaced to the apparatus was used to control the system as well as to collect and analyze the data. The TPD analyses were done in the 30-450 ^{o}C range at a temperature ramp of 4 ^{o}C/min. The PCI absorption and desorption measurements were carried out at temperatures ranging from 350-450 ^{o}C and the plateau pressures determined from the isotherms were used to make van't Hoff plots from which ΔHs were calculated. The apparatus for TPD and PCI analyses is shown in figure 2e below.

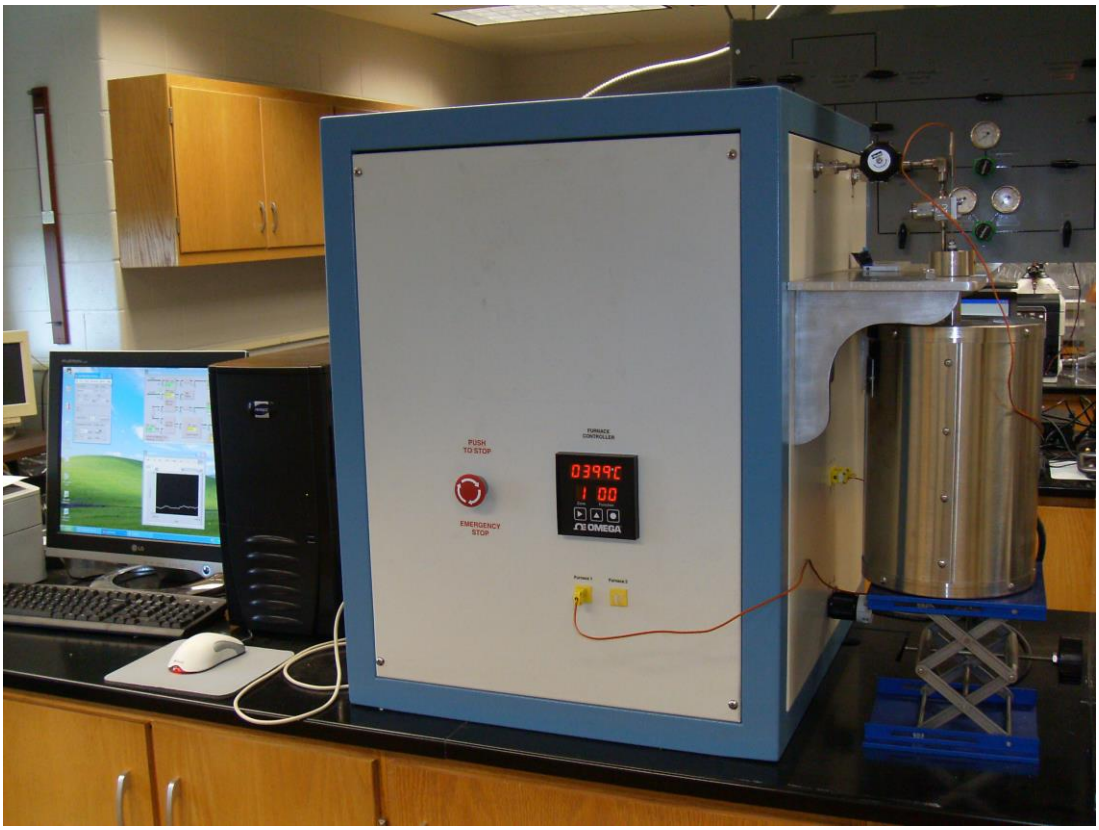

Figure 2e. Pressure Composition Isotherm Automated Hydriding Apparatus

2.6 KINETICS ANALYSIS

Kinetics measurements were done using a Sieverts type apparatus. The experiments were carried out using a method that allowed samples to be compared at the same constant

pressure driving force. The experimental apparatus was made essentially of stainless steel and equipped with ports for adding hydrogen, venting, and evacuating. Pressure regulators were installed to control the hydrogen pressure applied to the sample and to allow hydrogen to flow to and from the sample into a remote reservoir. The back pressure regulator helped to maintain a constant pressure in the sample chamber during desorption analyses. The software used in activating kinetics measurements, controlling it and obtaining data (Daqview) was installed on the computer connected to the Sieverts apparatus. A leak test was conducted before experimental procedure to ensure that all the valves were tightly connected and by so doing prevent pressure leakage. After passing the leak test, desorption kinetics for each sample was conducted. Approximately 2g of each sample mixture was measured and placed inside the sample holder in the glove box to prevent sample contamination. The sample holder was removed from the glove box, placed inside a tube furnace and connected to the kinetics apparatus via a quick connect fitting. Desorption kinetics measurements for MgH_2 with and without catalysts and for the composite mixture of $2LiBH_4 + MgH_2$ with and without catalysts were done 400 ^oC and 450 ^oC. Once the sample holder was attached to the apparatus, the reservoirs were vented and vacuumed for a while. The reservoir valves were then closed so that the pressure inside them would remain in vacuum. The middle valve was closed and a pressure slightly higher than the mid-plateau pressure P_m was set in the sample chamber. An opposing pressure P_{op}, determined from each sample's PCI plateau was set in the remaining system. The ratio of both pressure values (P_m/P_{op}) is defined as the N-value and it is kept constant for all samples measured. The vacuumed reservoir valves were then opened and the Daqview software was set ready to collect data. A low pressure

transducer was used to collect data for opposing pressures lower than or equal to 100 psi while a high pressure transducer was used to collect data for opposing pressures higher than 100. The sample holder was turned on after one minute of starting the experiment and the program was triggered to collect data every 30 seconds. The picture of the kinetics instrument is shown in figure 2f below.

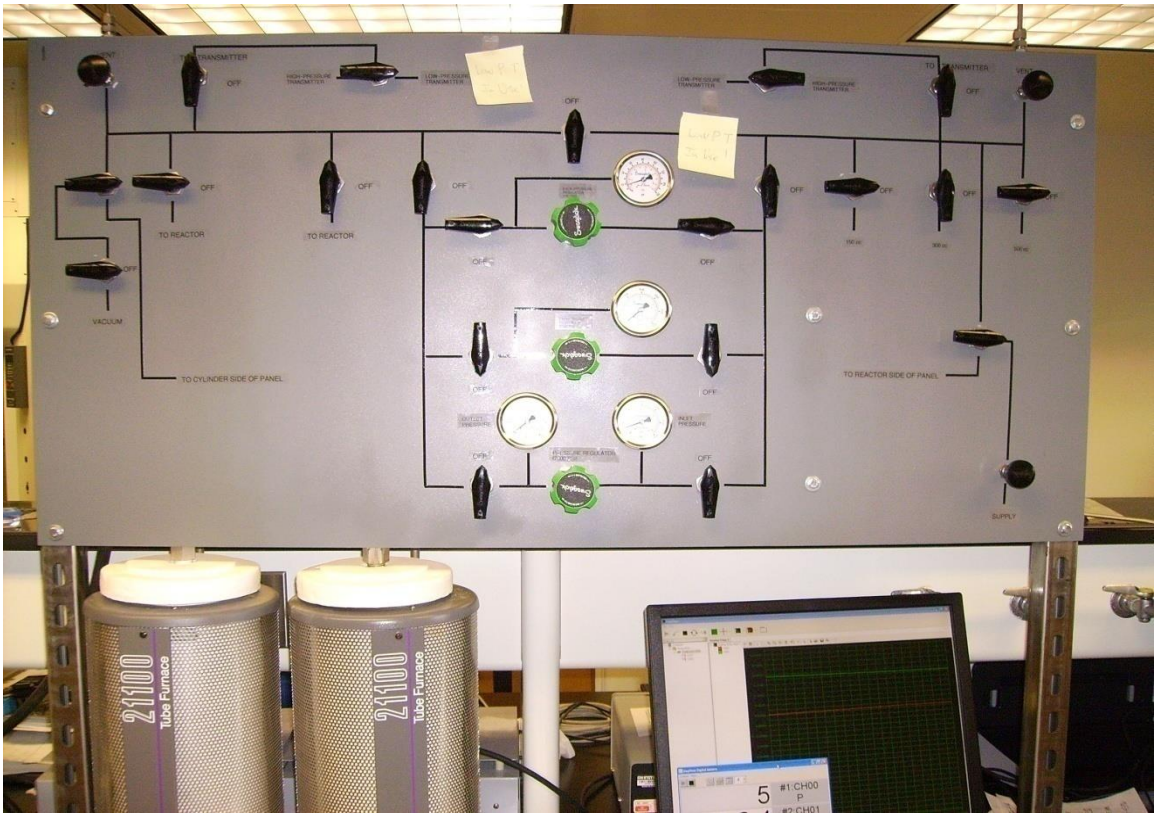

Figure 2f. Sieverts Apparatus

3.0 EFFECT OF TiH_2 AND Mg_2Ni ADDITIVES ON THE HYDROGEN STORAGE PROPERTIES OF MAGNESIUM HYDRIDE

In order to better understand the role that thermodynamic stability has on reaction temperature and rates, a study was done to determine the effect of TiH_2 and Mg_2Ni on the hydrogen sorption behavior of MgH_2. A series of mixtures were made in which MgH_2 was ball milled with various amounts of TiH_2, Mg_2Ni or a combination of both. X-ray diffraction analysis was carried out on a series of MgH_2–TiH_2 mixtures containing different amounts of TiH_2. Temperature Programmed Desorption (TPD) measurements were carried out to determine the effects of the additives on the hydrogen desorption temperature of MgH_2. Pressure Composition Isotherm measurements were done to determine the effect of TiH_2 and Mg_2Ni on the thermodynamic stability and the reaction rate for hydrogen absorption in MgH_2.

3.1 XRD ANALYSIS

A series of MgH_2–TiH_2 mixtures containing various amounts of TiH_2 ranging from 4 to 50 mol% were studied to determine the effect of TiH_2 on the hydrogen sorption properties of MgH_2. After each mixture was ball milled for 10 h, XRD measurements were used to determine if any alloying had taken place. Figure 3a contains XRD patterns for MgH_2, TiH_2 and a mixture containing MgH_2 + 4 mol% ofTiH_2. Scan (c) was done on the mixture before ball milling and scan (d) was done on the same mixture after ball milling. A comparison of the patterns in scans (c) and (d) shows the disappearance and emergence of some of the Mg and Ti reflections between 25^o and 75^o. This indicates that some alloying of the Mg and Ti had most likely taken place. It is also evident that the

diffraction peaks for the major phase, MgH_2, in the ball milled mixture are broader as the result of smaller particle size. This type of behavior was also observed by Shang et al. [89] who did a study on MgH_2 mechanically alloyed with various transition metals. Figure 3b contains XRD patterns for mixtures of MgH_2 with different mole percentages of TiH_2 (i.e. 4, 10, and 50). The diffraction patterns show a progressive decline in the peak intensity corresponding to MgH_2 in the region of 54^o as the mol% of TiH_2 in the mixture increases. There is also the emergence of prominent TiH_2 peaks in the regions of 60^o and 70^o as the amount of TiH_2 in the reaction mixture increases. This is a further indication that a new phase was starting to form.

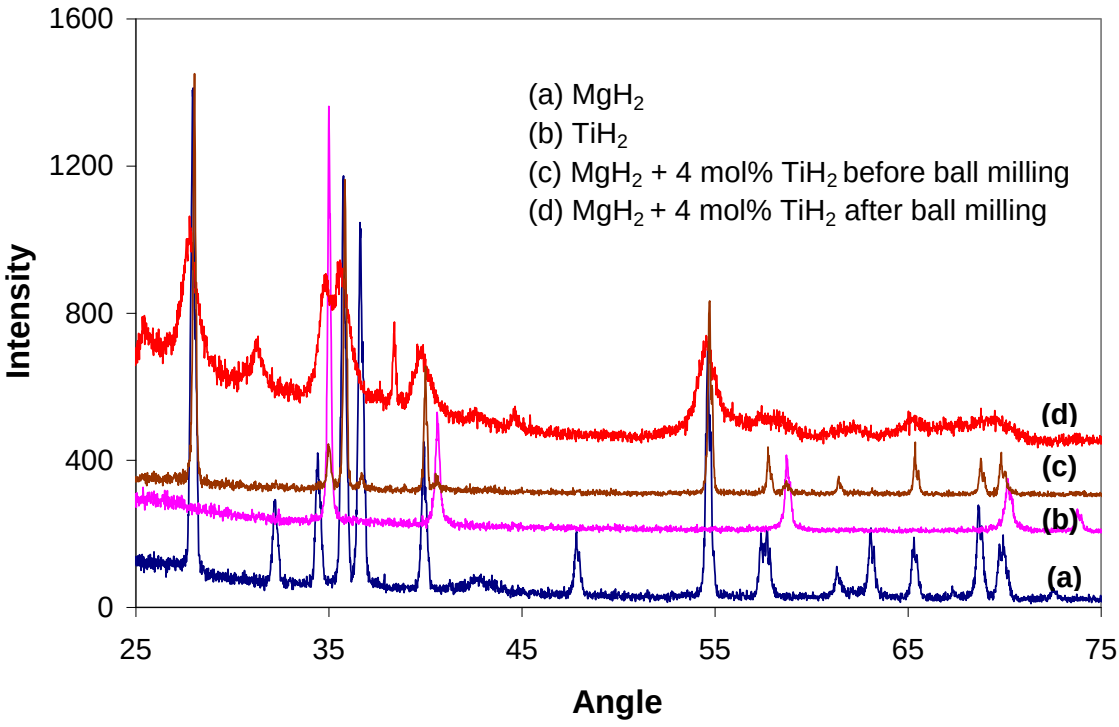

Figure 3a. X-ray diffraction patterns for MgH_2, TiH_2 and MgH_2 + 4 mol% TiH_2.

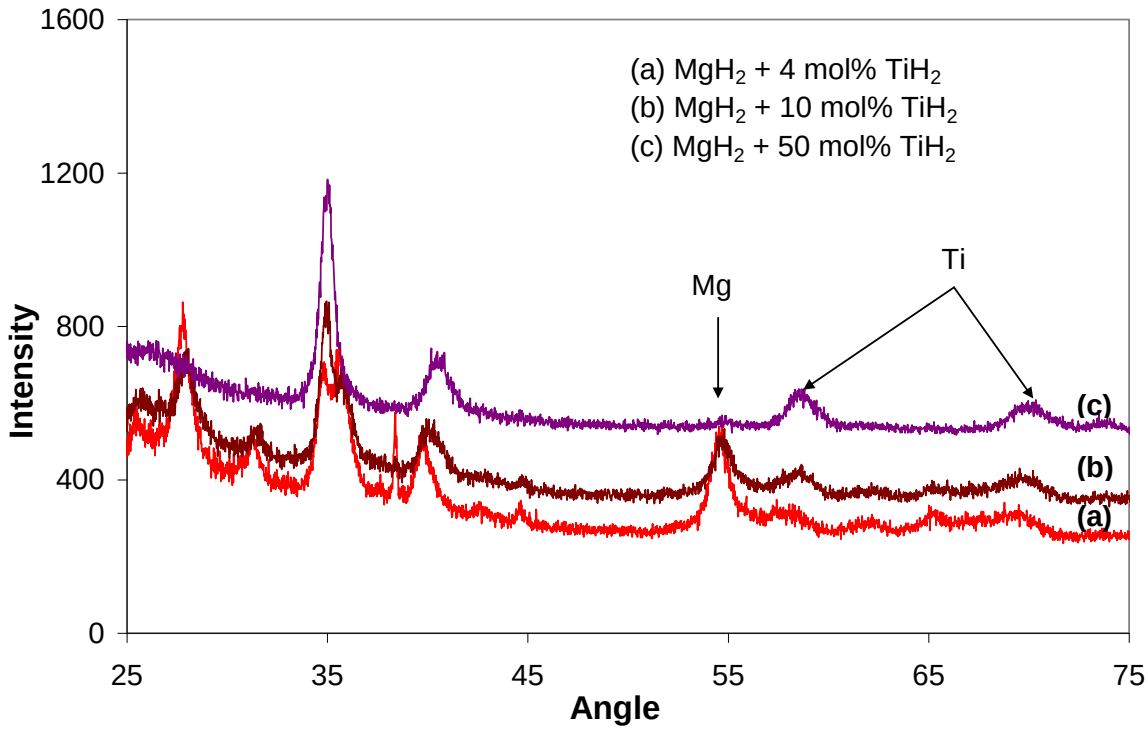

Figure 3b. X-ray diffraction patterns for several MgH_2–TiH_2 mixtures.

3.2 TEMPERATURE PROGRAMMED DESORPTION MEASUREMENTS

Temperature programmed desorption measurements were done on a series of MgH_2 mixtures containing 0, 4, 10, and 50 mol% TiH_2 in order to determine the effect of TiH_2 on the hydrogen desorption properties of MgH_2. The profiles in Figure 3c show the effect of various mole fractions of TiH_2 on the hydrogen desorption temperatures of MgH_2. In the case of pure MgH_2, the onset temperature which is the temperature at which hydrogen is desorbed was about 330 ^oC. This temperature systematically decreased to 250 ^oC as the relative amount of TiH_2 in the mixture increased to 50 mol%. The plots also show that as the mol% of TiH_2 increases the amount of H_2 released decreases from a high of about 7.5

wt% for pure MgH_2 to a low of about 2.4 wt% for the mixture containing 50 mol% TiH_2. This reduction in hydrogen weight percentage is most likely due to the fact that TiH_2 does not release its hydrogen in the temperature range used in this study. Temperatures in excess of the 450 ^oC used in these experiments must be reached before TiH_2 begins to release hydrogen. Thus, there is an increasing weight penalty that occurs as the percentage of TiH_2 in the mixture increases.

Since adding large amounts of TiH_2 to MgH_2 to lower reaction temperatures is accompanied by an excessive weight penalty, it was desirable to test another material to see if similar temperature lowering could be achieved with less weight penalty. Since nickel is known to be a good hydrogenation catalyst, the Ni-containing alloy, Mg_2Ni, was studied to determine if it would be more effective at lowering the reaction temperature. A mixture containing 10 mol% Mg_2Ni in MgH_2 was made by ball milling and the TPD curve is shown in Figure 3d. It can be seen that the onset temperature for the mixture containing 10 mol% Mg_2Ni is 195 ^oC, which is 55 ^oC lower than that for the mixture containing 50 mol% TiH_2, shown in Fig. 3c. Just as importantly, the weight penalty is significantly lower than the mixture containing 50 mol% TiH_2. This mixture releases about 6.3 wt% H_2, which is considerably better than the 2.4 wt% that was observed in the case of the 50 mol% TiH_2 mixture. Based on this, it appears that Mg_2Ni is a more effective catalyst than TiH_2. In order to determine if a combination of both catalysts might yield even better results, another mixture containing 4 mol% TiH_2 and 6 mol% Mg_2Ni, a total of 10 mol% catalyst, was also studied. The curves in Fig. 3d show that the mixed catalyst causes about the same temperature lowering as the mixture containing 10

mol% Mg_2Ni. Thus, in this case, the presence of TiH_2 does not produce any significant improvement in the results.

Since Mg_2Ni has such a large effect on the onset temperature for hydrogen desorption from MgH_2, a TPD profile was done on a sample of pure Mg_2NiH_4 to determine if it might have an even lower onset temperature than the MgH_2–Mg_2Ni mixtures. Surprisingly, the TPD curves in Fig. 3d for hydrogen desorption from the MgH_2–Mg_2Ni mixtures all show a lower onset temperatures than theMg_2NiH_4, which has an onset temperature of 245 ^oC. In addition, since Mg_2NiH_4 releases only 4.45 wt% hydrogen, its hydrogen storage potential is very limited. It is interesting to note that a similar phenomenon was also observed in the MgH_2 mixtures containing TiH_2. The TiH_2 is stable up to temperatures in excess of 500 ^oC. But when it is ball milled with MgH_2, the new phase releases hydrogen at a temperature which is lower than that of either constituent.

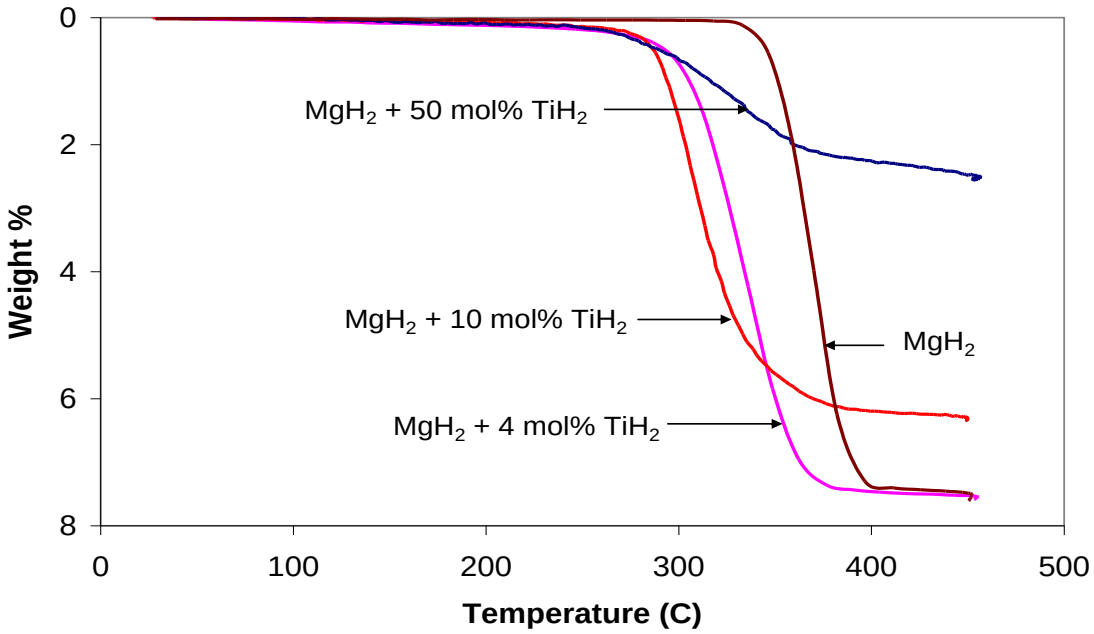

Figure 3c. TPD profiles for MgH_2 and several MgH_2–TiH_2 mixtures.

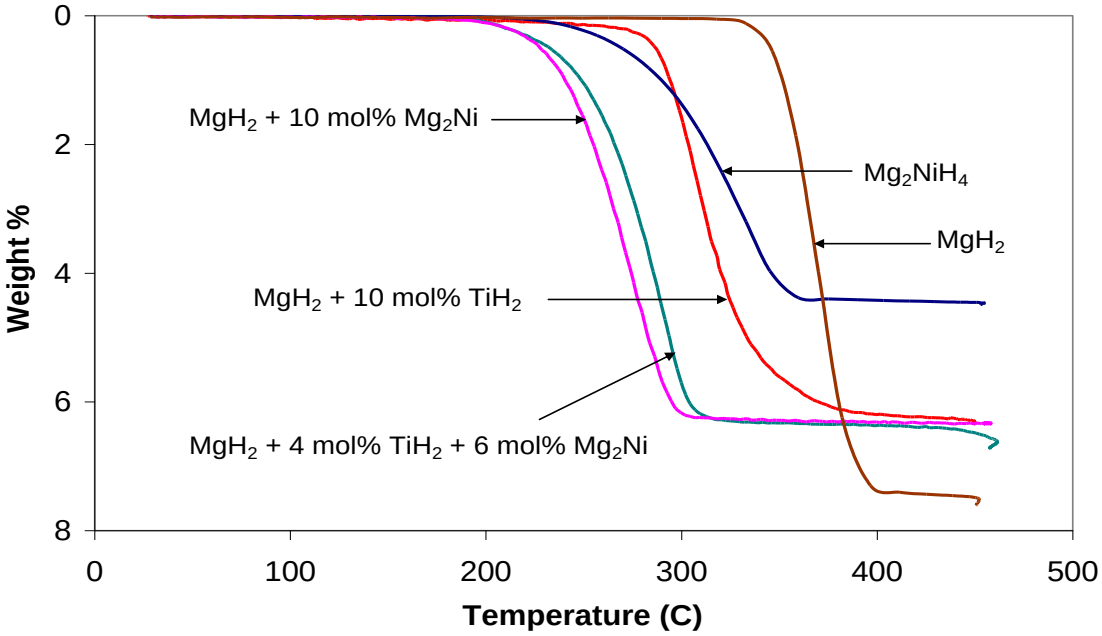

Figure 3d. TPD profiles for pure MgH_2, pure Mg_2NiH_4 and several mixtures containing various amounts of TiH_2 and/or Mg_2Ni.

3.3 PRESSURE COMPOSITION ISOTHERM MEASUREMENTS

Since TiH_2 and Mg_2Ni are both able to lower the reaction temperature of MgH_2, it was also of interest to determine their effect on the thermodynamic stability of MgH_2. Reilly and Wiswall [90] had already established that Mg_2NiH_4 had a lower stability than MgH_2 and thus it was expected that incorporating TiH_2 might produce a similar effect. Pressure-composition-isotherms were constructed for the MgH_2–TiH_2 mixtures shown in Fig. 3c. Figure 3e shows the absorption isotherms for these mixtures at 350 ^oC. It is evident from the curves that the plateau pressure increases with increasing TiH_2 content. It is also evident that the hydrogen-holding capacity decreases as the TiH_2 content increases. This was also observed in the TPD profiles. Pressure composition isotherms were constructed for each mixture at several temperatures and thus it was possible to construct the van't Hoff plots shown in Fig. 3f. The value of ΔH for each mixture could be determined from the slopes of these plots. Table 3a gives the values of ΔH for each mixture. It is evident that the values of ΔH systematically decrease from a high of 76 kJ/mol for pure MgH_2 to a low of 65 kJ/mol for the mixture containing 50 mol% TiH_2. This indicates that the thermodynamic stability of MgH_2 mixtures decreases with increasing TiH_2 content. This finding is somewhat different than that reported by Liang et al. [57]. They studied the catalytic effect of transition metals on hydrogen sorption by MgH_2 and found that the formation enthalpy of MgH_2 was not altered by milling with transition metals. In addition to lowering reaction temperatures, it is also important to have fast reaction rates. Huot et al. [64] reported that adding Mg_2Ni to MgH_2 actually decreases reaction rates. Therefore a series of experiments were done in order to determine the effect of additives on the reaction rates of H_2 with magnesium. Fig. 3g contains plots of reacted fraction versus

time for the uptake of hydrogen by the MgH_2–TiH_2 for mixtures containing 0, 4, 10, and 20 mol% TiH_2. In these experiments the pressure in the reaction chamber was initially set to 100 atm. Then the pressure decrease in the constant volume system was monitored as the sample mixture absorbed hydrogen. It can be seen that reaction rates increase with increasing percentage of TiH_2 in each mixture. The reaction rates of hydrogen in mixtures containing both TiH_2 and Mg_2Ni were also measured. Figure 3h contains the rate curves for mixtures containing 10 mol% TiH_2, 10 mol% Mg_2Ni, or a mixed catalyst containing 4 mol% TiH_2 + 6 mol% Mg_2Ni. From the curves it is evident that the Mg_2Ni is more effective than TiH_2 in increasing reaction rate. This is somewhat different than the findings of Huot et al. [64] who reported a decrease in reaction rates of desorption reactions. It is also evident that the mixed catalyst is more effective than the individual catalysts at increasing reaction rates. This is significant because it indicates that using an appropriate mixture of catalysts is a promising way to make MgH_2 a suitable material for hydrogen storage purposes. These findings are in agreement with those of Lu et al. [91]. They studied the hydrogen storage behavior of MgH_2 mechanically alloyed with Ti and Ni catalysts and found that a combination of Ti and Ni is more effective catalyst for increasing reaction rates than Ti or Ni alone (Table 3b).

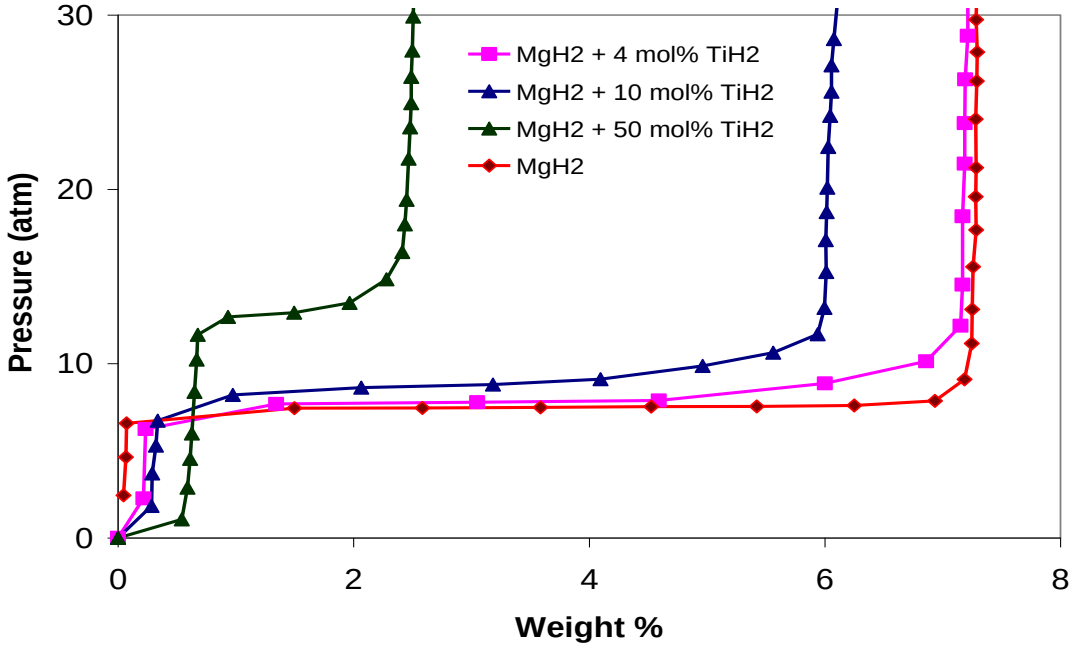

Figure 3e. Absorption isotherms for MgH_2 and several MgH_2–TiH_2 mixtures.

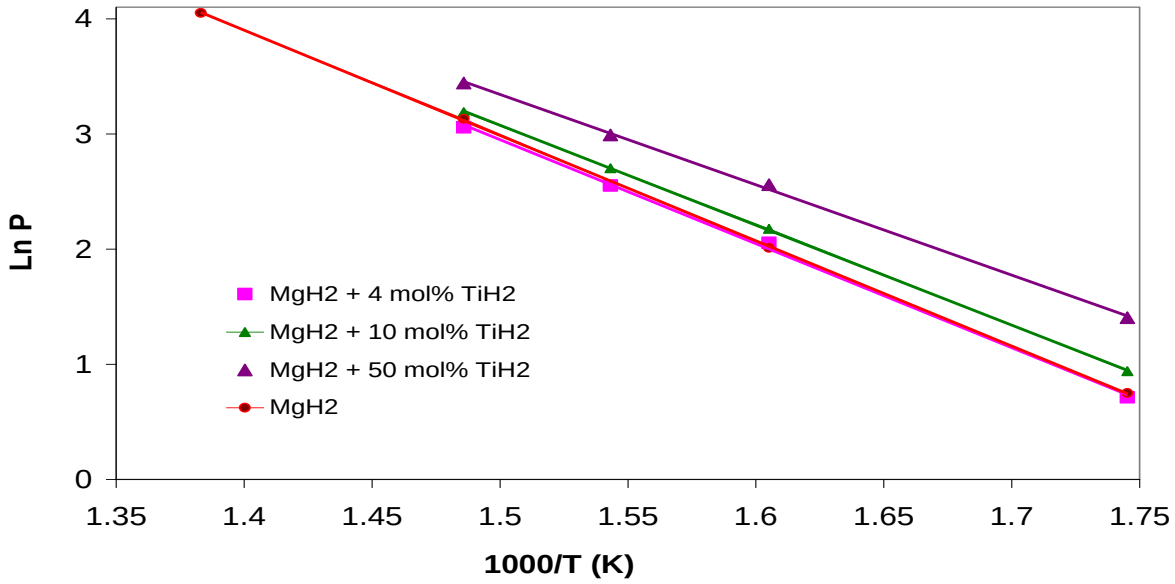

Figure 3f. Van't Hoff absorption plots for MgH_2 and several MgH_2–TiH_2 mixtures.

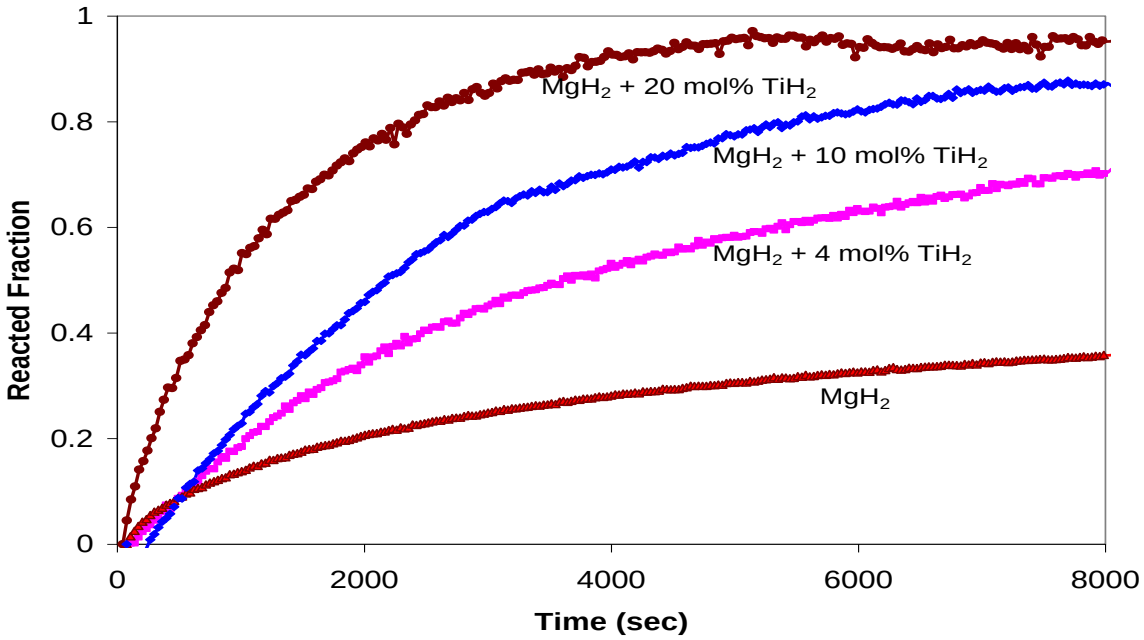

Figure 3g. Reaction rate plots for MgH_2 and several MgH_2–TiH_2 mixtures.

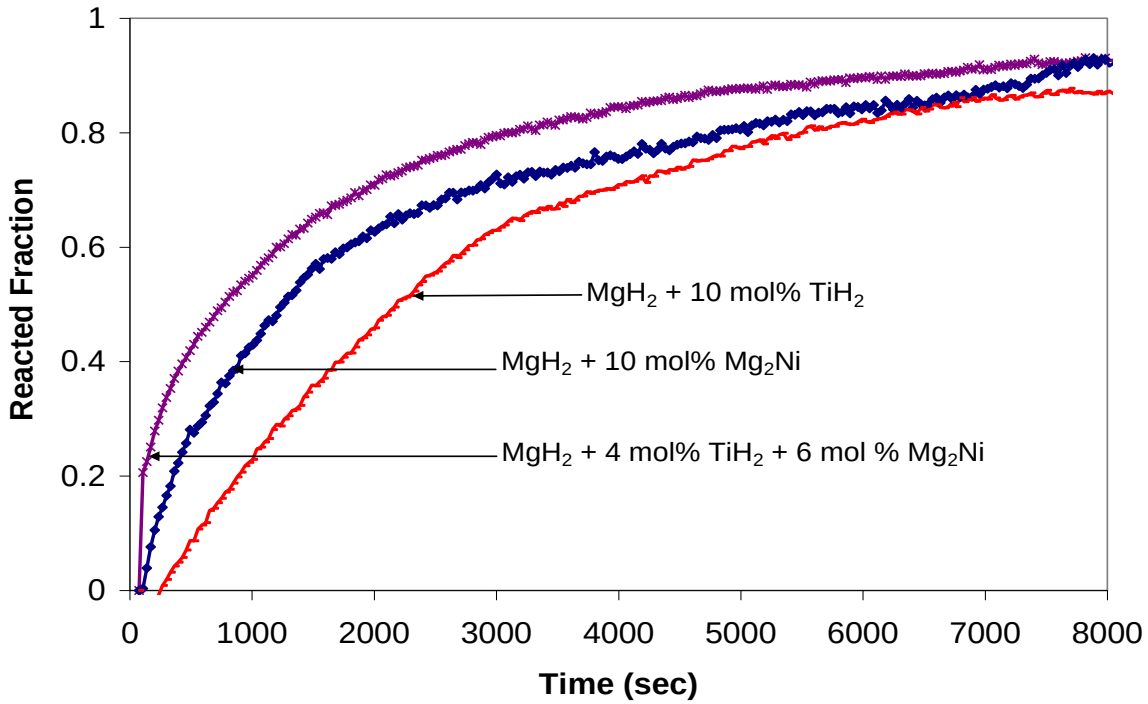

Figure 3h. Reaction rate plots for mixtures containing 90 mol% MgH_2 and 10 mol% of TiH_2, Mg_2Ni or both.

Composition	Onset Temp. (^{o}C)	Wt%	Pm (at 350 ^{o}C)	ΔH (kJ/mol)
MgH_2	346	7.50	7.49	76.0
MgH_2 + 4 mol% TiH_2	276	7.60	7.79	75.1
MgH_2 + 10 mol% TiH_2	265	6.25	8.81	72.2
MgH_2 + 50 mol% TiH_2	250	2.40	12.93	65.2

Table 3a. Thermodynamic parameters obtained for pure MgH_2 and MgH_2–TiH_2 mixtures.

Composition	Reacted Fraction at 1000secs
MgH_2	0.138
MgH_2 + 4 mol% TiH_2	0.185
MgH_2 + 10 mol% TiH_2	0.229
MgH_2 + 20 mol% TiH_2	0.522
MgH_2 + 10 mol% Mg_2Ni	0.430
MgH_2 + 4 mol% TiH_2 + 6 mol% Mg_2Ni	0.551

Table 3b. Reacted fractions obtained for pure MgH_2 and mixtures containing MgH_2, TiH_2, and/or Mg_2Ni after 1000 seconds of reaction time. All reactions were done at 350 ^{o}C.

3.4 CONCLUSION

This research has shown that TiH_2 and Mg_2Ni are both effective catalysts for lowering the reaction temperature of MgH_2 and increasing reaction rates, with Mg_2Ni being the more effective of the two. The research has also shown that a mixed catalyst is better at increasing reaction rates than a single catalyst. This indicates that an optimum amount of two or more catalysts is the most promising way to make MgH_2 a suitable material for hydrogen storage purposes. The research has also demonstrated that the enthalpy for the reaction of hydrogen with MgH_2 decreases with the addition of TiH_2. Thus it appears that the thermodynamic stability and reaction rates can be affected by ball milling MgH_2 with TiH_2.

4.0 KINETICS AND MODELING STUDY OF MAGNESIUM HYDRIDE WITH VARIOUS ADDITIVES AT CONSTANT PRESSURE THERMODYNAMIC DRIVING FORCES.

In this study, an attempt was made to compare the intrinsic dehydriding kinetics of MgH_2 ball milled with various catalysts using constant pressure thermodynamic driving forces. This is a novel procedure in which the ratio of the equilibrium plateau pressure (P_m) to the opposing pressure (P_{op}) was the same in all cases and also to determine the rate-controlling process. MgH_2 was ball milled with 4 mol% of TiH_2, Mg_2Ni or Nb_2O_5 and the effects of each catalyst on the thermodynamics and desorption kinetics of MgH_2 was studied. This will help us better understand the role that catalysts may have on reaction temperature and rates.

4.1 TEMPERATURE PROGRAMMED DESORPTION MEASUREMENTS

Several mixtures were made in which MgH_2 was ball milled with 4 mol% of TiH_2, Nb_2O_5 or Mg_2Ni. After each mixture was ball milled for 10 hours, TPD measurements were done in order to determine the effect of each catalyst on the hydrogen desorption properties of MgH_2. The profiles in Fig. 4a show that pure MgH_2 has the highest onset temperature of about 310 ^oC. The onset temperatures for all the catalyzed mixtures are summarized in Table 4a and are in the order: Pure MgH_2 > TiH_2 > Nb_2O_5 ≥ Mg_2Ni. The plots also show that all of the mixtures released greater than 6 wt% hydrogen except the Nb_2O_5 catalyzed mixture, which released about 5 wt% hydrogen. This lower weight percentage could possibly result from partial oxidation of the Mg in the alloy caused by the presence of oxide in Nb_2O_5.

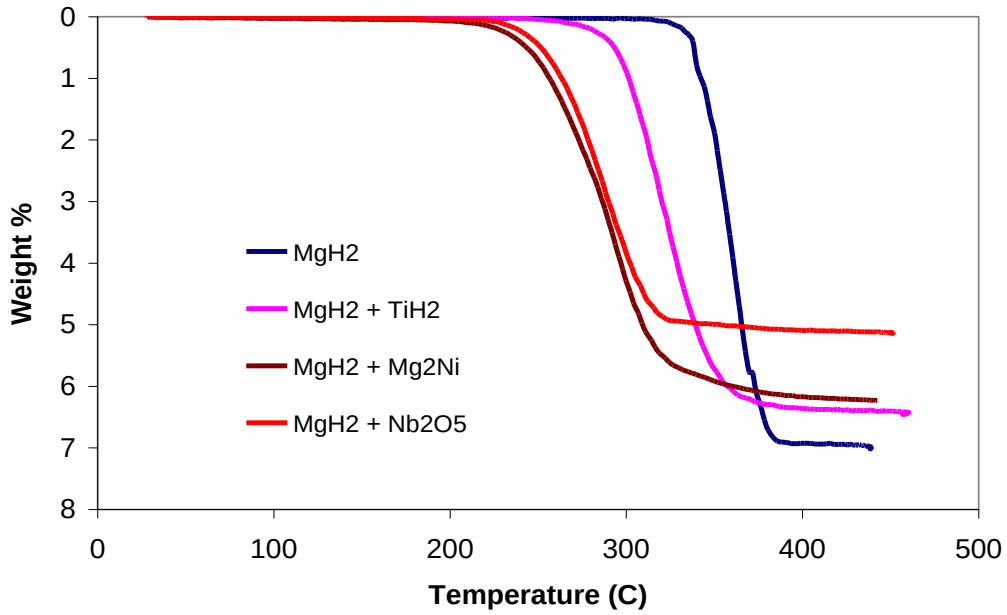

Figure 4a. TPD profiles for catalyzed MgH_2 mixtures.

4.2 KINETICS AND MODELING STUDIES

In addition to lowering reaction temperatures, it is important to have fast reaction rates. Therefore several experiments were done in order to determine the effect of catalyst additives on the hydrogen desorption rates from MgH_2. Fig. 4b contains plots of reacted fraction versus time for the desorption of hydrogen from the MgH_2 mixtures. These desorption measurements were performed using a novel concept of constant pressure thermodynamic driving forces. This was accomplished by first adjusting the hydrogen pressure in the reactor to a value just slightly higher than that of the mid-plateau pressure (P_m), to assure that only the hydrogen rich phase was initially present, and sealing off the reactor. The pressure in the remaining system (P_{op}) was then adjusted to a value such that

the ratio of the mid-plateau pressure to the opposing pressure (P_m/P_{op}) was a small whole number. This small whole number in the remainder of the text is defined as the N-value. In these experiments the N-value, and thus the thermodynamic driving force, was the same in all cases. This represents the first time that this technique has been applied to a kinetic study of the MgH_2 system. The plots show that, under the conditions used, the reaction times are in the order: Pure MgH_2 > TiH_2 > Mg_2Ni > Nb_2O_5. The times required for 90% of the reaction to be completed are also summarized in Table 4a. The rapid kinetics of Nb_2O_5 is in agreement with the results of others [53, 65].

The dehydriding reactions can possibly be described by any of several kinetics models. These include: diffusion, moving boundary and nucleation and growth. To determine which, if any, of these kinetics models describe these reactions it was necessary to construct plots corresponding to the theoretical equations. The theoretical equations are summarized below.

$$(1-f)^{1/3} = 1-\frac{\sqrt{kt}}{R} \qquad (4a)$$

$$(1-f)^{1/3} = 1-\left(\frac{k}{R}\right)t \qquad (4b)$$

$$f = 1-\exp\left(-kt^n\right) \qquad (4c)$$

In these equations, "f" corresponds to the reacted fraction, "k" is a constant, "t" is the time, "R" is the gas constant and "n" is a constant that depends on the geometry of the system. Eq. (4a) corresponds to a diffusion-controlled process; Eq. (4b) depicts a process that is limited by reaction at a moving boundary; and Eq. (4c) represents a nucleation and growth controlled process. If diffusion were controlling the rates then, according to Eq.

(4a), a plot of $(1-f)^{1/3}$ versus time$^{1/2}$ should be linear. The nonlinear plot in Fig. 4e indicates that diffusion does not control the reaction rate. In addition, according to the nucleation and growth model represented by Eq. (4c), a plot of $-\ln(1-f)$ versus t should be linear, assuming that n = 1. The assumption that n = 1 was reached based on a method of comparing the kinetics of solid state reactions that was proposed by Hancock and Sharp [92]. In their method, plots of $-\ln\ln(1-f)$ vs. $\ln(time)$ were used to determine values of "n" in Eq. (4c). Since values in these experiments ranged from 0.7 to 1.6, it was decided that an average value of 1 would be used for the analyses. The plots based upon a nucleation and growth model shown in Fig. 4c have a pronounced curvature, which indicates that the nucleation and growth model is not applicable. That leaves the moving boundary model that is based on equation (4b). When a plot of $(1-f)^{1/3}$ versus $time$ was constructed it was found to be more linear than the other plots. Fig. 4d contains such plots for each of the four systems studied and they are very nearly linear over five half lives. Therefore the moving boundary model is the most plausible mechanism. It should be noted that since reaction at a moving boundary is a bulk process, this indicates that the additives did not merely coat the surface of the hydride particles upon ball milling but rather they were mechanically alloyed into the MgH_2 phase. If the additives had coated the surface then a surface reaction would have controlled the rate and a plot of reacted fraction vs. time would be linear. We did not observe this.

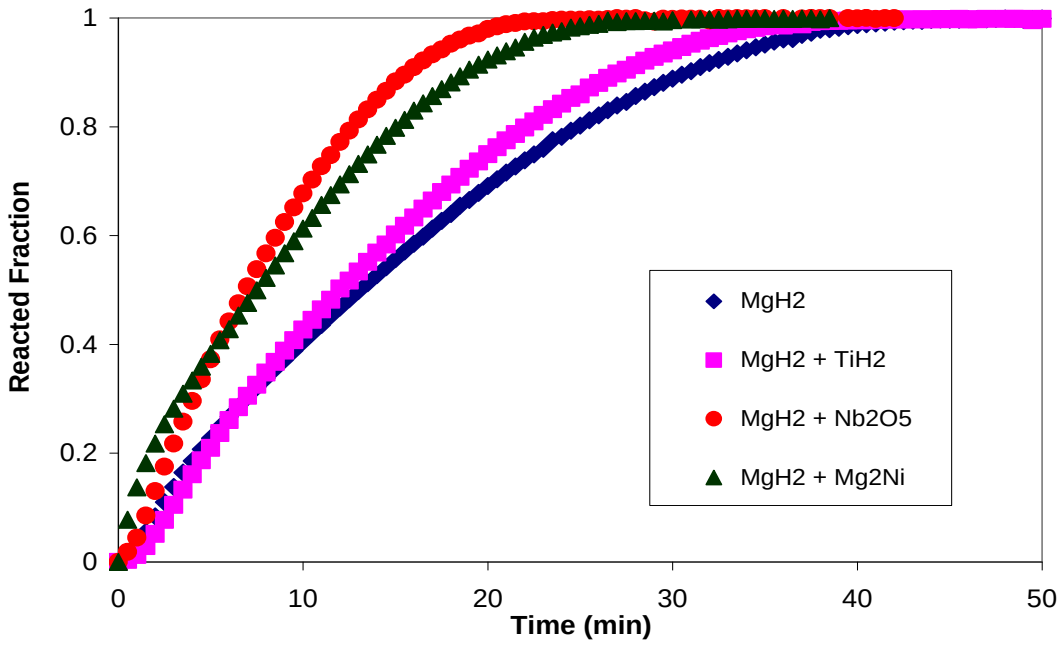

Figure 4b. Desorption kinetics for catalyzed MgH_2 materials at 400 ^oC and N=5.

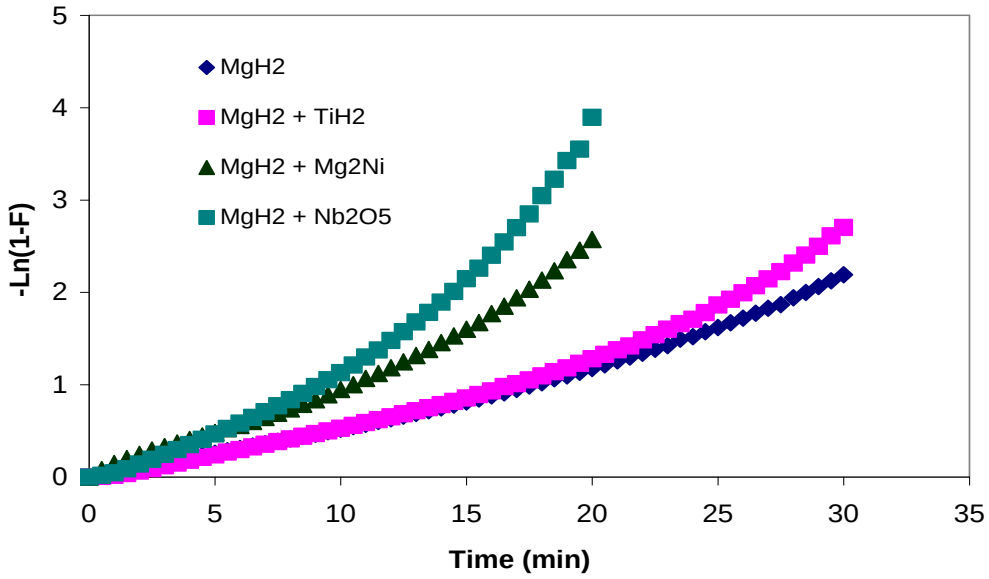

Figure 4c. Modeling for catalyzed MgH_2 materials at 400 ^oC and N=5 using nucleation and growth model.

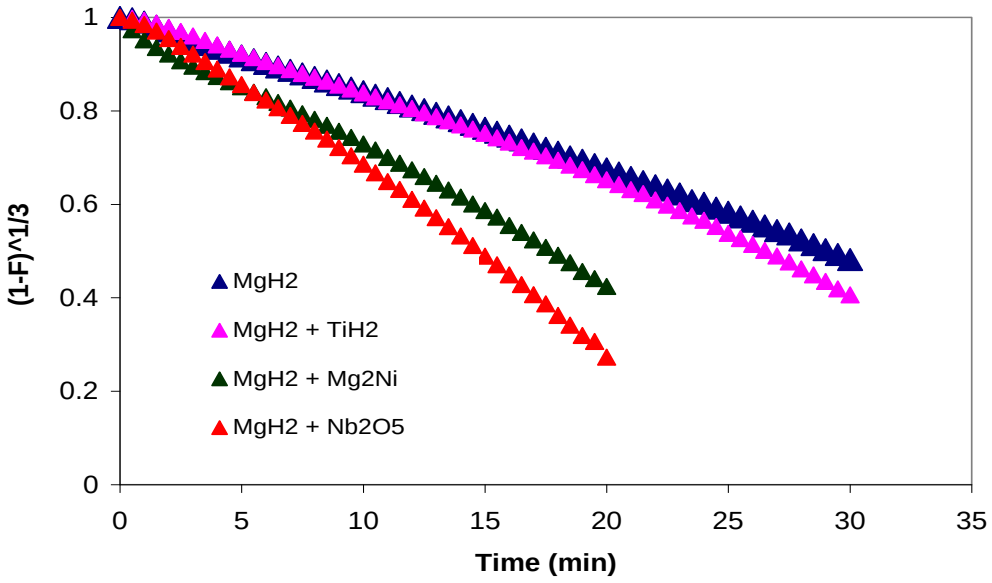

Figure 4d. Modeling for catalyzed MgH_2 materials at 400 ^oC and N=5 using moving boundary model.

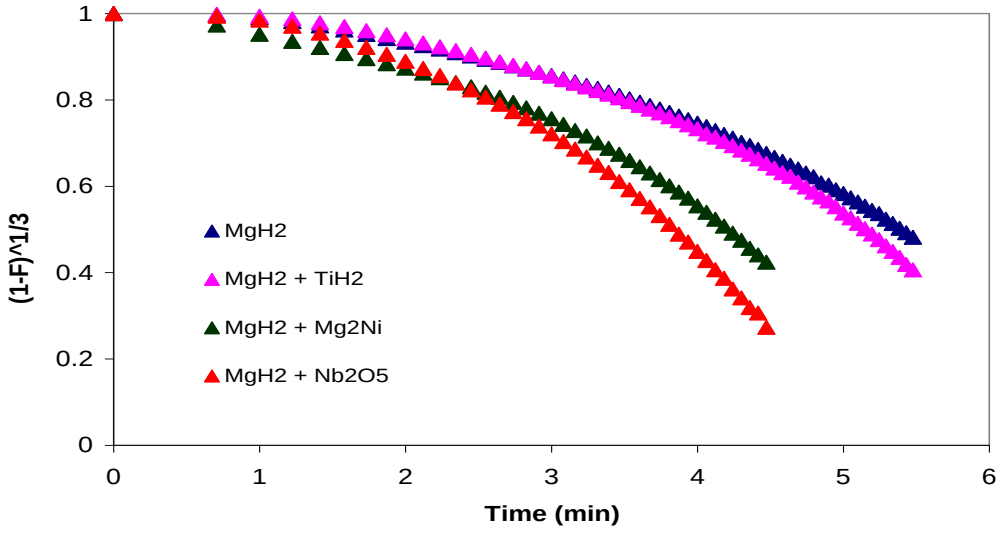

Figure 4e. Modeling for catalyzed MgH_2 materials at 400 ^oC and N=5 using diffusion model.

4.3 DIFFERENTIAL THERMAL ANALYSIS AND KISSINGER PLOTS

To further understand the effects of catalyst additives on the dehydrogenation of MgH_2, the activation energy of dehydrogenation for the samples with different catalysts were investigated using an isoconversion method based on the Kissinger equation [93]:

$$\ln\left(\frac{\beta}{T^2_{\max}}\right) = \frac{E_a}{R}\left(\frac{1}{T_{\max}}\right) + F_{KAS(\alpha)} \quad (4d)$$

Where $T_{\max}$ is the temperature at the maximum reaction rate, β the heating rate, E_a the activation energy, α the fraction of transformation, $F_{KAS(\alpha)}$ a function of the fraction of transformation, and R is the gas constant.

Fig. 4f shows the DTA curves for MgH_2–TiH_2 mixtures. As expected the endothermic peak corresponding to the maximum rate of dehydrogenation shifts to higher temperatures as the heating rate is increased. The same trend was also observed for the samples with Mg_2Ni and Nb_2O_5 additives. The plot based on the Kissinger equation is shown in Fig. 4g. It is seen that good linear relationships between $\ln\left(\frac{\beta}{T^2_{\max}}\right)$ and $\frac{1}{T_{\max}}$ are present for all the samples and that the activation energy of dehydrogenation can be calculated from the slope of the straight lines. The calculated activation energies are summarized in Table 1 and are in the order: Pure MgH_2 > TiH_2 > Mg_2Ni > Nb_2O_5. It should be noted that the desorption kinetics follows the same trend as the activation energies in so far as mixtures with lower activation energies have faster kinetics. A similar trend can be seen in the desorption temperatures. Mixtures with lower activation energies have lower desorption temperatures. However, there is one exception. The mixture containing Mg_2Ni has a slightly lower desorption temperature than the one

containing Nb_2O_5 even though the Nb_2O_5-containing mixture has a faster desorption rate and lower activation energy. The reason for this is not clearly understood at this time but it could simply because their catalytic effects are too close.

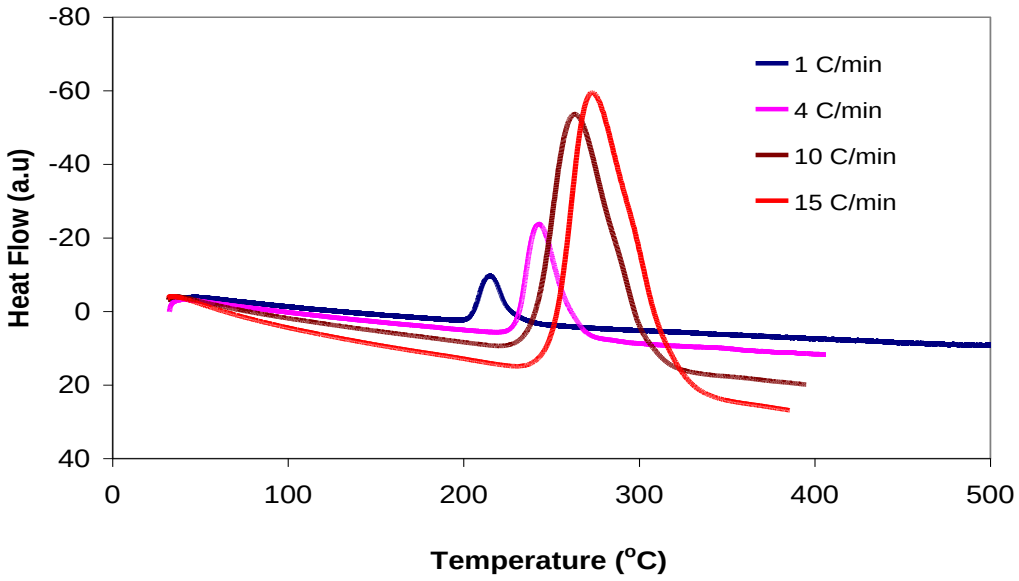

Figure 4f. DTA for MgH_2 catalyzed with TiH_2 done at different scan rates.

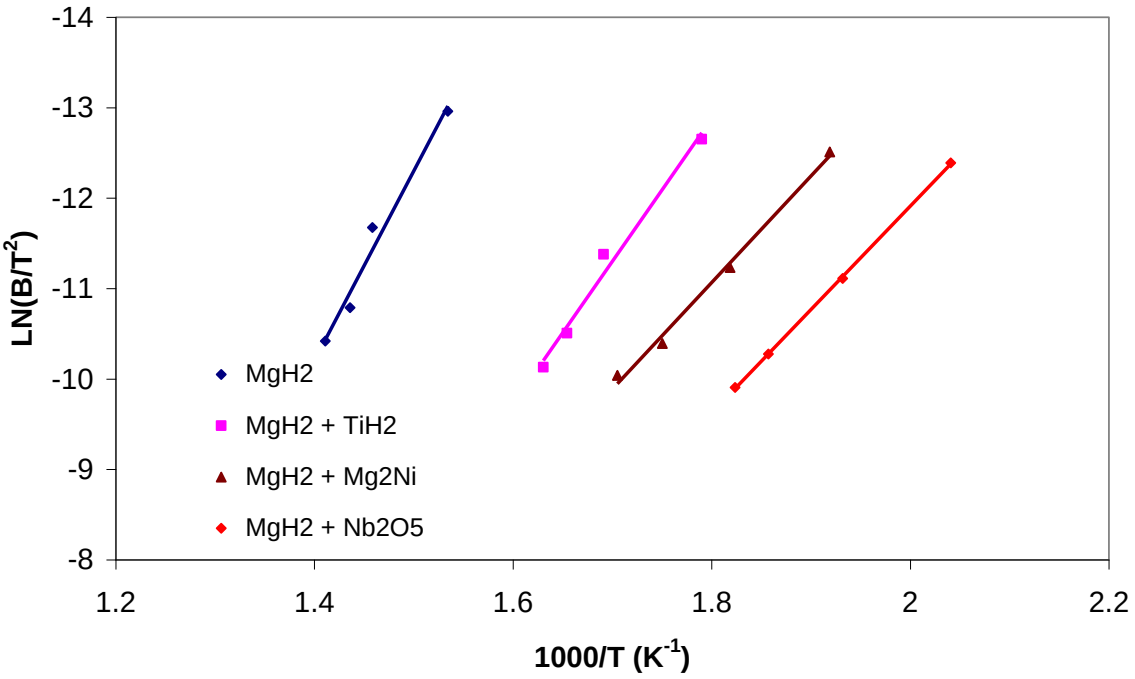

Figure 4g. Kissinger plots for catalyzed MgH_2 materials.

System	Onset Temperature (^oC)	T_{90} (min)	E_a (kJ/mol)
MgH_2	310	32	174
MgH_2 + TiH_2	250	26	131
MgH_2 + Mg_2Ni	190	19	98
MgH_2 + Nb_2O_5	205	16	95

Table 4a. Kinetics and TPD results for some MgH_2-based systems.

4.4 CONCLUSION

This study has shown that it's possible to compare the intrinsic dehydriding rates of MgH_2 mixed with various additives. Since constant pressure driving forces were used, it is evident that the desorption rates are in the order Nb_2O_5 > Mg_2Ni > TiH_2 > pure MgH_2. As expected, the mixtures with the fastest reaction times also had the lowest activation energies. In addition, the mixtures with the fastest reaction times generally had the lowest reaction temperatures. The one exception is that Nb_2O_5 had a slightly higher desorption temperature than Mg_2Ni even though it reacted faster than Mg_2Ni. Modeling studies indicate that reaction at a moving boundary is the most probable rate-controlling process for desorption of hydrogen from MgH_2.

5.0 DEHYDROGENATION KINETICS AND MODELING STUDIES OF MAGNESIUM HYDRIDE ENHANCED BY NIOBIUM (V) FLOURIDE CATALYST USING CONSTANT PRESSURE THERMODYNAMIC FORCES

In this research, the effect of NbF_5 as an additive on the hydrogen desorption kinetics of MgH_2 was investigated and compared to TiH_2, Mg_2Ni and Nb_2O_5 catalysts. The kinetics measurements were done using the method explained in earlier chapters in which the ratio of the equilibrium plateau pressure to the opposing pressure was the same for all the reactions. Two new modeling studies were done to determine the effect of catalysts on the rate-controlling process.

5.1 TEMPERATURE PROGRAMMED DESORPTION MEASUREMENTS

Temperature programmed desorption (TPD) measurements were done on several mixtures of MgH_2 ball milled for 10 hours with 4 mol% of TiH_2,Mg_2Ni,Nb_2O_5 andNbF5. The thermal desorption performance of each sample mixture was carried out to determine how each catalyst affects the hydrogen desorption temperature of MgH_2.The results are shown in Fig. 5a. The curves show that the onset temperatures of the catalyzed mixtures are in the order: Pure MgH_2> TiH_2> Nb_2O_5≥ Mg_2Ni> NbF_5. It can also be seen that not all the samples released the same amount of hydrogen. All of the samples released greater than 6 wt% of hydrogen except the Nb_2O_5 and NbF_5 catalyzed mixtures which released 5 and 4.5 wt% of hydrogen respectively. The reduced hydrogen capacity for MgH_2, in the case of Nb_2O_5, could be caused by the partial oxidation of the Mg due to the presence of oxide in Nb_2O_5 [70]. For NbF_5, the lower hydrogen capacity could be due to the formation of hydrogen fluoride which would reduce the amount of hydrogen available for release. It also seemed likely that the amount of HF production would be proportional to the amount of NbF_5 that was present in the mixture. If this were the case, improved

hydrogen capacity would result by decreasing the amount of NbF_5. To verify this, another sample mixture was prepared with 1 mol% NbF_5.The onset temperature for this mixture was somewhat higher than that of the mixture with 4 mol% NbF_5 and it released about 6.5 wt% hydrogen. This is significantly better than the 4.5 wt% released from the mixture with 4 mol% NbF_5. Also, the difference in the thermal desorption performances between the 1 and 4 mol% NbF_5 catalyzed mixtures agrees with the fact that increase in the amount of catalyst in a reaction mixture results in lower desorption temperatures accompanied by excessive weight penalty [71].

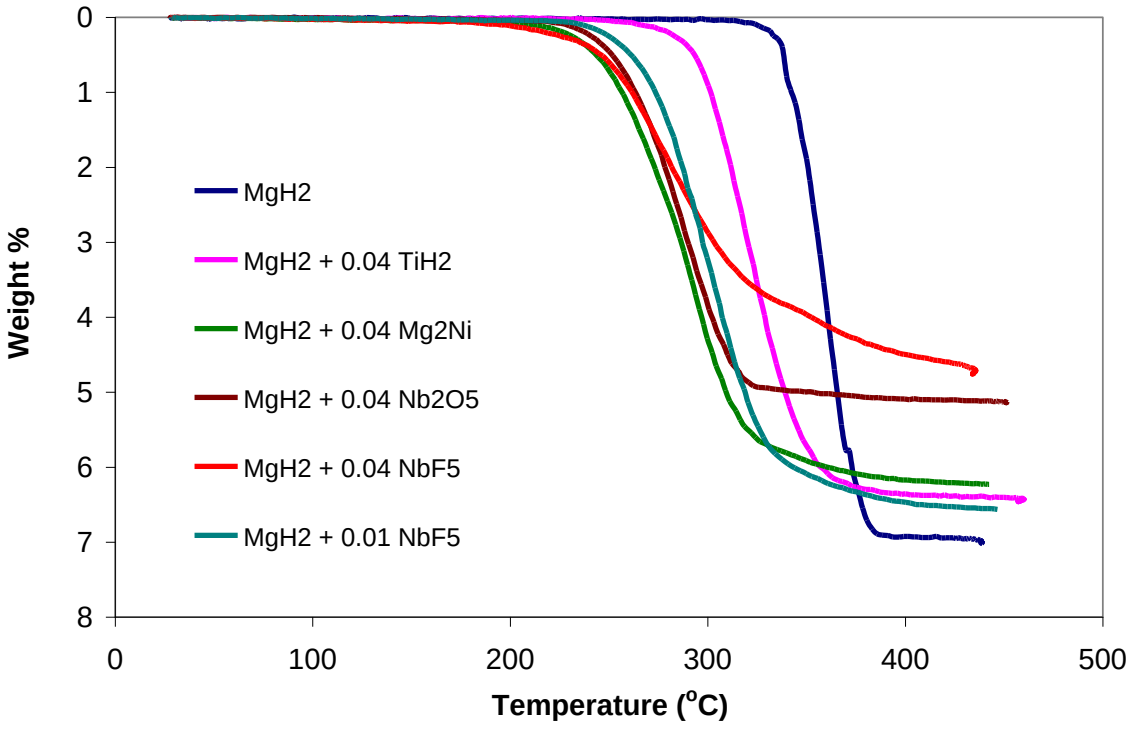

Figure 5a. TPD profiles for MgH_2 and catalyzed MgH_2 materials.

5.2 PRESSURE COMPOSITION ISOTHERM MEASUREMENTS

Pressure composition isotherm (PCI) analyses were done for MgH_2 and the MgH_2 catalyzed reaction mixtures. Fig. 5b shows the desorption isotherms for these samples at 400 ^oC. The results show that the plateau pressure is about the same for all the samples except the MgH_2 + 4 mol% NbF_5 mixture with a lower plateau pressure. The PCIs also show that the mixtures catalyzed by NbF_5 and Nb_2O_5 release considerably less hydrogen than the pure MgH_2 and the TiH_2 catalyzed mixture. This is consistent with the TPD results in Fig. 5a. The PCI results were used to construct the Van't Hoff plots shown in Fig. 5c. Values of ΔH were calculated for each mixture and the results are listed in Table 5a. It is evident from the values obtained for ΔH that the thermodynamic stability of MgH_2 is directly proportional to the onset temperature.

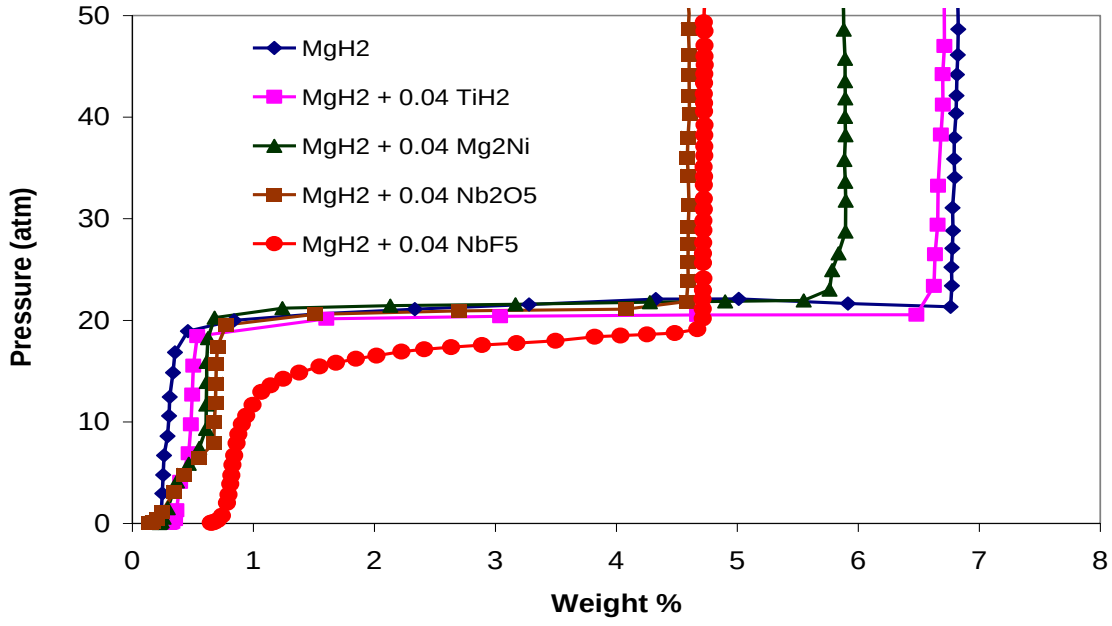

Figure 5b. Desorption isotherms for MgH_2 and catalyzed MgH_2 materials.

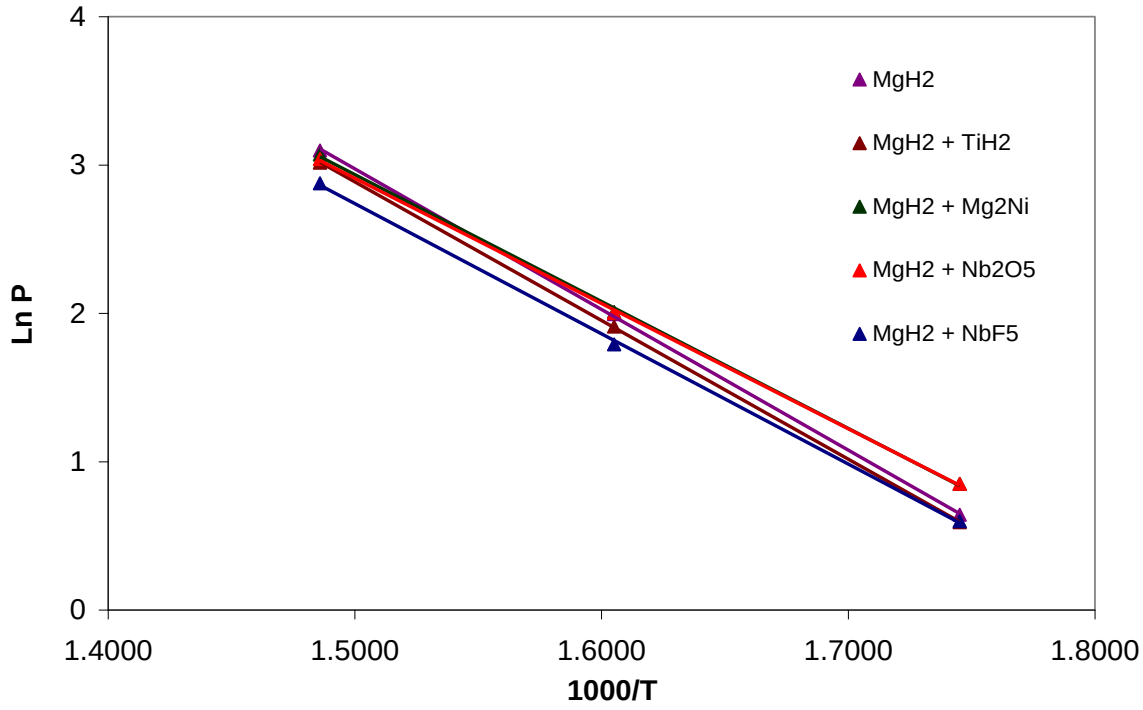

Figure 5c. Van't Hoff desorption plots for MgH_2 and catalyzed MgH_2 materials.

5.3 KINETICS MEASUREMENTS

Kinetics measurements were done on each sample in the two phase region at 400 ^{o}C in order to determine the catalytic effect of each additive on the hydrogen desorption rates from MgH_2. A novel concept of constant pressure thermodynamic driving force as fully described in chapter 4 was used to achieve these desorption kinetics measurements. The theoretical basis for constant pressure thermodynamic driving forces is that the Gibbs free energy $\Delta G = \Delta G^{o} + RT\ Ln(P_m/P_{op})$. If the N-value (P_m/P_{op}) is constant then ΔG will be the same for all determinations. In these experiments, the N-value was set at 5 for all the sample mixtures. Fig. 5d shows plots of the transducer pressure readings in the sample chamber and the remote reservoir at N = 5. It can be seen that the opposing pressure is

very nearly constant throughout the experiment. This is an indication that the thermodynamic driving force (ΔG) is constant. The transducer readings in the remote reservoir increased as a function of time during the course of the reaction. The rate of pressure increase is a direct measurement of the kinetics. Fig. 5e contains plots of the reacted fraction versus time for hydrogen desorption from the MgH_2 mixtures. The data show that the mixture with MgH_2 + 4 mol% NbF_5 desorbs hydrogen fastest while the pure MgH_2 sample desorbs hydrogen the slowest. It can also be seen that the time required for the reaction to reach 90 percent completion (T_{90}) is about 9 min while it takes 32 min for the same percentage of hydrogen to be released from the pure MgH_2. Desorption kinetics was also done for a mixture of MgH_2 + 1 mol% NbF_5. The plot showed that even at reduced level, NbF_5 still has a faster desorption rate than all other catalysts. The reaction times can be put in this order: Pure MgH_2 > TiH_2 > Mg_2Ni > Nb_2O_5 » NbF_5. Table 5a contains a summary of the times required for 90 percent of the hydrogen to be released from each mixture.

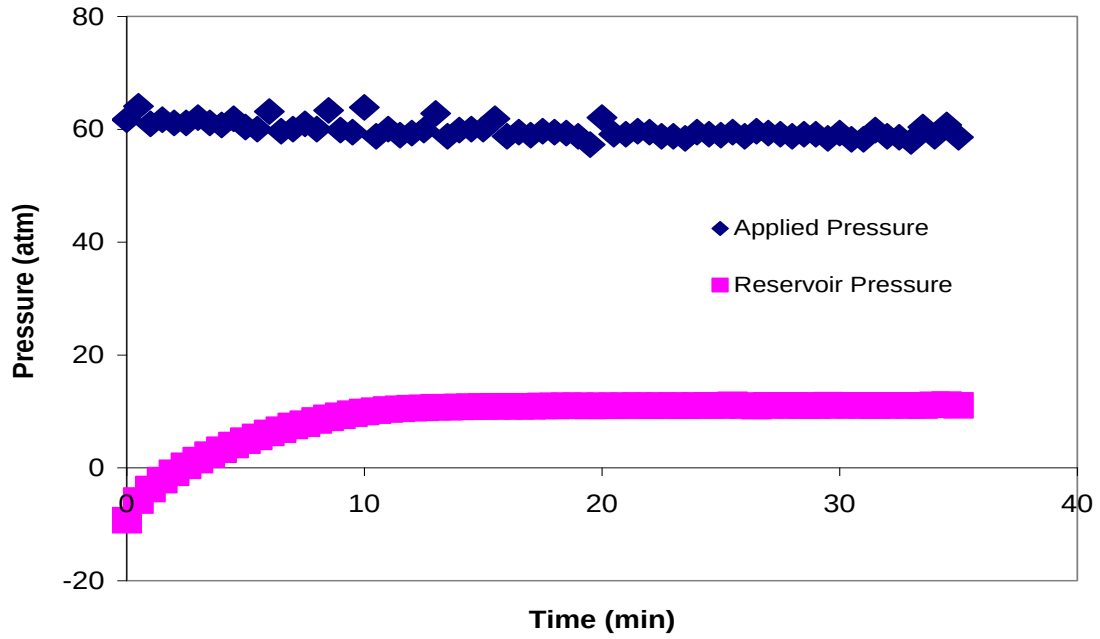

Figure 5d. Pressure transducer plot for MgH_2 + 4 mol% NbF_5 kinetics at 400 ^oC.

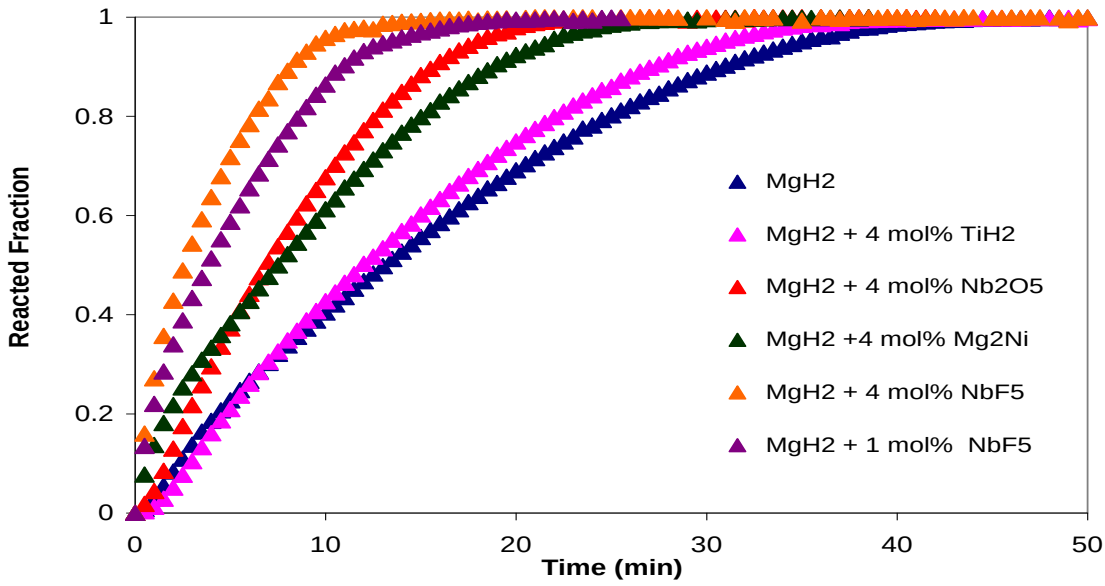

Figure 5e. Desorption kinetics for MgH_2 and catalyzed MgH_2 materials at 400 ^oC and N = 5.

5.4 KINETIC MODELING STUDIES

Diffusion, moving boundary and nucleation and growth are some of the kinetics models that can be used to describe dehydriding reactions. Plots corresponding to theoretical equations were constructed to determine which model describes the reactions in this study. The theoretical equations are summarized in chapter 4. Fig. 5f shows plots of $(1-f)^{1/3}$ versus *time* for each of the mixtures used in this study. These plots were much more linear than the other plots and thus chemical reaction at the moving boundary is believed to be the most likely mechanism for the reactions in this study. In order to confirm that chemical reaction at a moving boundary is indeed the rate-limiting process in these reactions, a second modeling approach was used. Smith and Goudy [87] had performed kinetics modeling studies on the $LaNi_{5-x}Co_x$ hydride system using equations that correspond to chemical reaction at a phase boundary and diffusion through a solid. These equations are as follows:

$$\frac{t}{\tau} = 1-(1-X_B)^{1/3} \qquad (5a)$$

Where $\tau = \dfrac{\rho_B R}{bk_s C_{Ag}}$

$$\frac{t}{\tau} = 1-3(1-X_B)^{2/3}+2(1-X_B) \qquad (5b)$$

Where $\tau = \rho_B R^2 / 6bD_e C_{Ag}$, t is the time at a specific point in the reaction and X_B is the fraction of the metal reacted. All of the other parameters are constants that have been fully described elsewhere [87]. A reaction based on equation (5a) will have chemical reaction at the phase boundary (i.e. the moving boundary) controlling the reaction rate

whereas a reaction based on equation (5b) is expected to have diffusion controlling the overall reaction rate. Equations (5a) and (5b) were fitted to the kinetic data presented in Fig. 5e and plots similar to those in Fig. 5g were obtained for each mixture. Fig. 5g contains three plots for the MgH_2 system. In the figure, one curve was based on the experimental data taken from Fig. 5e, a second curve was based on the diffusion model in Eq. (5b) and a third curve was based in Eq. (5a) with chemical reaction at the phase boundary controlling the rate. In order to determine the theoretical curves, it was necessary to determine a value for τ in Eqs. (5a) and (5b). This was done statistically by determining the value of τ necessary to minimize the standard deviation between the experimental and theoretical curves. As seen in Fig. 5g, the phase boundary controlled model is a better fit with the experimental data than the diffusion controlled model. This behavior was also observed in all the other systems. Since two different modeling techniques gave the same result, we can thus say that chemical reaction at the phase boundary is the most likely rate-controlling process in these systems.

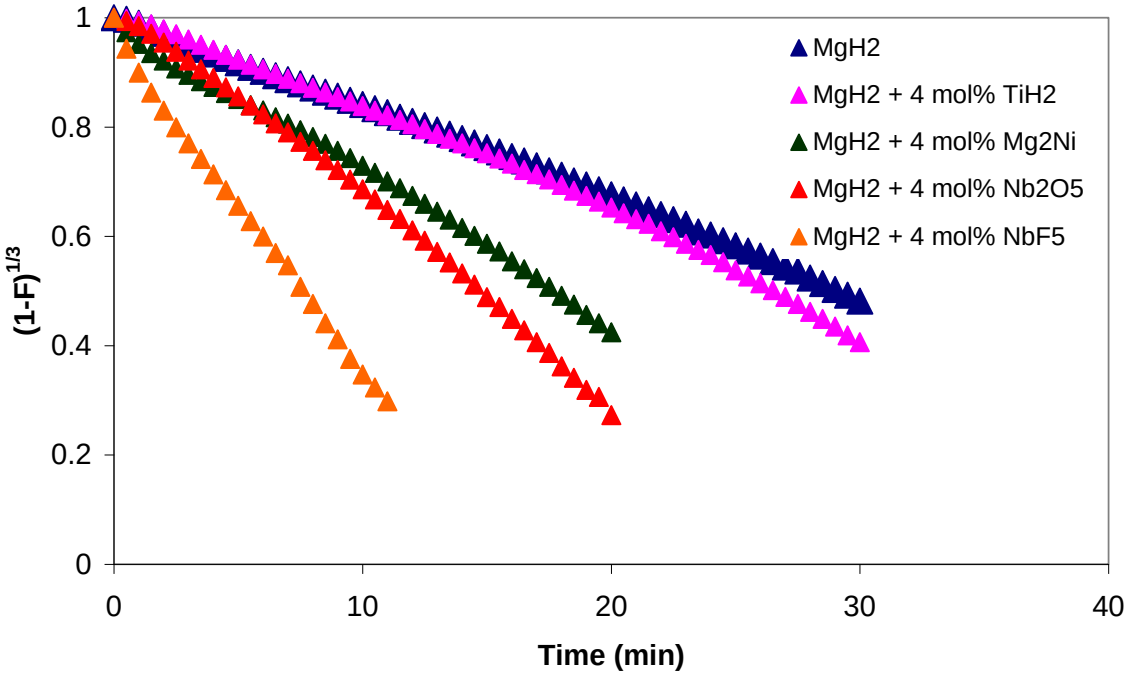

Figure 5f. Moving boundary model for MgH_2 and catalyzed MgH_2 materials at 400 ^{o}C and N= 5.

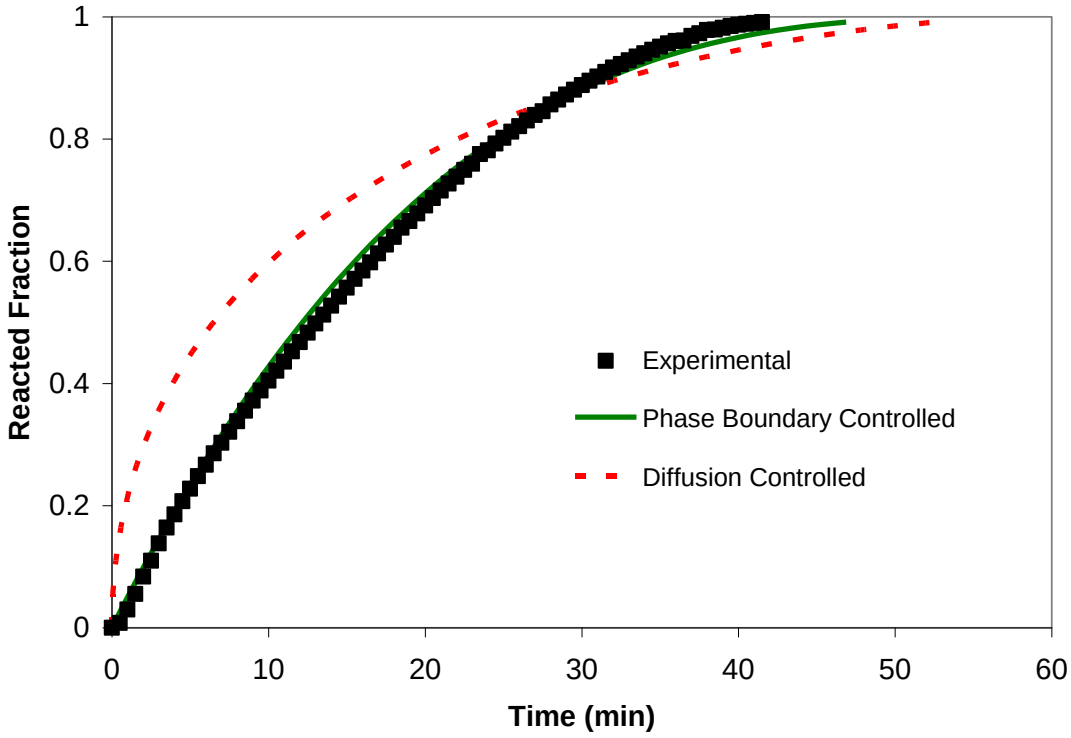

Figure 5g. Plots of reacted fraction versus time for MgH_2 at 400 ^oC.

5.5 DIFFERENTIAL THERMAL ANALYSIS AND KISSINGER PLOTS

The activation energies for dehydrogenation from the systems studied were determined using the Kissinger method described in chapter 4. A comparison of activation energies will be useful in more fully understanding the effects of catalysts on the dehydriding kinetics of MgH_2. Fig. 5h shows the DTA curves for the sample containing MgH_2 + 4 mol% Nb_2O_5 at heating rates ranging from1 to 15 ^oC per minute. The figure reveals that as the heating rate is increased, the peak corresponding to the maximum dehydriding rate moves to higher temperatures. This same behavior was observed in all the other samples. Using the DTA curves, Kissinger plots of $\ln(\beta/T_{max}^2)$ versus $1/T_{max}$ were constructed to

determine the activation energy for all the samples. Fig. 5i contains the Kissinger plots and the activation energies that were calculated from them are listed in Table 5a. The results show a good correlation between the activation energies and the times required for 90% reaction completion. The data in the table also show a direct correlation between activation energy thermal stability. The addition of catalysts to MgH_2 helped lower its activation energy and as a result the thermal stability is reduced as well.

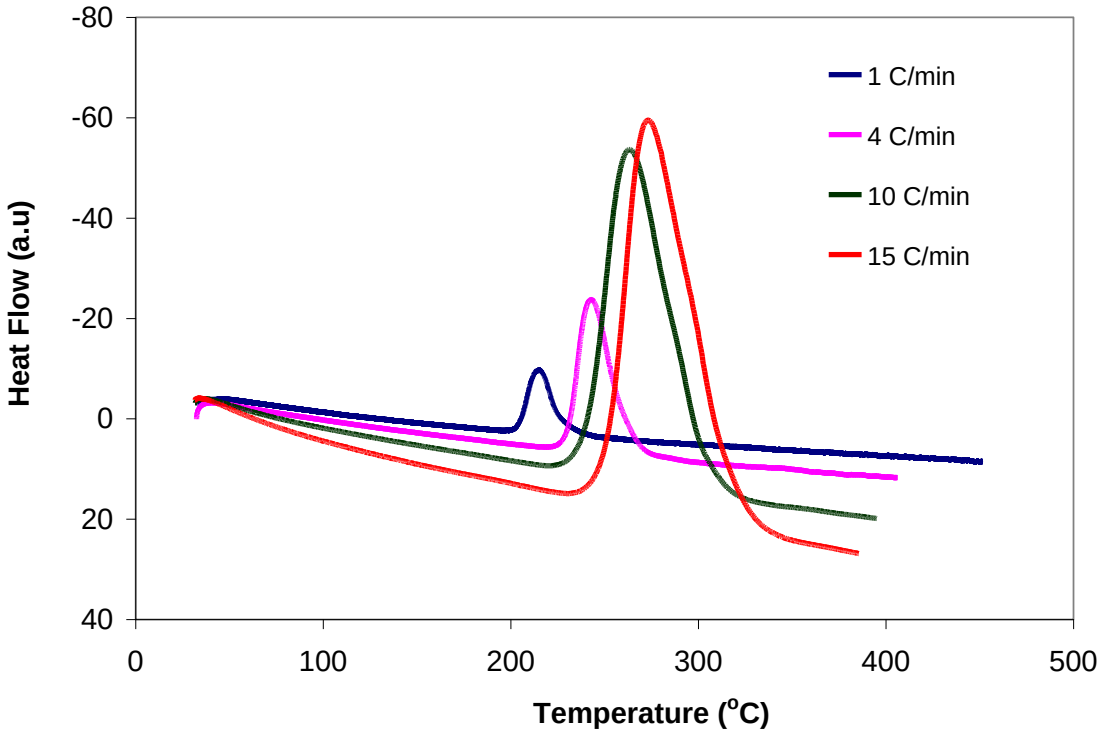

Figure 5h. DTA curves for MgH_2 + 4 mol% Nb_2O_5 at heating rates of 1, 4, 10 and 15 ^{o}C/min.

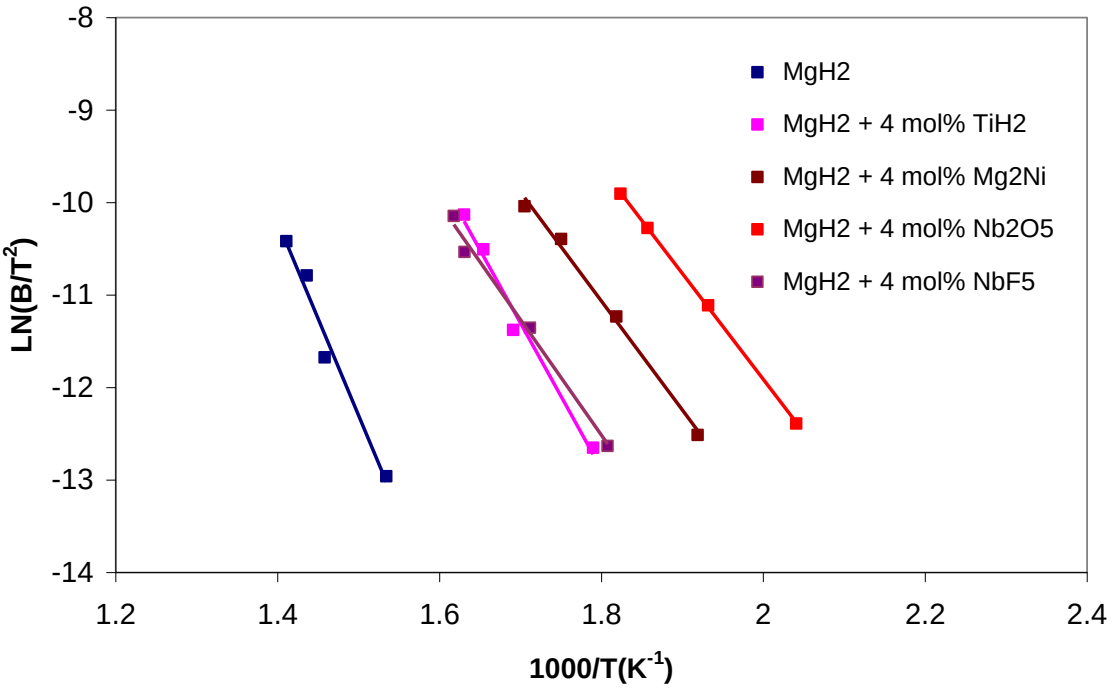

Figure 5i. Kissinger plot for MgH_2 and catalyzed MgH_2 materials.

Sample	**Onset Temp. (^oC)**	**ΔH (kJ/mol)**	**T_{90} (min)**	**E_a (kJ/mol)**
MgH_2	310	78.8	32	174
MgH_2 + 4 mol% TiH_2	250	77.7	26	131
MgH_2 + 4 mol% Mg_2Ni	190	71.1	19	98
MgH_2 + 4 mol% Nb_2O_5	205	70.2	16	95
MgH_2 + 4 mol% NbF_5	185	69.1	9	91

Table 5a. Thermodynamic and kinetics parameters for catalyzed MgH_2 materials.

5.6 CONCLUSION

This research has shown that the dehydriding rates of MgH_2 mixed with catalysts can be compared using constant pressure thermodynamic driving force. The desorption rates are in the order NbF_5 » Nb_2O_5 > Mg_2Ni > TiH_2 > pure MgH_2.The mixture with NbF_5 has the lowest desorption temperature as well as the fastest kinetics accompanied by some weight penalty. A reduction in the amount of NbF_5 reduces the onset temperature of MgH_2 by about 80 ^oC and the desorption kinetics was also faster than all other catalysts used in this study. This showed NbF_5 to be a very potent catalyst in destabilizing MgH_2 regardless of the amount added. Modeling studies, done by two different methods, showed that the reaction rates in all the reactions are controlled by chemical reaction at the phase boundary.

6.0 DEHYDROGENATION KINETICS AND MODELING STUDIES OF MAGNESIUM HYDRIDE ENHANCED BY TRANSITION METAL OXIDE CATALYSTS USING CONSTANT PRESSURE THERMODYNAMIC DRIVING FORCES

In this study, the influence of transition metal oxide catalysts (ZrO_2, CeO_2, Fe_3O_4 and Nb_2O_5) on the hydrogen desorption kinetics of MgH_2 was investigated using constant pressure thermodynamic driving forces in which the ratio of the equilibrium plateau pressure (P_m) to the opposing plateau (P_{op}) was the same in all the reactions studied. MgH_2 was ball milled with various transition metal oxides. TPD, PCI and kinetics measurements were taken to provide insight into the role that transition metal oxide catalysts may have on reaction temperature and rates.

6.1 TEMPERATURE PROGRAMMED DESORPTION MEASUREMENTS

Temperature Programmed Desorption (TPD) measurements were done on several ball milled mixtures of MgH_2 with 4 mol% of Nb_2O_5, ZrO_2, CeO_2 and Fe_3O_4. The samples were ball milled for 10 hours and their thermal desorption performance was studied to determine the temperature at which hydrogen was released from the sample mixtures. By so doing, we can understand the effect of each catalyst on the hydrogen desorption properties of MgH_2. It can be seen from the desorption curves shown in Fig. 6a that MgH_2 has the highest onset temperature of about 310 °C and that the catalyzed samples have lower desorption temperatures. The mixture of MgH_2 + Fe_3O_4 has the lowest onset desorption temperature of about 200 °C. The onset temperatures of the reacting mixtures are in the order: pure MgH_2 > CeO_2 > ZrO_2 > Nb_2O_5 > Fe_3O_4. The plot also revealed that all of the samples released less than 6 wt% of hydrogen. The reduction in hydrogen weight percentage is most likely due to the partial oxidation of the Mg in the alloy caused

by the presence of oxide in all the transition metal oxide catalysts. These results confirm that the addition of transition metal oxide catalysts is effective in reducing the desorption temperature of MgH_2, although accompanied with a small weight penalty. The values of the onset temperatures are summarized in Table 6a.

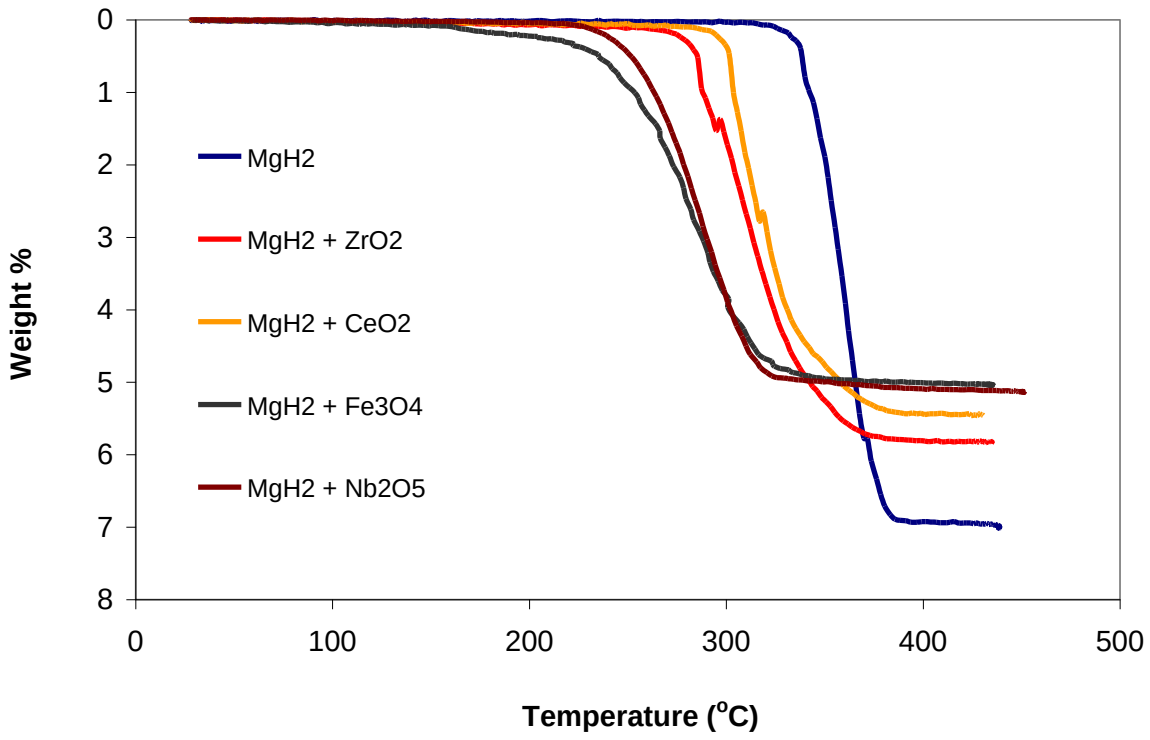

Figure 6a. TPD profiles for MgH_2 and catalyzed MgH_2 materials.

6.2 PRESSURE COMPOSITION ISOTHERM MEASUREMENTS

Pressure Composition Isotherms were constructed for MgH_2 and the catalyzed MgH_2 mixtures. Figure 6b shows the desorption isotherms for these samples at 400 °C. It can be seen from the curves that the plateau pressures are about the same for all the samples. The data from these isotherms were used to construct the Van't Hoff plots shown in

Figure 6c. The reaction enthalpies for the mixtures were determined from the slopes of these plots and the values are summarized in Table 6a. It is evident from the ΔH values that the thermodynamic stability of MgH_2 decreases with the addition of transition metal oxide catalysts.

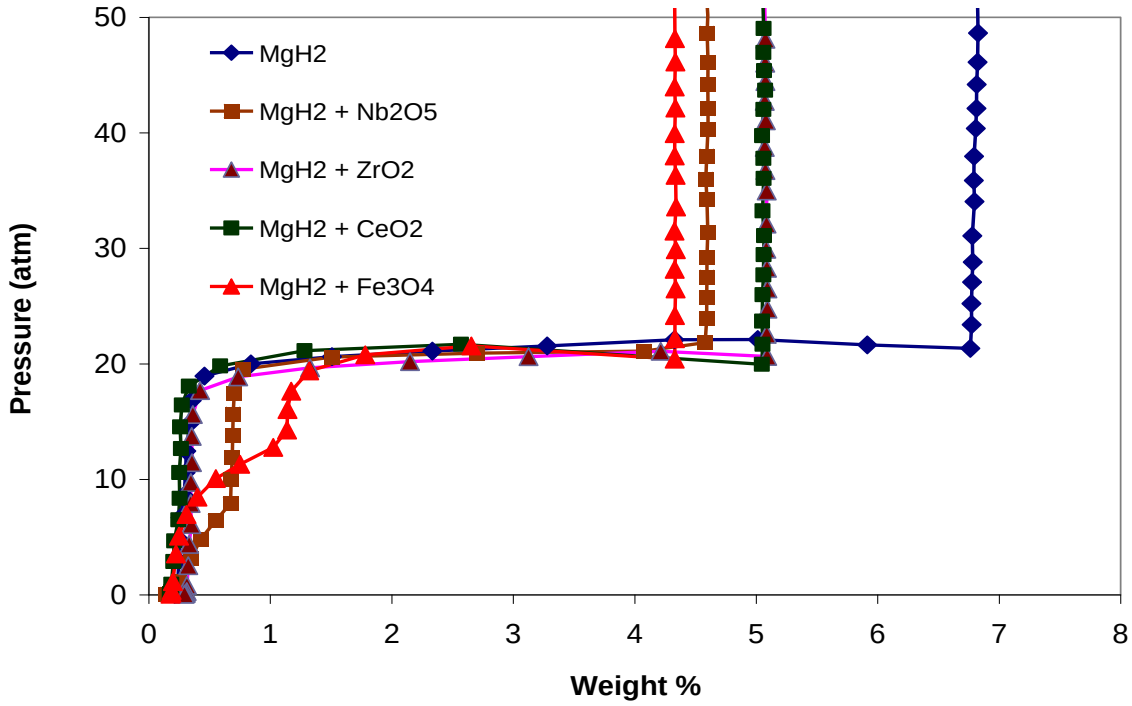

Figure 6b. Desorption isotherms for MgH_2 and catalyzed MgH_2 materials.

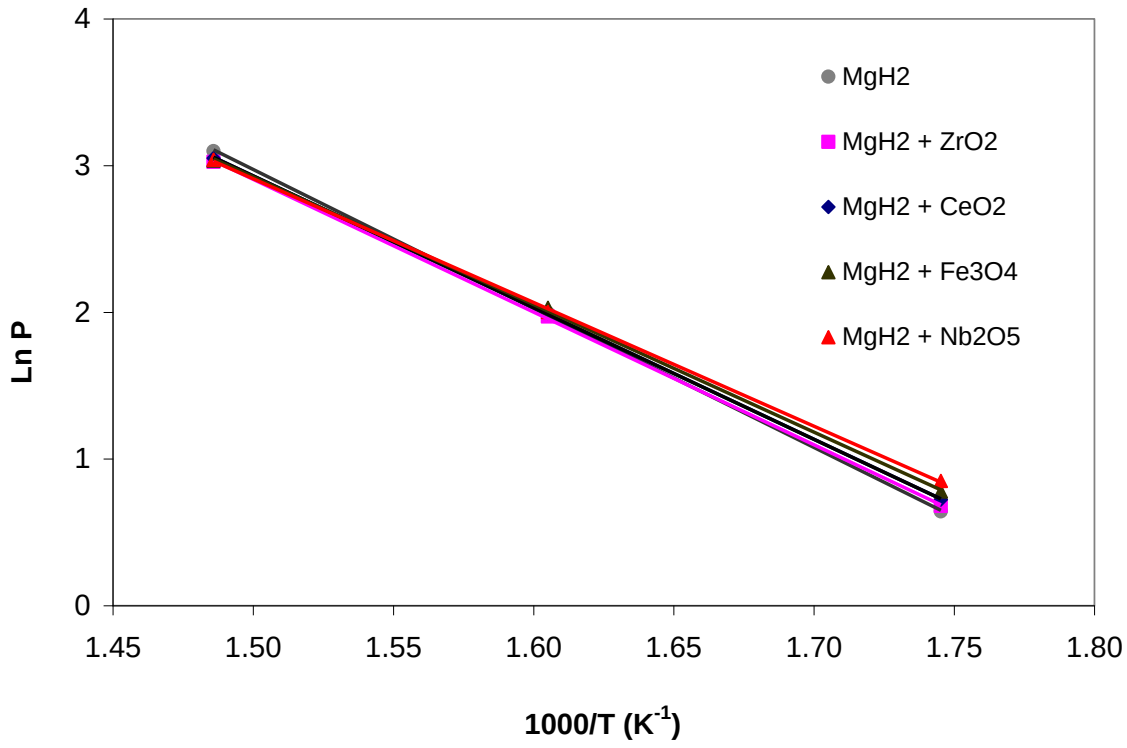

Figure 6c. Van't Hoff desorption plots for MgH_2 and catalyzed MgH_2 materials.

6.3 KINETICS MEASUREMENTS

In addition to having a low desorption temperature, it is also important that samples have fast reaction rates. Desorption kinetics experiments were carried out on each sample at 400 °C to determine the catalytic effect of transition metal oxides on hydrogen desorption rates from MgH_2. A concept of constant pressure thermodynamic driving force as described in previous chapters was used to achieve these desorption kinetics measurements. Figure 6d contains plots of the reacted fraction versus the time for hydrogen desorption from the MgH_2 mixtures with and without catalysts. It can be seen that the uncatalyzed MgH_2 sample has the slowest hydrogen desorption rate. The addition of transition metal oxides improved the kinetics of MgH_2 with Nb_2O_5 and Fe_3O_4 having

the fastest desorption reaction kinetics. The times required for all of these reactions to reach 90 percent completion (T_{90}) are summarized in Table 6a.

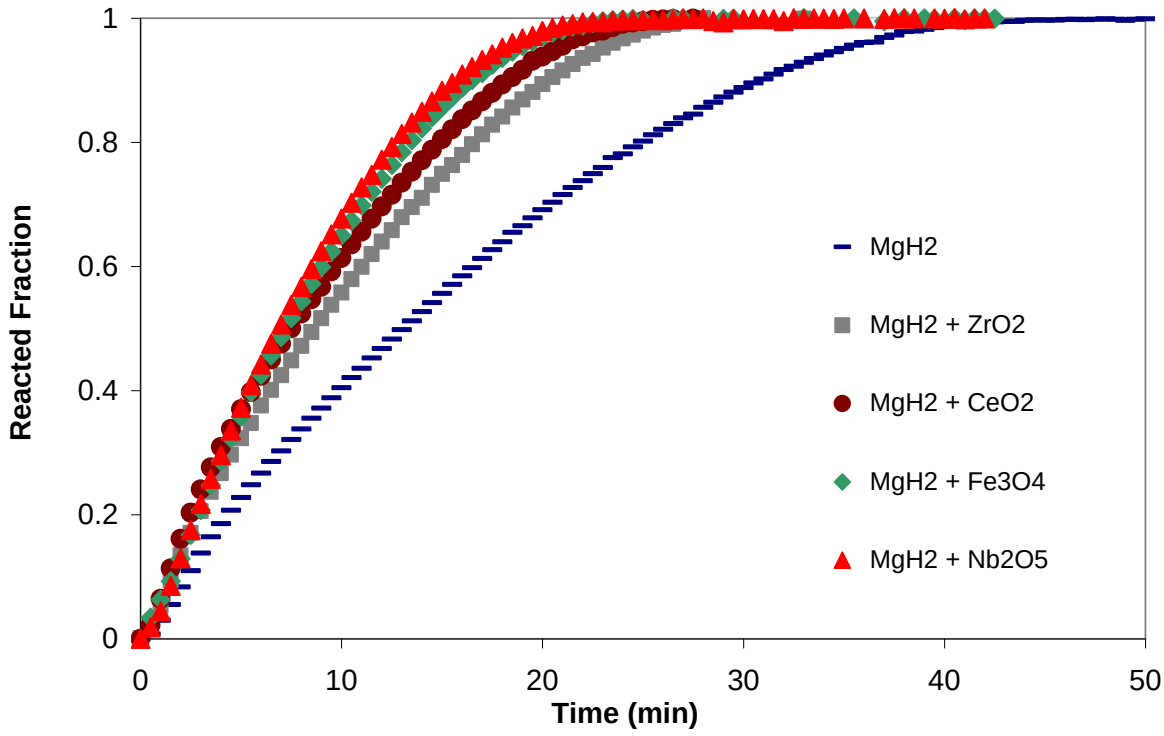

Figure 6d. Desorption kinetics for MgH_2 and catalyzed MgH_2 materials at 400 ^{o}C and N=5.

6.4 KINETICS MODELING STUDIES

A modeling approach by Smith and Goudy [87] was used to determine which kinetic model best describes the reactions in this study. The theoretical equations used to describe these modeling patterns are listed in chapter 5. Figures 6e–6i each contains three curves. One is an experimental curve taken from the desorption kinetics curve shown in Figure 6d, a second curve was calculated from the SCM with diffusion controlling the overall reaction and a third curve was calculated with chemical reaction at the phase

boundary controlling the rate. As shown in Figures 6e–6i, data generated from the SPM with chemical reaction at the phase boundary controlling the overall rate fits the experimental data better than the data generated from the SCM with diffusion controlling the overall reaction rate. Therefore we can say that chemical reaction at the phase boundary is the most likely mechanism for all the reactions in this study.

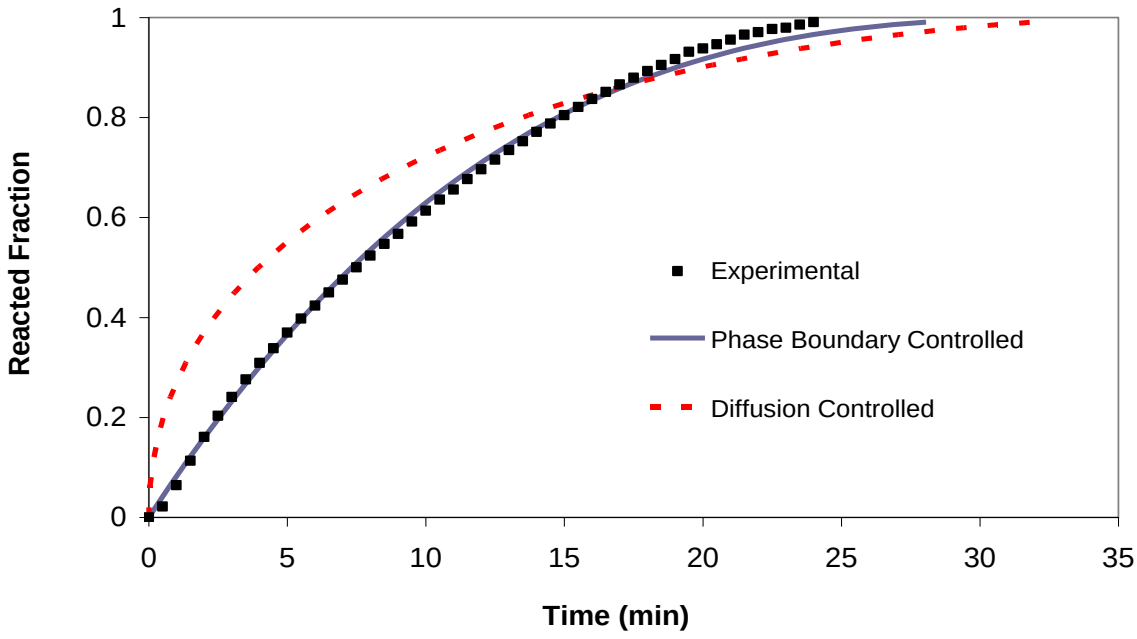

Figure 6e. Modeling results for MgH_2 + 4 mol% CeO_2.

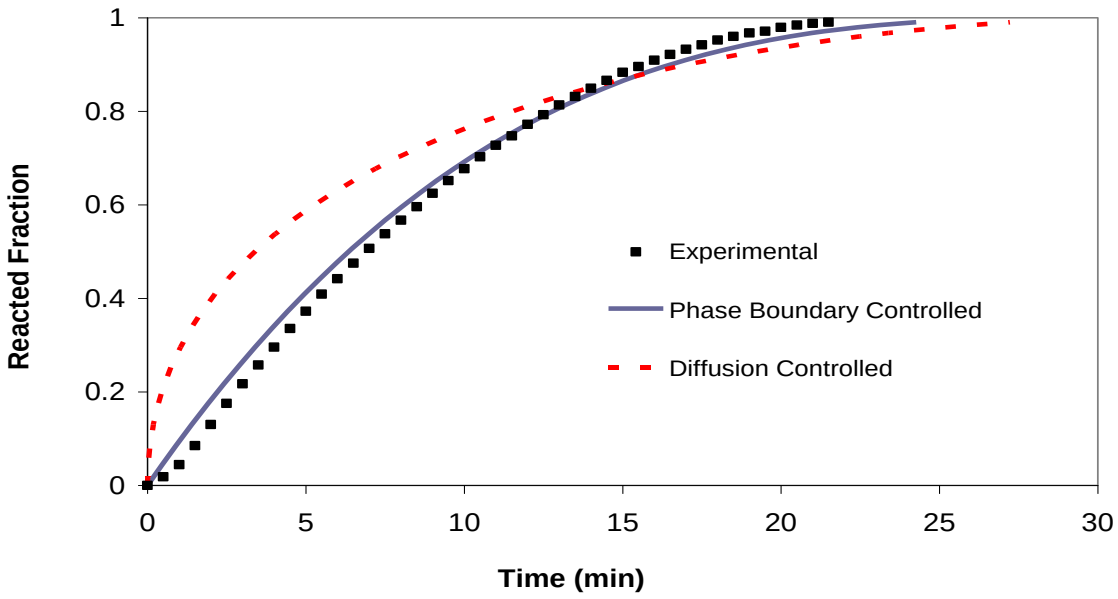

Figure 6f. Modeling results for MgH_2 + 4 mol% Nb_2O_5.

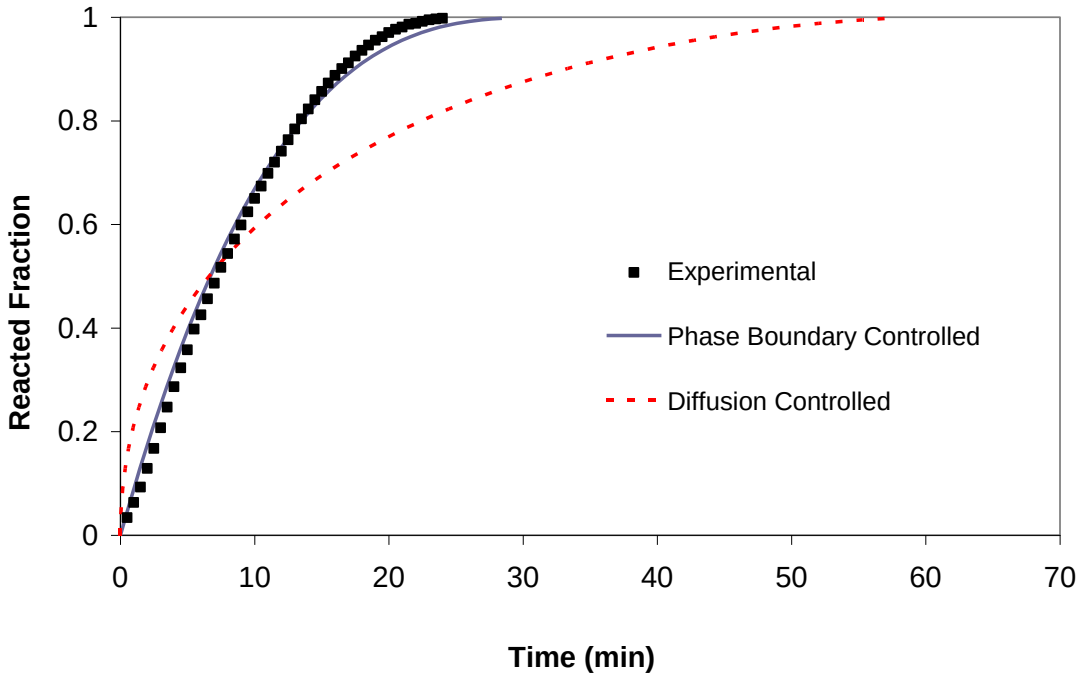

Figure 6g. Modeling results for MgH_2 + 4 mol% ZrO_2.

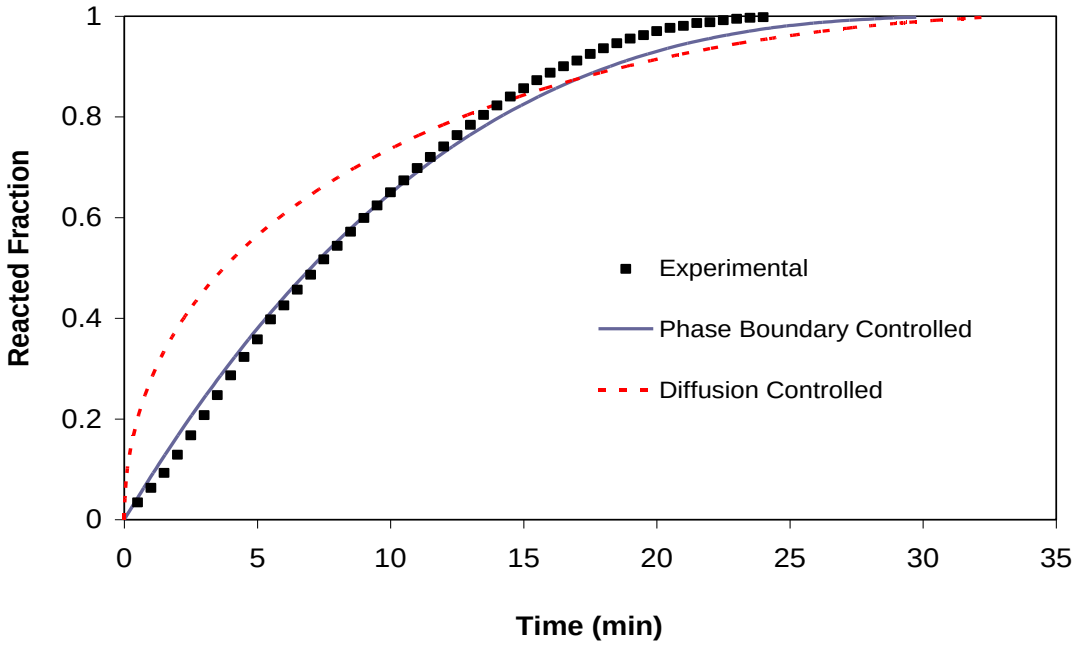

Figure 6h. Modeling results for MgH_2 + 4 mol% Fe_3O_4.

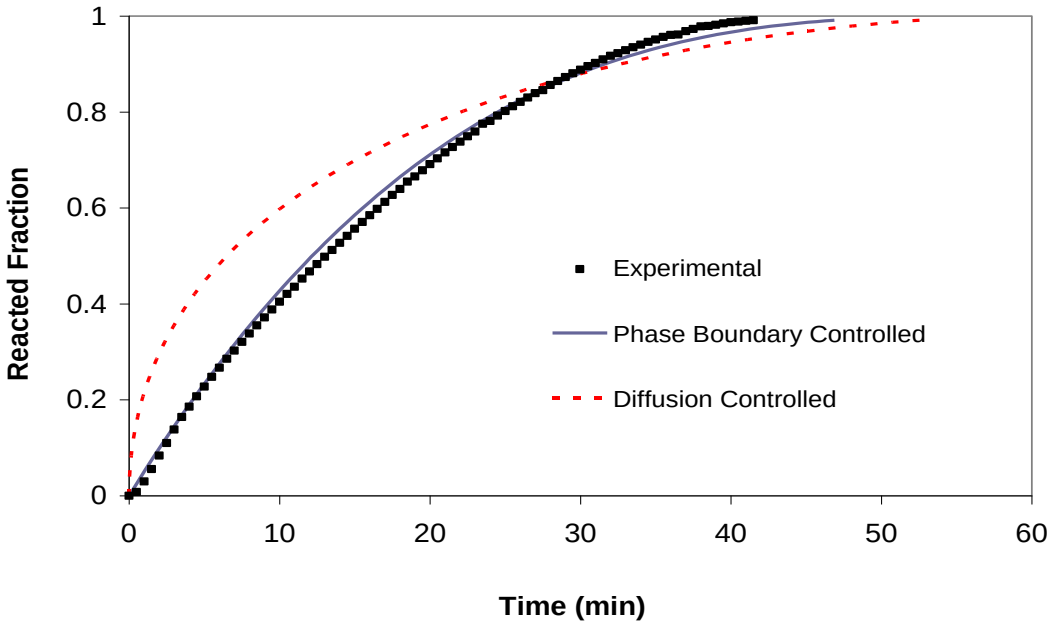

Figure 6i. Modeling results for MgH_2.

6.5 DIFFERENTIAL THERMAL ANALYSIS AND KISSINGER PLOTS

To further understand the effects of the transition metal oxide catalysts on the dehydrogenation of MgH_2, the activation energy of dehydrogenation for the systems studied were investigated using an isoconversion method based on the Kissinger equation described earlier. Figure 6j shows the DTA curves for one of the samples (MgH_2 + 4 mol% Nb_2O_5) at different heating rates from 1 to 15 °C per minute. The figure shows that the endothermic peak corresponding to the maximum rate of dehydrogenation shifts to higher temperatures as the heating rate is increased. The same trend was observed in all the other samples. The plots based on the Kissinger equation are shown in Figure 6k. A good linear relationship between $\ln(\beta/T_{max}^2)$ versus $1/T_{max}$ existed for all the samples. Activation energies of dehydrogenation were calculated from the slopes of the straight lines. The calculated activation energies are summarized in Table 6a. From the values it is clear that the addition of transition metal oxide catalysts to MgH_2 helped lower its activation energy. The calculated activation energies correlate well with the times required for 90% of the hydrogen to desorb from the samples (T_{90}). Lower activation energies correspond to faster desorption kinetics. There was also a slight correlation between the activation energy and desorption temperatures as well. Samples with high activation energies tended to have high thermal stabilities.

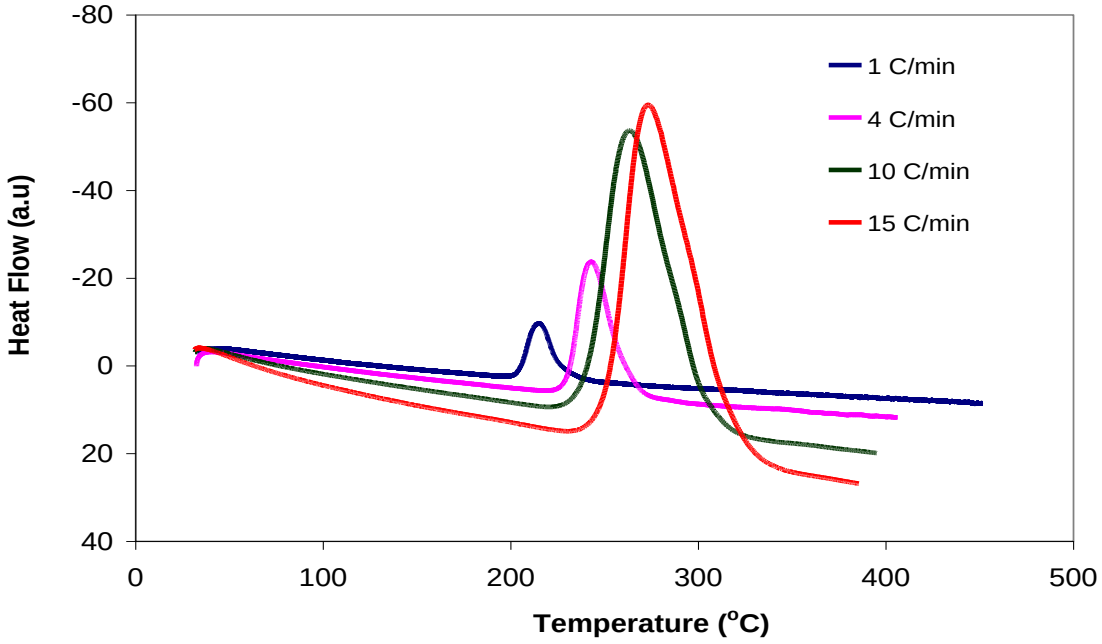

Figure 6j. DTA curves for MgH_2 + 4 mol% Nb_2O_5 at heating rates of 1, 4, 10 and 15 ^oC/min.

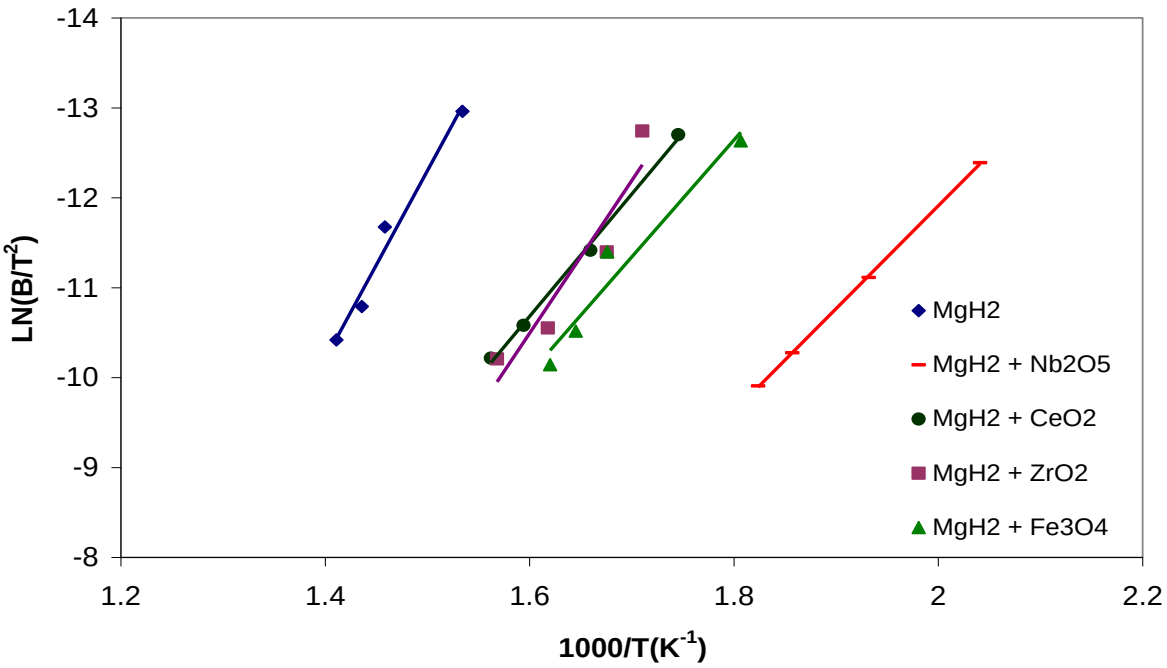

Figure 6k. Kissinger plot for MgH_2 and catalyzed MgH_2 materials.

Sample	Onset Temperature (^oC)	ΔH (kJ/mol)	T90/min	Ea (kJ/mol)
MgH_2	310	78.8	32	174
MgH_2 + 4 mol% ZrO_2	260	75.2	21	140
MgH_2 + 4 mol% CrO_2	270	74.7	19	113
MgH_2 + 4 mol% Fe_3O_4	200	72.4	17	108
MgH_2 + 4 mol% Nb_2O_5	205	70.2	16	95

Table 6a. Thermodynamic and kinetics parameters for catalyzed MgH_2 materials.

6.6 CONCLUSIONS

This study has shown that transition metal oxide catalysts are effective catalysts for lowering the reaction temperature and increasing the reaction rates of MgH_2. The dehydriding rates of MgH_2 mixed with transition metal oxide metals were in the order Nb_2O_5 > Fe_3O_4 > CeO_2 > ZrO_2 > pure MgH_2. The mixtures with Nb_2O_5 and Fe_3O_4 both have the lowest desorption temperatures as well as the fastest kinetics although the mixture with Nb_2O_5 has a slight advantage. As seen in Table 6a, the mixtures with the fastest reaction times also had the lowest activation energies and ΔH values. Modeling studies show that reaction at the phase boundary is the mechanism controlling the reaction rates in all the reaction mixtures.

CHAPTER 7

7.0 DEHYDROGENATION KINETICS AND MODELING STUDIES OF 2LiBH4 + MgH2 ENHANCED BY NbF5 CATALYST.

In earlier studies, Sabitu et al. [72] have compared the intrinsic dehydriding kinetics of MgH_2 ball milled with TiH_2, Mg_2Ni, Nb_2O_5 and NbF_5 using constant pressure thermodynamic forces and found that the reaction rates are in the order $NbF_5 > Nb_2O_5 > Mg_2Ni > TiH_2$. Because these catalysts were effective for MgH_2, the possibility of them being effective in improving the thermodynamics and desorption kinetics of $2LiBH_4 + MgH_2$ system was investigated. An attempt was made to study the kinetic behavior of the $2LiBH_4 + MgH_2$ composite after adding 4 mol% Mg_2Ni, Nb_2O_5 and NbF_5 to the mixture. XRD, TPD, PCI and kinetics measurements were conducted. An attempt was also made to determine the process that controls the rate of hydrogen desorption from the composite and catalyzed mixtures.

7.1 TEMPERATURE PROGRAMMED DESORPTION MEASUREMENTS

TPD measurements were carried out on a series of $2LiBH_4$-MgH_2 mixtures containing either 8.4 wt% NbF_5, 11.5 wt% Nb_2O_5, or 5.0 wt% Mg_2Ni. Each of the weight percentages chosen corresponds to 4 mol% catalyst. TPD measurements were also done on a "neat" $2LiBH_4 + MgH_2$ mixture and a sample of pure MgH_2 for comparison. The variable temperature hydrogen desorption behavior of the samples was examined to determine the effect of each catalyst on the hydrogen desorption properties of $2LiBH_4$-MgH_2. Figure 7a shows the TPD curves of the composites, and it can be seen that the $2LiBH_4$-MgH_2 mixture and pure MgH_2 have the highest onset temperatures. The onset temperatures for the catalyzed mixtures are in the order $Mg_2Ni > Nb_2O_5 > NbF_5$. The two

Nb-based catalysts were both able to lower the onset temperature to <150 °C compared with 250 °C for the "neat" mixture.

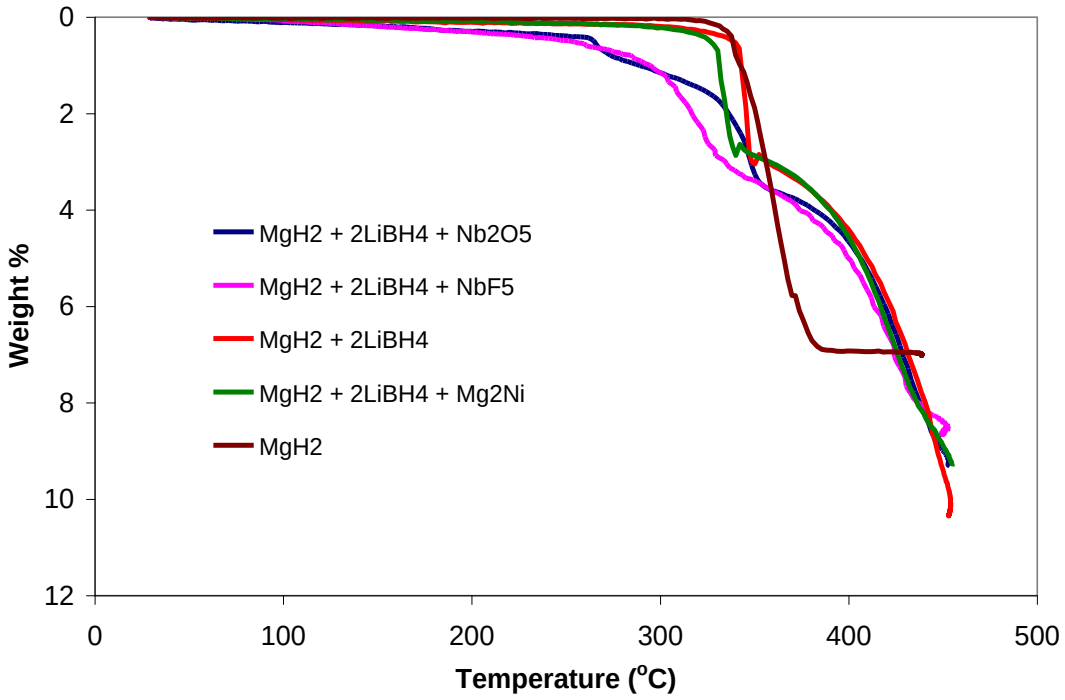

Figure 7a. TPD profiles for $2LiBH_4 + MgH_2$ with and without catalysts.

7.2 KINETICS MEASUREMENTS

Desorption kinetics experiments were carried out on each sample in the two-phase region at 450 °C. To do this, it was first necessary to construct PCIs for $2LiBH_4$-MgH_2 with and without catalysts at 450 °C. Figure 7b shows the desorption isotherms for each of the catalyzed samples. As seen on the curves, the sample mixtures have two plateaus showing that there are two steps in the overall reaction. It is also evident that each mixture released a different amount of hydrogen. Because the mixtures contain 5.0 wt% Mg_2Ni, 8.4 wt% NbF_5, and 11.5 wt% Nb_2O_5, it can be seen that the amount of hydrogen

released from each mixture is inversely proportional to the weight percentage of hydrogen in the mixture. The Mg_2Ni-catalyzed sample with the lowest weight percentage had the highest wt% H_2 release, whereas the Nb_2O_5-catalyzed sample with the highest weight percentage had the lowest wt% H_2 release. If one compares the total amount of hydrogen released from the sample mixtures during the TPD analyses (Figure 7a) with those released during the PCI analyses (Figure 7b), then it is evident that more hydrogen was released during the TPD analysis. The reason for this is that TPD analyses were done on freshly ball-milled samples, whereas the PCI analyses were done on samples that had been cycled several times. This indicates that the borohydride mixtures are not fully reversible. This lack of full reversibility in borohydride systems has also been reported elsewhere [94]. Desorption isotherms were also obtained for each sample at 425 and 475 °C. The data obtained from these isotherms were used to construct the van't Hoff plots shown in Figure 7c. The reaction enthalpies obtained from the slopes of these plots are given in Table 7a. The enthalpies are seen to be in the order: $Mg_2Ni > Nb_2O_5 > NbF_5$, which is the same trend that was seen in the onset temperatures that were obtained from the TPD curves in Figure 7a. This indicates that the catalysts are effective in destabilizing the reaction mixtures. Desorption kinetics experiments were carried out on the lower plateau at 450 °C. The kinetics measurements were all done at the same constant pressure thermodynamic driving force as described earlier. In these experiments, the N value was set to 3 for all of the sample mixtures. For example, at the temperature used in these experiments, P_m for the lower plateau in the NbF_5-catalyzed sample was 14 atm. Therefore, the P_{op} necessary for N = 3 in this sample was 4.67. This represents the first time that this technique has been applied to the kinetic study of the $2LiBH_4$-MgH_2

system. Figure 7d contains plots of reacted fraction versus time for hydrogen desorption from the samples. It can be seen from the plots that the uncatalyzed borohydride sample mixture has the slowest hydrogen desorption rate. The addition of 4 mol% Mg_2Ni to the $2LiBH_4$-MgH_2 mixture does not have any significant effect on the reaction kinetics. However, the niobium-based catalysts are very effective in improving the kinetics of the mixture. The sample mixture doped with 4 mol% NbF_5, in particular, has exceptionally fast desorption reaction kinetics. Under the conditions used, the NbF_5-catalyzed mixture releases ~80% of its hydrogen in 6.5 min, whereas the Nb_2O_5-catalyzed mixture takes 20 min, and the uncatalyzed borohydride sample takes 30 min to release the same percentage of hydrogen. It is interesting to note that the NbF_5-catalyzed borohydride mixture is the only one to release hydrogen faster than pure MgH_2. The MgH_2 sample does, however, complete desorbing 100% of its hydrogen more quickly than any of the borohydride mixture. A possible explanation for this is that the plateau region in MgH_2 is known to be very broad and well-defined with over 95% of the hydrogen desorption occurring in the two-phase plateau region. However, in the case of the borohydride mixtures, a smaller percentage of hydrogen desorbs along the plateau region. As can be seen from the isotherm for the NbF_5-catalyzed sample in Figure 7b, hydrogen release along the lower plateau results in a weight percentage change from 3.7 to 1.5. Only ~80% of the hydrogen is released along the two-phase plateau region with the remaining hydrogen being released in the single phase region. Once the reaction gets into the single-phase region, the desorption rate for the borohydride mixtures slows down significantly. In addition, the thermodynamic driving force decreases as hydrogen is released from the single-phase region. This effect is not seen the case of MgH_2.

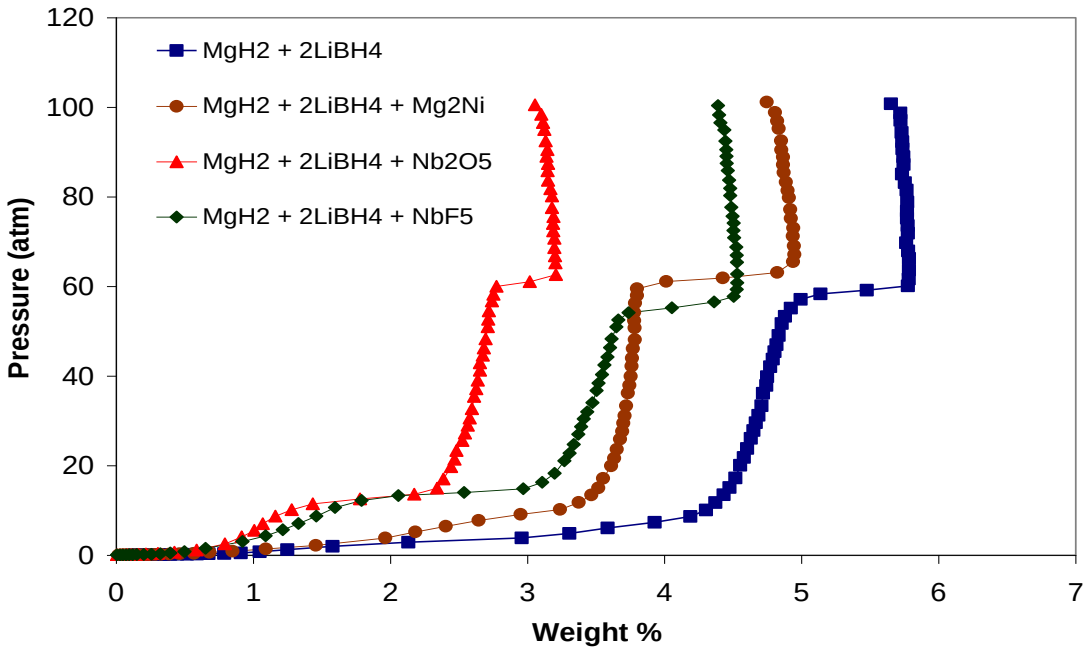

Figure 7b. Desorption isotherms for $2LiBH_4 + MgH_2$ systems catalyzed by 4 mol% NbF_5, Nb_2O_5, and Mg_2Ni.

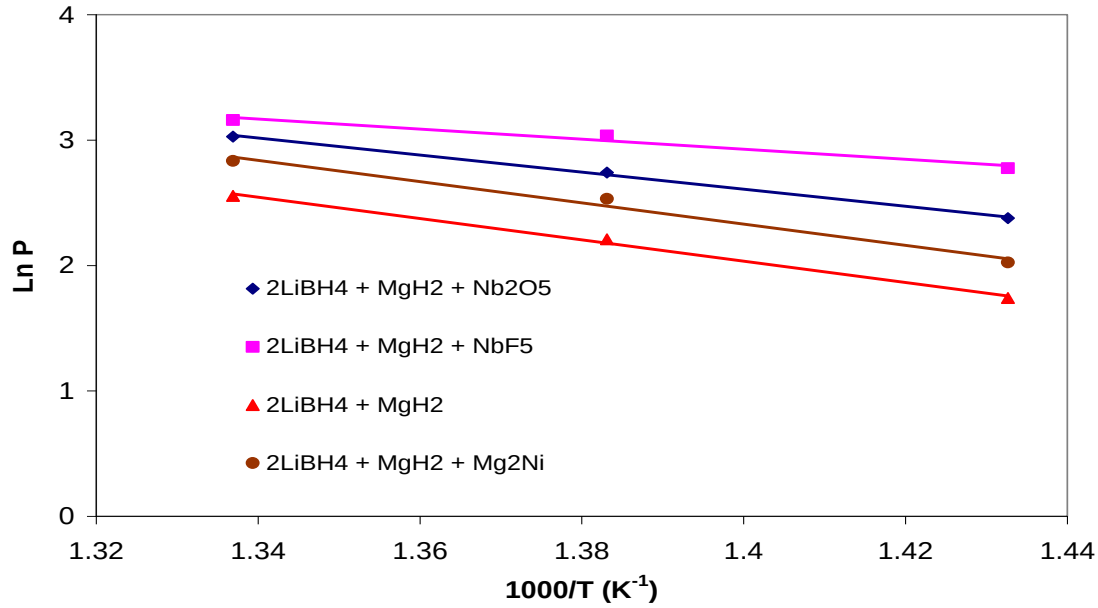

Figure 7c. Van't Hoff plots for $2LiBH_4 + MgH_2$ systems (lower plateau).

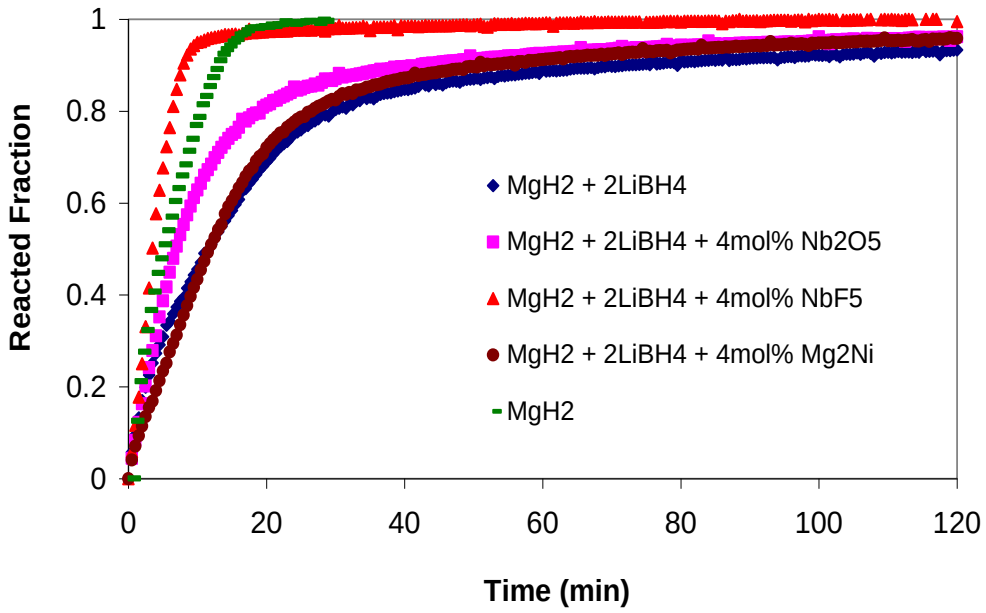

Figure 7d. Desorption kinetics for $2LiBH_4 + MgH_2$ with and without catalysts.

7.3 KINETICS MODELING STUDIES

A modeling approach by Smith and Goudy [87] was used to determine which kinetic model best describes the reactions in this study. The theoretical equations used to describe these modeling patterns are listed in earlier chapters. Figure 7e shows three curves for the $2LiBH_4 + MgH_2$ + 4 mol% NbF_5 system. One is an experimental curve taken from Figure 7d, a second curve was a theoretical curve that was calculated from a mathematical equation stating diffusion as the mechanism controlling the overall reaction; and a third curve was calculated from another mathematical equation stating that chemical reaction at the phase boundary is controlling the reaction rate. Both

equations are listed in chapter 5. As shown in Figure 7e, the data generated from the model with chemical reaction at the phase boundary controlling the overall rate fit the experimental data better than the data generated from the model with diffusion controlling the overall reaction rate. This is true during the first 80% of the reaction. Kinetic modeling studies were also attempted on the other mixtures as well as a sample of pure MgH_2. The results for the Nb_2O_5 and Mg_2Ni catalyzed mixtures are given in Figures 7f and 7g, respectively. The modeling results for these systems also show that chemical reaction at the phase boundary is also the likely rate-controlling process. Figures 7h and 7i contain modeling curves for the uncatalyzed mixture and the pure MgH_2 sample. The results for these two systems are not clear. Neither of the theoretical curves is a good fit with the experimental data. Because diffusion and chemical reaction at the phase boundary are always occurring simultaneously in these reactions, it could be that the kinetics in the case of MgH_2 and the uncatalyzed $2LiBH_4$-MgH_2 mixture are under the mixed control of both processes. The fitting of data with the mathematical equations described earlier can provide the values of the rate constant. In these model equations, $1/\tau = k$, where k is the rate constant. Values of k for each catalyzed mixture are listed in Table 7a. It can be seen that the rate constants increase as the times required for 90% reaction completion decreases. The NbF_5-catalyzed mixture has the largest rate constant, the smallest reaction time, the smallest enthalpy, and the lowest onset temperature. All of these findings indicate that NbF_5 is vastly superior to the other materials for catalyzing the $2LiBH_4$-MgH_2 system. The finding that reaction at the phase boundary controls reaction rates indicate that the catalysts employed may not merely coat the surface of the hydride particles during ball milling but are rather alloyed mechanically

into the $2LiBH_4$-MgH_2 phase. To determine if this was the case, we obtained some XRD patterns for the NbF_5 catalyst and for the $2LiBH_4$-MgH_2 mixture that was ball-milled with the NbF_5 catalyst or manually mixed with NbF_5 catalyst. Figure 7j contains the patterns. It can be seen that the pattern for the $2LiBH_4$-MgH_2 mixture manually mixed with the NbF_5 catalyst contains some small reflections that correspond to the NbF_5 reflections. However, the ball-milled mixture does not contain any of the NbF_5 reflections. This is a good indication that the NbF_5 in the ball-milled mixture is part of the phase.

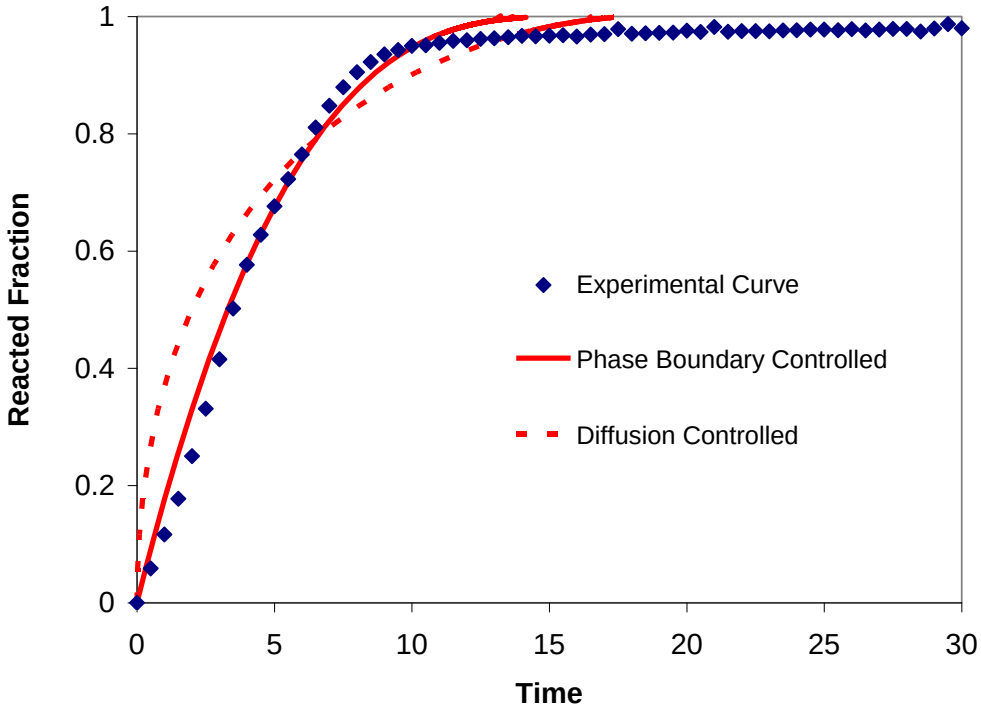

Figure 7e. Modeling results for $2LiBH_4 + MgH_2 + 4$ mol% NbF_5 at 450 ^oC.

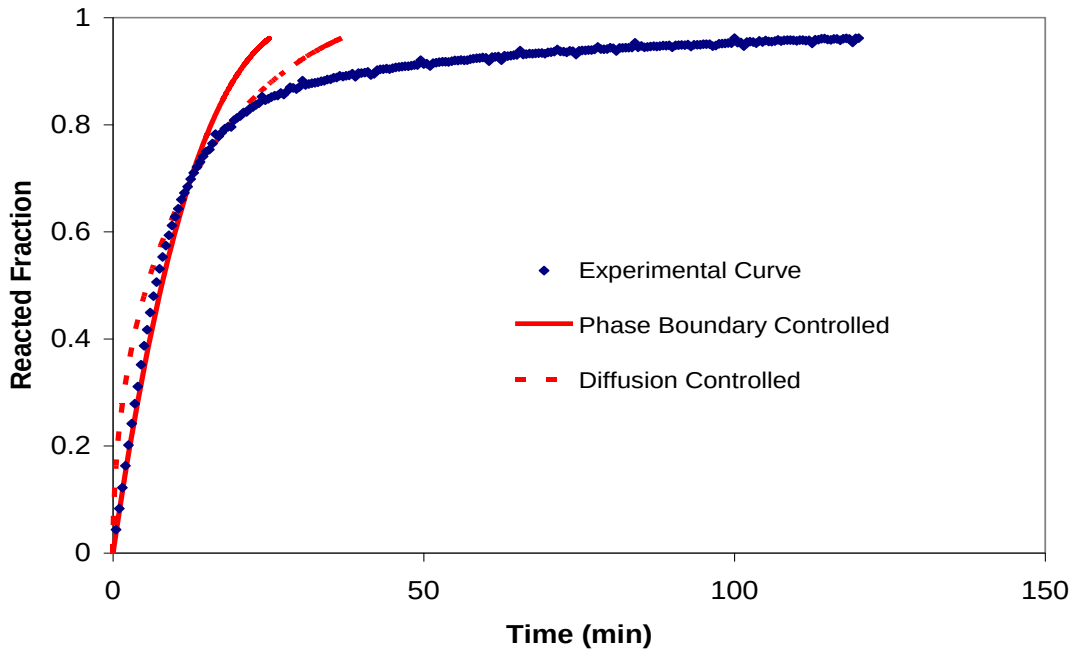

Figure 7f. Modeling results for $2LiBH_4 + MgH_2$ + 4 mol% Nb_2O_5 at 450 ^oC.

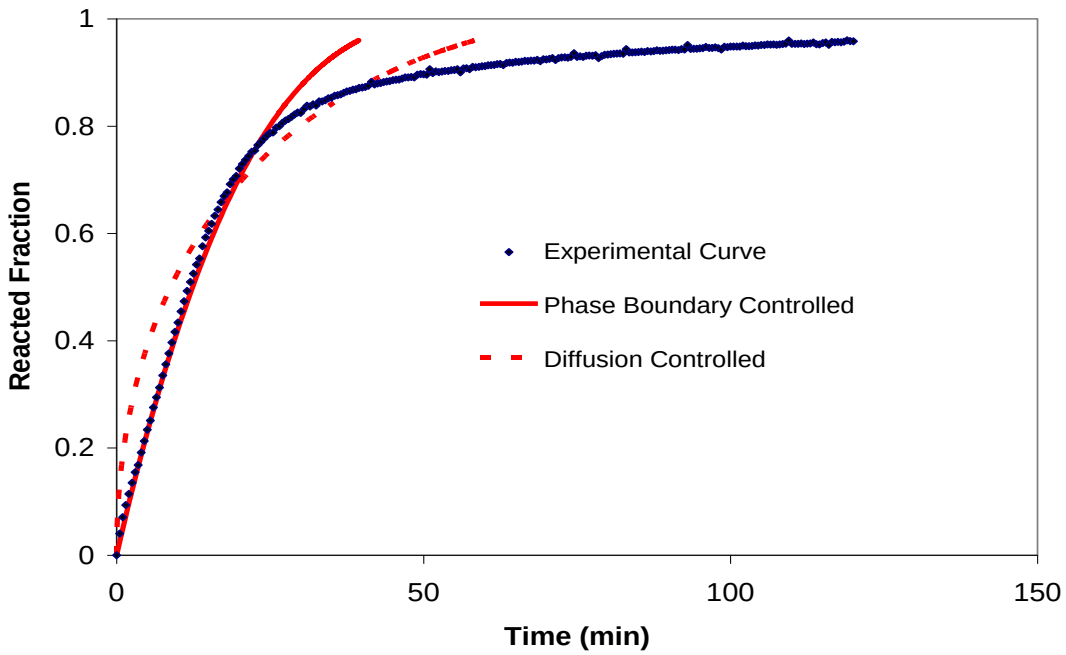

Figure 7g. Modeling results for $2LiBH_4 + MgH_2$ + 4 mol% Mg_2Ni at 450 ^oC.

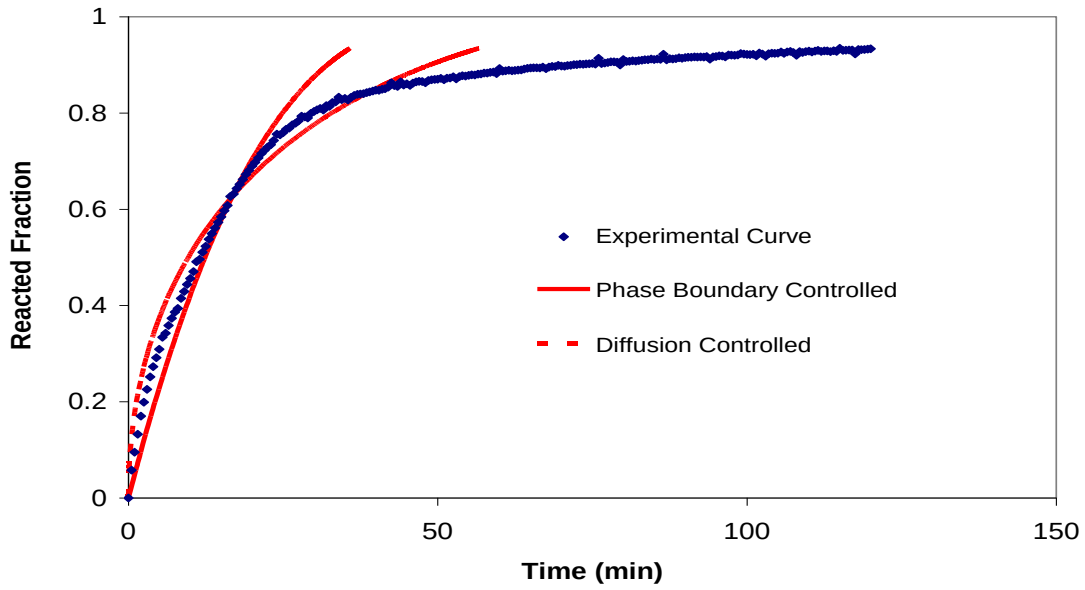

Figure 7h. Modeling results for $2LiBH_4 + MgH_2$ uncatalyzed at 450 ^oC.

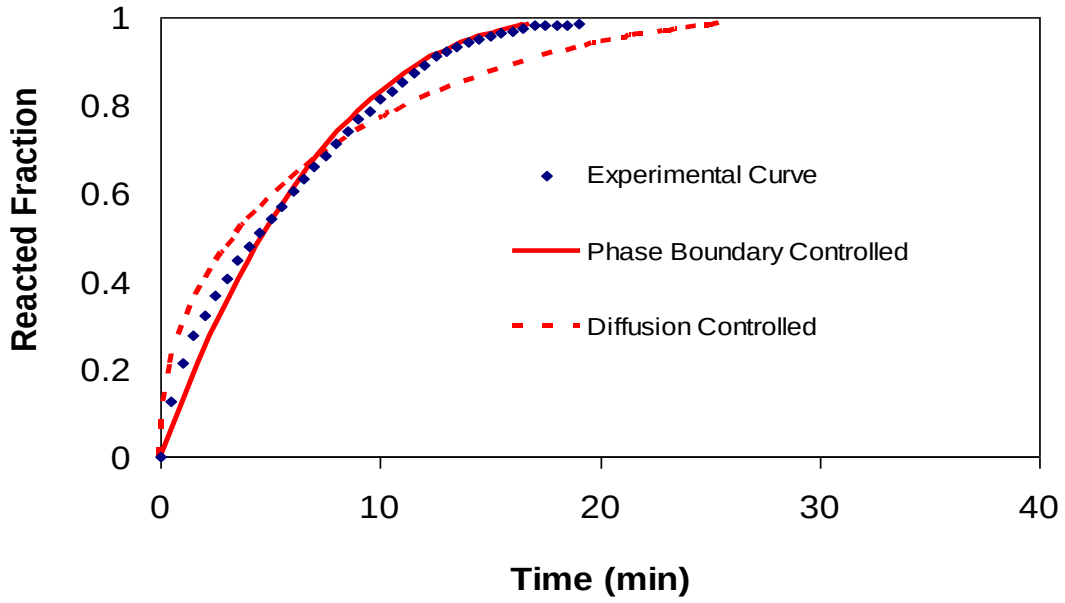

Figure 7i. Modeling results for MgH_2 at 450 ^oC.

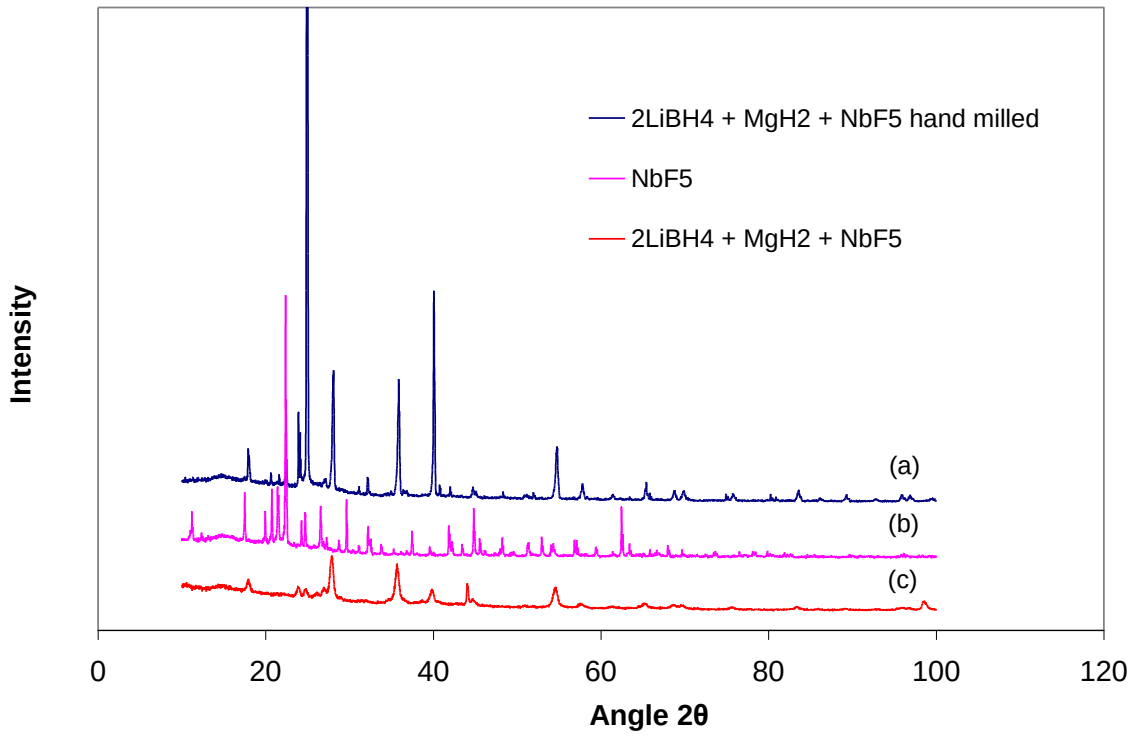

Figure 7j. XRD plots for (a) NbF_5 (b) $2LiBH_4 + MgH_2$ ball milled with 4 mol% NbF_5 and (c) $2LiBH_4 + MgH_2$ manually mixed with 4 mol% NbF_5.

Sample	**Onset Temp. (^oC)**	$k = 1/\tau$ **(min^{-1})**	T_{90} **(min)**	**ΔH (kJ/mol)**
Pure MgH_2	310		12	79
$2LiBH_4 + MgH_2 + Mg_2Ni$	315	0.0167	53.5	70
$2LiBH_4 + MgH_2 + Nb_2O_5$	240	0.0263	47.5	57
$2LiBH_4 + MgH_2 + NbF_5$	235	0.0625	8	33
$2LiBH_4 + MgH_2$	320		72	71

Table 7a. Thermodynamic and kinetics parameters.

7.4 CONCLUSION

The results of this study demonstrate that the hydrogen storage properties of a $2LiBH_4 + MgH_2$ composite can be significantly improved by the addition of several catalysts. Comparisons of the van't Hoff plots and TPD analyses of the catalyzed mixtures show that the hydrogen desorption enthalpies and onset temperatures are in the order: $Mg_2Ni > Nb_2O_5 > NbF_5$. This indicates that NbF_5 is the most effective additive for thermodynamically destabilizing the $2LiBH_4 + MgH_2$ composite. The results also show the hydrogen desorption rates are in the order: $Mg_2Ni < Nb_2O_5 \ll NbF_5$. All of these findings indicate that NbF_5 is vastly superior to the other materials for catalyzing the $2LiBH_4 + MgH_2$ system. The modeling studies based on the kinetics data indicate that chemical reaction at the phase boundary is the likely rate controlling process in all of the catalyzed mixtures. However, in the case of MgH_2 and the uncatalyzed $2LiBH_4 + MgH_2$ mixture, the results indicate that their kinetics may be under the mixed control of more than one process.

CHAPTER 8

8.0 CONCLUSION

The effect of additives such as TiH_2, Mg_2Ni, Nb_2O_5, NbF_5, etc on the thermodynamics and kinetics of MgH_2 was investigated throughout this study. Of all the catalyst studied, NbF_5 proved to be the most potent catalyst in destabilizing MgH_2. When compared with others, the mixture of MgH_2 with NbF_5 had the lowest desorption temperature. In terms of thermodynamic stability, NbF_5 had the most effect on MgH_2. This is evident from the ΔH values obtained for the MgH_2-catalyzed mixtures. Comparing the onset temperatures and ΔH values for MgH_2 and the catalyzed mixtures, it can be deduced that thermodynamic stability is directly proportional to the onset temperature. The effect of each catalyst on the hydrogen desorption kinetics of MgH_2 was compared using constant pressure thermodynamic driving force in which the ratio of the equilibrium pressure to the opposing pressure was the same for all the reactions. The mixture of MgH_2 and NbF_5 had the fastest kinetics of all the systems studied even when the amount of NbF_5 in the reaction mixture was reduced. The mixture also had the lowest activation energy. This proved that NbF_5 is a very potent catalyst in improving the reaction kinetics of MgH_2. Two modeling methods were used to describe the likely mechanism for the reactions in this study. The modeling studies showed that the reaction rates in all the reactions are controlled by chemical reactions at the phase boundary.

The effect of additives such as Mg_2Ni, Nb_2O_5 and NbF_5 on the thermodynamics and desorption kinetics of $2LiBH_4 + MgH_2$ composite mixture was also investigated. NbF_5 stood out as the most effective catalyst for thermodynamic destabilization of the composite mixture. In terms of improving the desorption kinetics, NbF_5 had the most

effect of all catalyst studied. The modeling studies based on the kinetics data showed that chemical reaction at the phase boundary is the likely rate controlling process in all of the catalyzed mixtures.

REFERENCES

1. Edwards, P. P.; Kuznetsor, V. L.; David, W. I. F.; Brandon, N. P. Hydrogen and fuel cells: Towards a sustainable energy future, *Energy Policy* **2008**, 36(12), 4356-4362.

2. Jain, I. P.; Chaagan, L.; Jain, A. Hydrogen storage in Mg: A most promising material, *Int. J. of Hydrogen Energy* **2010**, 35(10), 5133-5144.

3. Alternative and Advanced Fuels (US Department of Energy, Energy Efficiency and Renewable Energy) available at http://www1.eere.energy.gov/femp/pdfs/federal_fleet_faq.pdf

4. Hydrogen available at http://www.need.org/needpdf/infobook_activities/IntInfo/HydrogenI.pdf

5. US Department of Energy-Energy Efficiency and Renewable Energy. Fuel Cell Technologies Program-Hydrogen Delivery available at http://www1.eere.energy.gov/hydrogenandfuelcells/delivery/printable_versions/index.html

6. Hydrogen available at http://www1.eere.energy.gov/hydrogenandfuelcells/storage/printable_versions/doe_rd.html

7. Hydrogen available at http://www1.eere.energy.gov/hydrogenandfuelcells/pdfs/doe_overview_satyapal.pdf

8. Satyapal, S.; Petrovic, J.; Read, C.; Thomas, G.; Ordaz, G. The U.S. Department of Energy's National Hydrogen Storage Project: Progress towards meeting hydrogen-powered vehicle requirements, *Catalysis Today* **2007**, 120(3-4), 246-256.

9. Alternative Fuels Data Center (Hydrogen Benefits and Considerations) available at http://www.afdc.energy.gov/fuels/hydrogen_benefits.html

10. Hydrogen benefits and challenges available at http://www.fueleconomy.gov/feg/fcv_benefits.shtml

11. Advantages and benefits of fuel cell and hydrogen technologies available at http://www.fuelcellmarkets.com/fuel_cell_markets/5,1,1,663.html

12. Hydrogen Storage Challenges available at http://www1.eere.energy.gov/hydrogenandfuelcells/storage/printable_versions/storage_challenges.html

13. Zuttel, A. Materials for Hydrogen Storage, *Materials Today* **2003**, 6(9), 24-33.

14. Pukazhselvan, D.; Kumar, V.; Singh, S. K. High capacity hydrogen storage: Basic aspects, new developments and milestones, *Nano Energy* **2012,** 1(4), 566-589.

15. Schlapbach, L.; Zuttel, A. Hydrogen-storage materials for mobile applications, *Nature* **2001**, 414(6861), 353-358.

16. Levesque, S.; Ciureanu, M.; Roberge, R.; Motyka, T. Hydrogen storage for fuel cell systems with stationary applications. Transient measurement technique for packed bed evaluation, *Int. J. Hydrogen Energy* **2000**, 25(11), 1095-1105.

17. Selvam, P.; Viswanathan, B.; Swamy, C. S.; Srinivasan, V. Magnesium and magnesium alloy hydrides, *Int. J. Hydrogen Energy* **1986**, 11(3), 169-192.

18. Long, L. H. The mechanisms of thermal decomposition of diborane and of interconversion of the boranes: A reinterpretation of the evidence, *J. Inorg. Nucl. Chem.* **1970**, 32(4), 1097-1115.

19. Orimo, S.; Nakamori, Y.; Zuttel, A. Material properties of MBH_4 (M=Li, Na, and K), *Mater. Sci. Eng. B* **2004**, 108(1-2), 51-53.

20. Nakamori, Y.; Miwa, K.; Ninomiya, A.; Li, H.; Ohba, N.; Towata, S.; Zuttel, A.; Sichi, O. Correlation between thermodynamical stabilities of metal borohydrides and cation electronegativites: First-principles calculations and experiments, *Phys. Rev. B* **2006**, 74(4), 45126-45134.

21. Frankcombe, T. J.; Kroes, G. J.; Zuttel, A. Theoretical calculation of the energy of formation of $LiBH_4$, *Chem. Phys. Lett.* **2005**, 405(1-3), 73-78.

22. Ohba, N.; Miwa, K.; Aoki, M.; Noritake, T.; Towata, S.; Nakamori,Y.; Orimo, S.; Zuttel, A. First-principles study on the stability of intermediate compounds of $LiBH_4$, *Phys. Rev. B* **2006**, 74(7), 75110-75116.

23. Araujo, C. M.; Li, S.; Ahuja, R.; Jena, P. Vacancy-mediated hydrogen desorption in $NaAlH_4$, *Phys. Rev. B* **2005**, 72(16), 165101-165106.

24. Liu, X.; Langmi, H. W.; Beattie, S. D.; Azenwi, F. F.; McGrady, G. S.; Jensen, C. M. Ti-Doped $LiAlH_4$ for Hydrogen Storage: Synthesis, Catalyst Loading and Cycling Performance, *J. Am. Chem. Soc.* **2011**, 133(39), 15593-15597.

25. Liu, X.; McGrady, G. S.; Langmi, H. W.; Jensen, C. M. Facile Cycling of Ti-Doped $LiAlH_4$ for High Performance Hydrogen Storage, *J. Am. Chem. Soc.* **2009,** 131(14), 5032-5033.

26. Zaluska, A.; Zaluski, L.; Strom-Olsen, J. O. Sodium alanates for reversible hydrogen storage, *J. Alloys Compd.* **2000**, 298(1-2), 125-134.

27. Blade, C. P.; Hereijgers, B. P. C.; Bitter, J. H.; de Jong, K. P. Sodium Alanate Nanoparticles − Linking Size to Hydrogen Storage Properties, *J. Am. Chem. Soc.* **2008**, 130 (21), 6761-6765.

28. Arroyo, C. P.; Dompablo, Y.; Ceder, G. First principles investigations of complex hydrides AMH_4 and A_3MH_6 (A=Li, Na, K, M=B, Al, Ga) as hydrogen storage systems, *J. Alloys Compd.* **2004**, 364(1-2), 6-12.

29. Ares, J. R.; Aguey-Zinsou, K.; Leardini, F.; Jimenez, I.; Ferrer, J.; Fernandez,J. F.; Gou, Z.; Sanchez, C. Hydrogen Absorption/Desorption Mechanism in Potassium Alanate ($KAlH_4$) and Enhancement by $TiCl_3$ Doping, *J. Phys. Chem. C* **2009**, 113(16), 6845-6851.

30. Jeloaica, L.; Zhang, J.; Cuevas, F.; Latroche, M.; Raybaud, P. Thermodynamic Properties of Trialkali (Li, Na, K) Hexa-alanates: A Combined DFT and Experimental Study, *J. Phys. Chem. C* **2008**, 112(47), 18598-18607.

31. Fichtner, M.; Fuhr, O. Synthesis and structures of magnesium alanate and two solvent adducts, *J. Alloys Compd.* **2002**, 345(1-2), 286-296.

32. Kim, Y.; Lee, E.; Shim, J.; Cho, Y. W.; Yoon, K. B. Mechanochemical synthesis and thermal decomposition of $Mg(AlH_4)_2$, *J. Alloys Compd.* **2006**, 422(1-2), 283-287.

33. Varin, R. A.; Chiu, C.; Czujko, T.; Wronski, Z. Mechano-chemical activation synthesis (MCAS) of nanocrystalline magnesium alanate hydride [$Mg(AlH_4)_2$] and its hydrogen desorption properties, *J. Alloys Compd.* **2007**, 439(1-2), 302-311.

34. Liquid-Hydrogen Storage available at http://www.eolss.net/Sample-Chapters/C08/E3-13-07-05.pdf

35. Flynn, T. M. A liquidation of gases, *McGraw-Hill Encyclopedia of Science and Technology*, 7th Ed., Parker, SP (ed.), McGraw-Hill, New York, **1992**, 10, 106.

36. Hydrogen Production and Storage; R&D Priorities and Gaps. Hydrogen Implementing Agreement available at http://www.iea.org/publications/freepublications/publication/hydrogen.pdf

37. Mao, W. L.; Mao, H.; Goncharov, A. F.; Struzhkin, V. V.; Guo, Q.; Hu, J.; Shu, J.; Hemley, R. J.; Somayazulu, M.; Zhao, Y. Hydrogen Clusters in Clathrate, *Hydrate Science* **2002**, 297(5590) 2247-2249.

38. Lee, H.; Lee, J.; Kim, D.; Park, J.; Seo, Y.; Zeng, H.; Moudrakovski, I. L.; Ratcliffe, C. I.; Ripmeester, J. A. Tuning clathrate hydrates for hydrogen storage, *Nature* **2005**, 434(7034) 743-745.

39. Kazansky, V. B.; Borovkov, V. Y.; Serich, A.; Karge, H. G. Low temperature hydrogen adsorption on sodium forms of faujasites: barometric measurements and drift spectra *Micro. Mes. Mater.* **1998**, 22(1-3)251-259.

40. Langmi, H. W.; Walton, A.; Al-Mamouri, M. M.; Johnson, S. R.; Book, D.; Speight, J. D.; Edwards, P. P.; Gameson, I.; Anderson, P. A.; Harris, I. R. Hydrogen adsorption in zeolites A, X, Y and RHO, *J. Alloys Compd.* **2003**, 356-357, 710-715.

41. Sudan, P.; Zuttel, A.; Mauron, Ph.;, Emmenegger, Ch.; Wenger, P.; Schlapbach, L. Physiosorption of hydrogen in single-walled carbon nanotubes, *Carbon* **2003**, 41(2), 2377-2383.

42. Viswanathan, B.; Sankaran, M.; Schibioh, M. A. Carbon nanomaterials: are they appropriate candidates for hydrogen storage, *Bulletin of the catalysis society of India* **2003**, 2, 12-32.

43. Nijkamp, M. G.; Raaymakers, J. E. M. J.; van Dillen, A. J.; de Jong, K. P. Hydrogen storage using physiosorption-materials demands, *Appl. Phys. A* **2001**, 72(5), 619-623.

44. Dillon, A. C.; Jones, K. M.; Bekkedahl, T. A.; Kiang, C. H.; Bethune, D. S.; Heben, M. J. Storage of hydrogen in single-walled carbon nanotubes, *Nature* **1997**, 386(6623), 377-379.

45. Costa, P. M. F. J.; Coleman, K. S.; Green, M. L. H. Influence of catalyst metal particles on the hydrogen sorption of single-walled carbon nanotube materials, *Nanotechnology* **2005**, 16(4), 512-517.

46. Wu, Z.; Zhou, G.; Yin, L.; Ren, W.; Li, F.; Cheng, H. Graphene/metal oxide composite electrode materials for energy storage, *Nano Energy* **2012**, 1(1), 107-131.

47. Roswell, J. L. C.; Yaghi, O. M. Metal–organic frameworks: a new class of porous materials, *Micro. Mes. Mater*. **2004**, 73(1-2), 3-14.

48. Chen, B.; Ma, S.; Zapata, F.; Lobkovsky, E. B.; Yang, J. Hydrogen Adsorption in an Interpenetrated Dynamic Metal−Organic Framework, *J. Inorg. Chem.* **2006**, 45(15), 5718-5720.

49. Suh, M. P.; Park, H. J.; Prasad, T. K.; Lim, D. Hydrogen Storage in Metal–Organic Frameworks, *Chem. Rev.* **2012**, 112(2), 782-835.

50. Kojima, Y.; Kawai, Y. IR characterization of lithium imide and amide, *J. Alloys Compd*. **2005**, 395(1-2), 236-239.

51. Evard E.; Gabis I.; Yartys V. A. Kinetics of hydrogen evolution from MgH_2: Experimental studies, mechanism and modeling, *Int. J. Hydrogen Energy* **2010**, 35(17), 9060-9069.

52. Inamura H.; Masanari K.; Kusuhara M.; Katsumoto H.; Sumi T.; Sakata Y. High hydrogen storage capacity of nanosized magnesium synthesized by high energy ball-milling, *J. Alloys Compd.* **2005**, 386(1-2), 211-216.

53. Barkhordarian G.; Klassen T.; Bormann R. Effect of Nb_2O_5 content on hydrogen reaction kinetics of Mg, *J. Alloys Compd*. **2004**, 364(1-2), 242-246.

54. Hanada N.; Ichikawa T.; Fujii H. Catalytic effect of Ni nano-particle and Nb oxide on H-desorption properties in MgH_2 prepared by ball milling, *J. Alloys Compd.* **2005**, 404-406, 716-719.

55. Zhu M.; Wang H.; Ouyang L. Z.; Zeng M. Q. Composite structure and hydrogen storage properties in Mg-base alloys, *Int. J. Hydrogen Energy* **2006**, 31(2), 251-257.

56. Oelerich W.; Klassen T.; Bormann R. Metal oxides as catalysts for improved hydrogen sorption in nanocrystalline Mg-based materials, *J. Alloys Compd*. **2001**, 315(1-2), 237-242.

57. Liang G.; Huot J.; Boily S.; Van Neste A.; Schulz R. Catalytic effect of transition metals on hydrogen sorption in nanocrystalline ball milled MgH_2-Tm (Tm=Ti, V, Mn, Fe and Ni) systems, *J. Alloys Compd.* **1999**, 292(1-2), 247-252.

58. Yang W. N.; Shang C. X.; Guo Z. X. Site density effect of Ni particles on hydrogen desorption of MgH_2, *Int. J. Hydrogen Energy* **2010**, 35(10), 4534-4542.

59. Aguey-Zinsou K-F.; Ares Fernandez J. R.; Klassen T.; Bormann R. Effect of Nb_2O_5 on MgH_2 properties during mechanical milling, *Int. J. Hydrogen Energy* **2007**, 32(3), 2400-2407.

60. Luo Y.; Wang P.; Ma L.; Cheng H. Hydrogen sorption kinetics of MgH_2 catalyzed with NbF_5, *J. Alloys Compd.* **2008**, 453(1-2), 138-142.

61. Bogdanovic, B.; Bohmhamme, K.; Christ, B.; Reiser, A.; Schlichte, K.; Vehlen, R.; Wolf, U. Thermodynamic investigation of the magnesium-hydrogen system, *J. Alloys Compd*. **1999**, 282(1-2), 84-92.

62. Sohn H. Y.; Emami S. Kinetics of dehydrogenation of the Mg-Ti-H hydrogen storage system, *Int. J. Hydrogen Energy* **2011**, 36(14), 8344-8350.

63. Haussermann, U.; Blomqvist, H.; Noreus, D. Bonding and stability of the hydrogen storage material Mg2NiH4, *Inorg. Chem.* **2002**, 41(14), 3684-3692.

64. Huot J.; Akiba E.; Takada T. Mechanical alloying of Mg-Ni compounds under hydrogen and inert atmosphere, *J. Alloys Compd.* **1995**, 231(1-2), 815-819.

65. Barkhordarian G.; Klassen T.; Bormann R. Fast hydrogen sorption kinetics of nanocrystalline Mg using Nb_2O_5 as catalyst, *Scripta Materialia* **2003**, 49(3), 213-217.

66. Koh, J. T.; Goudy, A. J.; Huang, P.; Zhou, G. A comparison of the hydriding and dehydriding kinetics of $LaNi_5$ hydride, *J. Less. Common Metals* **1989**, 153(1), 89-100.

67. Yang H.; Ojo A.; Ogaro P.; Goudy A. J. Hydriding and dehydriding kinetics of sodium alanate at constant pressure thermodynamic driving forces, *J. Phys. Chem. C* **2009**, 113(32), 14512-14517.

68. Ibikunle A.; Goudy A. J.; Yang H. Hydrogen storage in a $CaH_2/LiBH_4$ destabilized metal hydride system, *J. Alloys Compd*. **2009**, 475(1-2), 110-115.

69. Durojaiye T.; Goudy A. J. Desorption kinetics of lithium amide/magnesium hydride systems at constant pressure thermodynamic driving forces, *Int. J. Hydrogen Energy* **2012**, 37(4), 3298-3304.

70. Sabitu S. T.; Fagbami O.; Goudy A. J. Kinetics and modeling study of magnesium hydride with various additives at constant pressure thermodynamic driving force, *J. Alloys Compd*. **2011**, 509(Supplement 2), S588-591.

71. Sabitu S. T.; Gallo G.; Goudy A. J. Effects of TiH_2 and Mg_2Ni additives on the hydrogen storage properties of magnesium hydride, *J. Alloys Compd*. **2010**, 449(1), 35-38.

72. Sabitu, S. T.; Goudy, A. J. Dehydrogenation kinetics and modeling studies of MgH_2 enhanced by NbF_5 catalyst using constant pressure thermodynamic forces, *J. Int. Hydrogen Energy* **2012**, 37(17), 12301-12306.

73. Sabitu, S. T.; Goudy, A. J. Dehydrogenation kinetics and modeling studies of MgH2 enhanced by transition metal oxide catalysts using constant pressure thermodynamic driving forces, *Metals* **2012**, 2(3), 219-228.

74. Zhou, Y.; Liu, Y.; Wu, W.; Zhang, Y.; Gao, M.; Pan, H. Improved Hydrogen Storage Properties of $LiBH_4$ Destabilized by in Situ Formation of MgH_2 and LaH_3, *J. Phys. Chem. C* **2012**, 116(1), 1588-1595.

75. Jiang, Y.; Liu, B. H. Dehydrogenation kinetics of $2LiBH_4 + MgH_2$ enhanced by hydrogen back pressure and a $CuCl_2$ catalyst, *J. Alloys Compd.* **2011**, 509(37), 9055-9059.

76. Xia, G.; Leng, H.; Xu, N.; Li, Z.; Wu, Z.; Du, J, Yu, X. Enhanced hydrogen storage properties of $LiBH_4$–MgH_2 composite by the catalytic effect of $MoCl_3$, *Int. J. Hydrogen Energy* **2011**, 36(12), 7128-7135.

77. Zhong, Y.; Zhu, H.; Shaw, L. L.; Ramprasad, R. Ab Initio Computational Studies of Mg Vacancy Diffusion in Doped MgB_2 Aimed at Hydriding Kinetics Enhancement of the $LiBH_4 + MgH_2$ System, *J. Phys. Chem. C* **2010**, 114(49), 21801-21807.

78. Deprez, E.; Justo, A.; Rojas, T. C.; Lopez-Cartes, C.; Minella, C.B.; Bosenberg, U.; Dornheim, M.; Bormann, R.; Fernandez, A. Microstructural study of the $LiBH_4$–MgH_2 reactive hydride composite with and without Ti-isopropoxide additive, *Acta Materialia* **2010**, 58(17), 5683-5694.

79. Price, T. E. C.; Grant, D. M.; Legrand, V.; Walker, G. S. Enhanced kinetics for the $LiBH_4$:MgH_2 multi-component hydrogen storage system – The effects of stoichiometry

and decomposition environment on cycling behavior, *Int. J. Hydrogen Energy* **2010**, 35(9), 4154-4161.

80. Zhang, Y.; Tian, Q.; Chu, H.; Zhang, J.; Sun, L, Sun, J.; Wen, Z. Hydrogen De/Resorption Properties of the $LiBH_4$−MgH_2−Al System, *J. Phys. Chem. C* **2009**, 113(2), 21964-21969.

81. Sudik, A.; Yang, J.; Siegel, D. J.; Wolverton, C.; Carter III, R. O.; Drews, A. R. Impact of Stoichiometry on the Hydrogen Storage Properties of $LiNH_2$−$LiBH_4$−MgH_2 Ternary Composites, *J. Phys. Chem. C* **2009**, 113(5), 2004-2013.

82. Fan, M.; Sun, L.; Zhang, Y.; Xu, F.; Zhang, J.; Chu, H. The catalytic effect of additive on the reversible hydrogen storage performances of composite, *Int. J. Hydrogen Energy* **2008**, 33(1), 74-80.

83. Gross, A. F.; Vajo, J. J.; Van Atta, S. L.; Olson, G. L. Enhanced Hydrogen Storage Kinetics of LiBH4 in Nanoporous Carbon Scaffolds, *J. Phys. Chem. C* **2008**, 112(14), 5651-5657.

84. Vajo, J. J.; Skeith, S. L. Reversible Storage of Hydrogen in Destabilized $LiBH_4$, *J. Phys. Chem. B* **2005**, 109(9), 3719-3722.

85. Vajo, J. J.; Salguero, T. T.; Gross, A. F.; Skeith, S. L.; Olson, G. L. Thermodynamic destabilization and reaction kinetics in light metal hydride systems, *J. Alloys Compd*. **2007**, 446-447, 409-414.

86. Zhang, W.; Cimato, J.; Goudy, A. J. The hydriding and dehydriding kinetics of some $LaNi_{5-x}Al_x$ alloys, *J. Alloys Compd*. **1993**, 201(1-2), 175-179.

87. Smith, G.; Goudy, A. J. Thermodynamics, kinetics and modeling studies of the $LaNi_{5-x}Co_x$ hydride system, *J. Alloys Compd.* **2001**, 316(1-2), 93-98.

88. Sabitu, S. T.; Goudy, A. J. Dehydrogenation kinetics and modeling studies of $2LiBH_4 + MgH_2$ enhanced by NbF_5 catalyst using constant pressure thermodynamic driving forces, *J. Phys. Chem. C* **2012** 116(25), 13545-13550.

89. Shang, C. X.; Bououdina, M.; Song, Y.; Guo, Z. X. Mechanical alloying and electronic simulations of (MgH_2 + M) systems (M=Al, Ti, Fe, Ni, Cu and Nb) for hydrogen storage, *Int. J. Hydrogen Energy* **2004**, 29(1), 73-80.

90. Reilly, J. J.; Wiswall, R. H. Reaction of hydrogen with alloys of magnesium and nickel and the formation of Mg_2NiH_4, *Inorg. Chem*. **1968**, 7(11), 2254-2256.

91. Lu, H. B.; Poh, C. K.; Zhang, L. C.; Guo, Z. P.; Yu, X. B.; Liu, H.K. Dehydrogenation characteristics of Ti- and Ni/Ti-catalyzed Mg hydrides, *J. Alloys Compd.* **2009**, 481(1-2), 152-155.

92. Hancock, J. D.; Sharp, J. H. Method of comparing soid-state kinetic data and its application to the decomposition of kaolinite, brucite, and $BaCO_3$, *J. Am. Cer. Soc*. **1972**, 55(2), 74-77.

93. Kissinger, H. E. Reaction kinetics in differential thermal analysis, *Anal. Chem*. **1957**, 29(11), 1702-1706.

94. Durojaiye, T.; Ibikunle, A.; Goudy, A.J. Hydrogen storage in destabilized borohydride materials, *Int. J. Hydrogen Energy* **2010**, 35(19), 10329-10333.

Saidi Temitope Sabitu
831 Gibbs Drive
Middletown, DE 19709
(302) 339-2253
topesabitu@gmail.com

Objective:

To obtain a position with a visionary institution that benefit from the knowledge and experiences I have acquired through education and professional work; and can afford me the opportunities for personal growth in the field of science and research.

Technical Qualifications:

- X-ray diffraction instrument for surface characterization
- Thermogravimetric/Differential Analyzer (TG/DTA) and Pressure Composition Isotherm (PCI) instruments for dehydrogenation profile and thermodynamic analysis
- Sieverts apparatus for kinetics and reaction rate analysis
- Microscopy, UV-Spectroscopy, FTIR, NMR
- Coordinate research activities and supervise undergraduate and high school students
- Excellent drive for research and possesses a strong sense of responsibility
- Excellent organizational and interpersonal skills

Education:

- **PhD in Applied Chemistry** **December 2012**
  Delaware State University, Dover, DE
- **Master of Science in Chemistry** **May 2008**
  Delaware State University, Dover, DE
- **Bachelor of Science in Biochemistry** **April 2002**
  University of Agriculture, Ogun State (Nigeria)

Professional Experience:

Graduate Assistant, September 2006 - Present

Center for Hydrogen Storage Research; Delaware State University, Dover, DE

- Led and conducted research and development on finding a suitable material (metal hydride) that can effectively store and release hydrogen according to the U.S. Department of Energy's guidelines for hydrogen storage and alternative energy sources for vehicular applications.

- Directed research efforts for the synthesis of metal hydrides for hydrogen storage and performed detailed characterization of the synthesized hydrides using X-ray diffraction.

- Thermodynamic and catalytic destabilization of magnesium hydride and lithium borohydride composite mixture to reduce their dehydrogenation temperature and effectively improve their reaction kinetics.

- Studying and comparing the effects of catalysts such as titanium hydride, magnesium nickel, transition metal oxides and niobium fluoride on the hydrogen storage properties of magnesium hydride.

- Compare the intrinsic dehydriding kinetics of destabilized metal hydrides using constant pressure thermodynamic driving forces.

- Modeling studies on destabilized metal hydrides to determine the rate controlling process.

- Supervised undergraduate and high school students in the planning and execution of research assignments and ensure the data from these research projects were translated into oral and written scientific reports.

Graduate Tutor, Delaware State University, Dover, DE September 2009 – December 2009

- Worked with students one-on-one as well as in small groups to help develop their understanding of Chemistry and its principles.

- Particularly worked with students enrolled in the 'Chemistry for Nursing' class

- Helped students prepare for standardized and no-standardized exams

Publications:

- **S.T. Sabitu**, G. Gallo, A.J Goudy. Effect of TiH_2 and Mg_2Ni additives on the hydrogen storage properties of magnesium hydride. *Journal of Alloys and Compounds* 499 (**2010**) 35-38.

- **S.T. Sabitu**, O. Fagbami, A.J. Goudy. Kinetics and modeling study of magnesium hydride with various additives at constant pressure thermodynamic driving forces. *Journal of Alloys and Compounds* 509S (**2011**) S588-S591.

- **S.T. Sabitu,** A.J. Goudy. Dehydrogenation kinetics and modeling studies of $2LiBH_4 + MgH_2$ enhanced by NbF_5 catalyst. *Journal of Physical Chemistry C* **2012**, 116, 13545-13550.

- **S.T. Sabitu,** A.J. Goudy. Dehydrogenation kinetics and modeling studies of MgH_2 enhanced by NbF_5 catalyst using constant pressure thermodynamic forces. *International Journal of Hydrogen Energy* 37 (**2012**) 12301-12306

- **S.T. Sabitu,** A.J. Goudy. Dehydrogenation kinetics and modeling studies of MgH_2 enhanced by transition metal oxides catalysts using constant pressure thermodynamic driving forces. *Metals* **2012**, 2, 219-228.

Conference/ Poster Presentations:

- **Thermodynamic studies on the interactions of TiH_2 and Mg_2Ni with MgH_2 for high capacity hydrogen storage.** National Organization for the Professional advancement of Black Chemists and Chemical Engineers (NOBCChe). September 2009, Maryland, USA.

- **Effect of TiH_2 and Mg_2Ni additives on the hydrogen storage properties of magnesium hydride.** National Hydrogen Association (NHA) Hydrogen Conference & Expo. May 2010, Long Beach, California, USA.

- **Kinetics and modeling study of magnesium hydride with various additives at constant pressure thermodynamic driving forces.** International Symposium on Metal-Hydrogen systems. July 2010, Moscow, Russia.

- **Attendee**, Gordon Research Conference (GRC). July 2011, Boston, USA.

- **Kinetics and modeling study of magnesium hydride with various catalysts as hydrogen storage material**. 2nd Annual Graduate Research Symposium. Delaware State University. April 2012, Dover, USA.

- **Kinetics and modeling studies of some alkaline earth borohydrides at constant pressure thermodynamic forces**. 244th American Chemical Society (ACS) National Meeting. August 2012, Philadelphia, USA.

Academic Honors & Awards:

- Best graduating Biochemistry student award **2002**
- Dr. Apampa's 1st place award in Biochemistry Department **2002**
- Student's Chemical Society of Nigeria (SCSN) award for best student in the Department of Biochemistry **2000-2002.**

Affiliations:

- Member; American Chemical Society (ACS)
- Member; Student Chemical Society of Nigeria (SCSN)

Personal Interest

- Choir, playing soccer and reading